Rossana Pasquino
Ph.D. Thesis in Chemical Engineering
(XXI cycle)

Rheology of viscoelastic suspensions

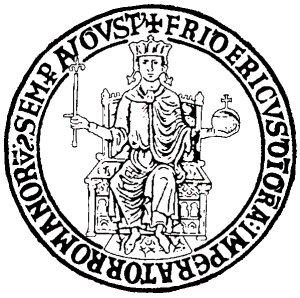

Jury

Prof. Nino Grizzuti, promotor
Dr. Francesco Greco
Prof. Pier Luca Maffettone
Prof. Jan Vermant

Non ho particolari talenti, sono solo appassionatamente curioso.
A. Einstein

A nonna Ninuccia

Acknowledgments

Mi piacerebbe poter ringraziare coloro i quali hanno contribuito in questi anni al mio lavoro di tesi di dottorato.
In primis vorrei ringraziare Nino (per una volta il "tu") per aver creduto in me fin dall'inizio (sperando che non se ne sia pentito..), per avermi inculcato l'entusiasmo della scoperta e per il supporto emotivo che non mi ha fatto mai mancare.
Grazie a Francesco, per le discussioni accademiche (e non), per i pianti, i sorrisi, i discorsi su quotidianitá e vita. Se sono migliorata, e non solo accademicamente (anche se non mi dirai mai di sì), buona parte del merito *è* suo.
Grazie a Pier Luca, per non avermi mai fatto sentire la differenza tra "il" professore e lo studente e per l'estrema disponibilit*à* che ha sempre dimostrato.
Thanks to the professor Jan Vermant, to give me the possibility to improve my professional knowledge and to support me during my "bad" period in Belgium. I will never forget our meetings and the words "it's amazing!", that well express all your curiosity and passion for research.
Grazie ai miei amici di sempre, a quelli di cui non ho mai sentito la mancanza, a quelli che ho incontrato da poco, a quelli che sono passati per poco e mi sono rimasti sulla pelle. In particolare ringrazio Alessia, Rita, Elisa, Gustavo, Alessandro, Erman e Cettina senza cui i miei mesi a letto sarebbero durati una eternitá. Ed i ragazzi del Paolella, in particolare Luisa, che è piú di una sorella.
Grazie a Ginia, per le mille telefonate e per avermi regalato il sorriso di Fede.
Grazie ai miei colleghi napoletani, Claudia, Stefano e Francesco e non ho bisogno di spiegare perchè, tutto è giá nelle intere giornate passate insieme.
Thanks to Frank (the angel of my office!) for our discussions on research and "life's purposes", to be always nice and "predictable", to correct this thesis...Basa (a good cook!), Naveen and Kasper without whom my experience in Belgium would have had surely less importance. In particular, Basa's rigor, integrity and curiosity serve as the standard that I shall aspire to throughout my professional life.
Grazie, ancora, ad Eleonora, Anneleen and Leen per le nostre indimenticabili serate belghe e per avermi regalato affetto incondizionato!
Thanks to all the people of the "Etna".
At last but not least, non posso che dire grazie ai miei genitori, presenza costante, accorta, sentita. Mi hanno dedicato buona parte della loro vita, rendendomi migliore giorno dopo giorno. Sono riusciti a farmi sentire sempre importante, amata. Spero di poter un giorno ricambiare con lo stesso intenso amore. Non avrei potuto desiderare genitori migliori.

Grazie, infine, ai miei fratelli, che, dovunque si trovino e mi trovi, sono e rimarranno sempre ad un passo da me.

"chi car' e s' áiz nun è mai carut..."

Summary

The rheology of suspensions of solid particles in viscoelastic fluids is important in many technological applications as exemplified by the processing of filled polymers e.g. injection molding, coating processes, application in food and health care products,...
Consequently, considerable attention in the literature is given to the rheology of suspensions of particles. Most studies are focused on highly filled systems (typically, volume fractions greater than 10%), with polydisperse particles of irregular shapes due to their technological importance. In contrast, realtively few studies are conducted on the rheology of dilute or semi-dilute suspensions of monodisperse spheres.
In the first part we elucidate the effect of viscoelasticity on the bulk rheological properties. The behavior of model suspensions composed of non Brownian, inertialess, rigid spheres immersed in Newtonian and viscoelastic matrices is investigated in the concentration range from 0 up to 10%, thus encompassing both the dilute and semidilute regimes. The data are fitted with quadratic polynomial functions of the particle volume fraction in order to compare with theoretical, empirical and experimental models.
As second part, new simulation technique for suspensions in Newtonian fluids under oscillatory shear flow is presented. The cases of a single sphere and two particles are studied and discussed.
Finally, the flow induced microstructure of suspensions in viscoelastic fluids is studied by rheo-optical techniques. More specifically, the flow-induced alignment of non-colloidal particles in viscoelastic fluids is investigated systematically in an attempt to quantify the alignment of the particles and correlate it with the shear rate, size of the particles and interactions with the wall.

List of Figures

1.1 Data from Rutgers. 21
1.2 Data from Saunders. The slope of 6.2 is in good agreement with Batchelor's prediction 22
1.3 Normalized effective viscosity of suspensions as a function of volume fraction of monosized hard spheres showing comparison between Hsueh's work and existing predictions [20]. 23
1.4 Time-averaged bulk shear viscosity as a function of solid area fraction, calculated from the single particle problem [23]. . . . 24
1.5 Relative bulk shear viscosity as a function of solid area fraction. Hwang and Hulsen results [24] are plotted as well (open squares). 25
1.6 Relative shear viscosity as a function of solid area fraction for different Weissenberg numbers [37]. 28
1.7 Alignment and aggregation effects in suspension of spheres in non Newtonian fluid (a) after loading (b)with few oscillations of the plate (c)after several oscillations (d)after long oscillatory times 33
1.8 Alignment of a bidisperse suspension in a non-Newtonian liquids [61]. 34
1.9 Imbalance of shear rate for two cylinders. 35

2.1 Particle size distribution for PMMA spheres. 39
2.2 Particle size distribution for glass beads. 39
2.3 TGA for aPP suspensions. 41
2.4 DFST for Newtonian Polyisobutylene, at 30°C. 44
2.5 DFST for the Dow Silicone Fluid, at 30°C. 45
2.6 DFST for the Rhodorsil fluid, at 30°C. 45
2.7 The steady shear viscosity of PIB based suspensions as function of shear rate at various filler concentrations. 46

2.8 Loss modulus for PDMS-B based suspensions as function of frequency at various filler concentrations; (a) for all measured frequencies (lines are guides to the eye); (b) in the low frequency range: lines are linear regressions of the data). Symbols as in the Fig. 2.7. 47
2.9 Normalized steady shear viscosity (top) and viscous modulus (bottom) for the PIB suspensions as function of volume fraction. Dashed line: Einstein's viscosity law; solid line: quadratic fit. 49
2.10 Normalized steady shear viscosity (top) and viscous modulus (bottom) for the PDMS-A suspensions as function of volume fraction. Dashed line: Einstein's prediction; solid line: quadratic fit. 50
2.11 Normalized steady shear viscosity (top) and viscous modulus (bottom) for the PDMS-B suspensions as function of volume fraction. Dashed line: Einstein's prediction; solid line: quadratic fit. 51
2.12 Intrinsic steady shear viscosity (top) and intrinsic loss modulus (bottom) for the three suspensions as function of volume fraction 54
2.13 The percent error for three different frequencies (0.1, 1 and 10 rad/s), for both the calculation of $G^{'}(\circ)$ and $G^{''}(\bigtriangledown)$ 55
2.14 The ratio of the loss over the storage modulus versus frequency for filled and unfilled PDMS fluids. 56
2.15 Comparison between normalized viscous modulus for PDMS based suspensions in the low frequency range and in the whole frequency range. Line is the best fit to data. 58
2.16 Relative storage modulus as function of volume fraction for the suspending media. The lines are best fits to the data. . . . 59
2.17 Comparison between data of viscous modulus for PDMS-B based suspensions at $70°C$ with those at $30°C$. 61
2.18 DFST for pure suspending atactic polypropylene 62
2.19 Loss (a) and storage (b) moduli for a-PP based suspensions as function of frequency at various filler concentrations. 63
2.20 Normalized viscous modulus for the a-PP suspension as function of bead volume fraction. 64
2.21 Normalized storage modulus for the a-PP suspension as function of bead volume fraction. 64
2.22 N_1 as function of shear rates for different volume fractions. Symbols as in Fig. 2.20. 65
2.23 Normalized value of N_1 as function of volume fraction. 66

2.24 Normalized viscous modulus as function of the longest relaxation time λ_{max} for the three suspending media, for different volume fractions. 68

3.1 The geometry used in the simulation technique. 73
3.2 The angular velocity as function of ωt. 75
3.3 Fluid (top) and particle (bottom) contributions to the shear bulk stress as function of particle size. 76
3.4 Viscous modulus as function of solid area fraction. The line is the best fit to the data. 76
3.5 The division of the domain box in four sub-domains; one particle is in the center of the box; the initial position of the other particle is changed. 77
3.6 The viscous modulus as function of solid area fraction. The dashed line is Einstein's result for 2-D flow [26]. The solid line is a quadratic regression to the data. 78

4.1 SEM micrographs of Polystyrene spheres. From the top to the bottom, 2.8 μm, 1.9 μm and 1.2 μm respectively. 82
4.2 Schematic diagram of SALS setup 84
4.3 Schematic layout of a SALS setup dipicting the incident and scattered beams, the 2-D detector and the definition of the scattered vector (q). 85
4.4 Real space image of a flow aligned structure and the corresponding image in the SALS pattern (respectively top left and top right). Scattering pattern before shearing and after shearing for PS suspensions in HPC. 87
4.5 The counterrotating rheometer combined with microscopy from [55]. 89
4.6 Viscosity of the fluids as function of shear rate. 90
4.7 First normal stress coefficients of the fluids as function of shear rate. 90
4.8 Weissenberg numbers of the fluids as function of shear rate. . . 91
4.9 Viscoelastic moduli for the suspending media as function of frequency. 92
4.10 Microscopy image of PEO's suspension with 3μm diameter spheres. 92
4.11 Microscopy images of a HPC suspension at $30s^{-1}$ and 200μm gap (diameter spheres=1.9 μm). After 1h: on the left side the microstructure on the plate; on the right side in the bulk. . . . 94

4.12 Microscopy image of a HPC suspension at $30s^{-1}$, 100μm gap (diameter spheres=3μm). Top left: before shearing. Top right: on the plate after shearing 1h. Bottom: in the bulk after shearing 1h. 94
4.13 Microscopy image of a HPC suspension at different shear rates (diameter spheres: 1.9μm) after shearing 1h at 100μm gap. . . 95
4.14 Microscopic image of HPC suspension with 1.2μm spheres in the bulk of the liquid after shearing at 1 s^{-1}. 96
4.15 The sign evaluation of cos2ϑ for the alignment factor. 97
4.16 Evaluation of percent error in a meaningful q range for 1.9 μm based suspension. 98
4.17 SALS patterns as function of shear rate for 1.2 μm size particle. At low shear rates, a weak vorticity alignment can be see. Increasing the shear rate reorients the strings in the flow direction. 98
4.18 Alignment factor as function of scattering vector at 360% strain for the 1.2 μm size suspension. 99
4.19 Alignment factor as function of scattering vector after 1h for 1.2 μm size spheres. 100
4.20 Alignment factor as function of shear rate at a scattering vector of $1\mu m^{-1}$. 100
4.21 Alignment factor (eq. 4.6) as function of scattering vector for the suspensions with 1.2μm particles at different shear rates after 1h of shearing. 101
4.22 Alignment factor at steady state as function of shear rate for suspensions with spheres of different sizes. Data for suspensions with 2.8μm spheres are from Scirocco *et al* [91]. 102
4.23 Effect of the gap width on the alignment factor for a dispersion of 1.9μm spheres in the HPC based suspending medium. Steady state at q=$1\mu m^{-1}$. 103
4.24 Alignment factor as function of the time for different gap sizes. 104
4.25 First derivative of the alignment factor in fig. 4.23 in the range 0-600s. 104
4.26 Alignment factor as function of time for a gap of 100μm at $30s^{-1}$. 105
4.27 Bands of particles at high shear rates. 105
4.28 SALS patterns as function of shear rate for 1.6 μm size charged particle. 106
4.29 Counterrotating image for HPC based suspensions. 108
4.30 Alignment factor as defined by eq. 4.7 at steady state as function of shear rate for suspensions of spheres with different sizes. 109

List of Tables

2.1 Zero shear viscosities of the suspending fluids 38
2.2 Comparison between required and effective volume fractions . 41
2.3 Fit values of the polynomial coefficients of Eqs. 1.2 and 1.7. Standard deviations are also shown. 52
2.4 Best fit values for b$'$ of eq. 1.8 and comparison with b'' of eq. 1.7 with the assumption that $a' = a'' = 2.5$. Standard deviations are also reported to appreciate the statistical error. 60
2.5 Parameters of eq. 1.7 and 1.8 for PDMS-B based suspensions at $30°C$ and $70°C$. 60
2.6 Longest relaxation time λ_{max} for the suspending media. 68

4.1 Molecular weights of the polymers and composition of the suspending media. 83
4.2 Weissenberg number and onset of alignment as function of shear rate. 96

List of symbols

Symbol	*Description*	*Units*
a, a', a'', b, b', b''	fitting parameters	[-]
A	area	[m^2]
A_f	area occupied by fluid	[m^2]
A_f	alignment factor	[-]
A_p	area occupied by particles	[m^2]
D	particle diameter	[m]
E	modulus of Young of suspension	[Pa]
E_0	modulus of Young of suspending medium	[Pa]
f	force	[N]
F_i	total force on the particle boundaries	[N]
T_i	total torque on the particle boundaries	[N $\cdot$ m]
g	acceleration gravity	[m $\cdot$ s^{-2}]
G^*	complex modulus of suspension	[Pa]
G_0^*	complex modulus of suspending medium	[Pa]
G''	viscous modulus of suspension	[Pa]
G'	elastic modulus of suspension	[Pa]
G_0''	viscous modulus of suspending medium	[Pa]
G_0'	elastic modulus of suspending medium	[Pa]
G_n''	normalized viscous modulus	[-]
G_n'	normalized elastic modulus	[-]
h	gap	[m]
I	intensity	[-]
k_i	incident wave vector	[-]
k_s	scattered wave vector	[-]
K_B	Boltzmann constant	[J $\cdot$ K^{-1}]
L	characteristic length	[m]
n	unit normal vector	[-]
N	number of particles	[-]
N_1	first normal stress difference	[Pa]
N_2	second normal stress difference	[Pa]
p	pressure	[Pa]
Pe	Peclet number	[-]
q	scattering vector	[m^{-1}]
r	radius of the plate	[m]
R	particle radius	[m]
Re	Reynolds number	[-]

Re_p	particle Reynolds number	[-]
s	spacing between two spheres	[m]
T	temperature	[K]
t	time	[s]
u	velocity vector	$[\mathrm{m} \cdot \mathrm{s}^{-1}]$
U_i, V_i	components of the translational velocity	$[\mathrm{m} \cdot \mathrm{s}^{-1}]$
v_z	migration velocity	$[\mathrm{m} \cdot \mathrm{s}^{-1}]$
w	angular velocity	$[\mathrm{s}^{-1}]$
Wi	Weissenberg number	[-]
Wi_{cr}	critical Weissenberg number	[-]
X_i, Y_i	coordinates of the particle center	[-]
x, y, z	coordinates	[-]

Greek symbols

α	polar angle	[-]
γ	deformation	[-]
γ_0	amplitude of deformation	[-]
δ	ratio between G'' and G'	[-]
$\dot{\gamma}$	shear rate	$[\mathrm{s}^{-1}]$
λ	wavelength of the light	[m]
λ_{max}	maximum relaxation time	[s]
η_0	viscosity of suspending medium	$[\mathrm{Pa} \cdot \mathrm{s}]$
η	viscosity of suspension	$[\mathrm{Pa} \cdot \mathrm{s}]$
η_n	normalized viscosity	[-]
θ	azimuthal angle	[-]
σ	shear stress	[Pa]
ρ_0	density of suspending medium	$[\mathrm{Kg} \cdot \mathrm{m}^{-3}]$
ρ_p	particle density	$[\mathrm{Kg} \cdot \mathrm{m}^{-3}]$
ϕ	volume fraction	[-]
ϕ_a	area fraction	[-]
ϕ_m	volume fraction at maximum packing	[-]
ψ_1	first normal stress coefficient	$[\mathrm{Pa} \cdot \mathrm{s}^{-2}]$
ω	frequency	$[\mathrm{s}^{-1}]$
Ω	bounded region	$[\mathrm{s}^{-1}]$

Contents

0.1 Introduction 15

1 State of the art **18**
1.1 Rheological properties of suspensions 18
1.1.1 Viscosity of suspensions of spheres in Newtonian media 18
1.1.2 Viscosity and viscoelastic properties for suspensions of spheres in non-Newtonian Media 26
1.2 Hydrodynamics and interaction forces 31
1.2.1 Newtonian media 31
1.2.2 Non-Newtonian media 32

2 Suspension Rheology **38**
2.1 Materials and Methods 38
2.1.1 Materials 38
2.1.2 Preparation of the suspensions 40
2.1.3 Rheological measurements 42
2.2 Experimental results-A 44
2.2.1 Rheology of suspending fluids 44
2.2.2 Rheology of suspensions 45
2.3 Experimental results-B 62
2.3.1 Rheology of atactic-polypropylene 62
2.3.2 Rheology of the suspensions 62
2.4 Conclusions 67

3 Simulation of circular disks in a Newtonian fluid under 2-D oscillatory flow **69**
3.1 Modeling aspects 70
3.2 Bulk stress 73
3.3 The single particle problem 74
3.4 The two particles problem 77
3.5 Conclusions 79

4 Flow-induced structure formation of spheres in viscoelastic fluids **80**
4.1 Materials 80
4.1.1 Polystyrene particles 80
4.1.2 Polymer solutions 82
4.2 Experimental techniques 83
4.3 Experimental results 90
4.3.1 Rheology of suspending fluids 90
4.3.2 Microscopy 92
4.3.3 Small angle light scattering 97
4.3.4 Counterrotating device 107
4.4 Conclusions 108

0.1 Introduction

Rheology is the science that studies the deformation and flow of matter.
It is a relatively young and multidisciplinary science that encompasses many different industrial areas of activity as plastics, ceramics, cosmetics, pharmaceutics, food and biotechnology, but also paints and inks, adhesives, lubricants and surfactants.
It is quite straightforward to list situations where the deformation or the flow of matter (which depends on the rheological characteristics of the involved materials) determines the performance of a product, the effectiveness of a service and the rate of a manufacturing process. Thus, rheology is a very attractive, dynamic, highly multidisciplinary and fast-growing area of activity.
In particular, in many industrial processes, materials consist of particles dispersed in rheologically complex fluids, the so called suspensions.

Suspensions of particles find applications in many different areas, including polymers, pharmaceuticals, cosmetics, food, ceramic pastes. The control of structure and flow properties of suspensions is often crucial to the commercial success of the product. The final properties of suspensions are affected by several factors, including shape, concentration and size of the filler. In particular, the size of solid inclusions can range from nanoscopic to macroscopic characteristic dimensions, leading to a wide range of different flow behaviors.

The rheological behavior of suspensions has received considerable attention in the literature. Most studies have focused on highly filled systems (typically, volume fractions greater than 10%), due to their importance in technological applications. Conversely, relatively few studies are done on the rheology of dilute or semi-dilute suspensions. Low concentrations are important, however, at least for two reasons: first, low concentration suspensions find applications in several fields (biomedical materials, cosmetics). Second, the experimental response of semi-dilute suspensions is a good test for theories that explore concentrations beyond the well known Einsteins infinite dilution result.

It must be added that most investigations in the low concentration range were carried out on particles suspended in a Newtonian liquid. Indeed, dispersing particles will be different depending on whether the suspending medium is Newtonian or non-Newtonian. Viscoelastic fluids, in particular, exhibit shear thinning, memory effects and first and second normal stress differences, as such increasing the rheological complexity of the whole system.
Compared to the Newtonian suspensions, suspensions with viscoelastic suspending media show differences in the flow induced structure.

The macroscopic response and the flow induced microstructure depend on the dynamics of the individual particles and the flow of the suspending fluid around and between the particles. The differences between Newtonian and viscoelastic suspensions are mainly due to the changes in hydrodynamic forces that are associated to the changes in the rheological behavior of the suspending fluids. Phenomena of chaining and alignment can occur in viscoelastic suspending media and there is no indication that this also happens in Newtonian media.

In order to understand the formation of such microstructures, one needs to fully consider the hydrodynamic interactions between particles and fluid, the inter-particle forces as well as the complex rheological properties of the fluid. To accommodate all these requests, the development of simulation methods has received great attention in recent years. In particular, direct numerical simulation techniques give sufficiently accurate results on velocity and stress fields in the fluid medium, along with full consideration of hydrodynamic and interparticular interactions with the usage of state-of-the-art viscoelastic constitutive models. To our knowledge, most investigations have been carried out on direct numerical simulations for inertialess non-Brownian hard particle suspensions, with Newtonian and viscoelastic fluids, in both simple shear and elongational two-dimensional flows.

Objectives

The main objective of this study is to elucitade the role and effect of the viscoelasticity of the dispersion medium on the rheology and microstructure of dilute suspensions of spherical particles.
In particular, the dependence of viscoelastic moduli and shear viscosity on volume fraction and frequency has been experimentally studied for different particle-polymer systems.
Moreover, a new simulation technique for non-Brownian inertialess hard sphere suspensions in oscillatory flow for a Newtonian fluid will be presented, in order to understand how the complex viscosity changes as a function of solid area fraction (two-dimensional flow).
The microstructure generated in flowing suspensions has been also considered. The knowledge of this study provides the basis for understanding the processing of suspensions as well as predicting and controlling the final properties of the processed products.

Approach

The macroscopic rheology of several non-colloidal, inertialess rigid spheres in both Newtonian and viscoelastic fluids is investigated. Volume fractions up to 10% were used, thus exploring both the dilute regime, which is commonly delimited to a concentration of about 5% [1], and the semi-dilute regime, where interparticle interactions are expected to become relevant. The experimental results are compared with the predictions of existing theories, in particular those based on purely hydrodynamic calculations.

In addition, suspensions of monodisperse polystyrene spheres in different suspending media have been studied. The goal is to use microscopy and scattering techniques to understand how particle dynamics are altered and how the overall suspension rheology is affected in a viscoelastic fluid. The effect of the size of the spheres on flow-induced alignment has been considered. Walls effects and migration have been considered.

This thesis is organized as follows: in chapter 1 the state of the art is reviewed. This chapter covers the rheology of suspensions of spheres in both Newtonian and viscoelastic suspending media, with particular attention to the theoretical models and experimental background, and also focuses on the motion and suspension microstructure.
The experimental results are divided in three sections. In the first section results on the macroscopic rheological response for a Newtonian and some viscoelastic suspensions are presented. The behavior of model suspensions composed of non Brownian, inertialess, rigid spheres immersed in Newtonian and viscoelastic matrices is investigated in the range of volumetric concentrations up to 10%, thus encompassing both the dilute and semidilute regimes. The data are modeled by means of quadratic polynomial functions of the particle volume fraction in order to make a comparison with theoretical, empirical and experimental models.
The second section reports on a new simulation technique for suspensions in Newtonian fluid with imposed oscillatory flow. The case of a single sphere and of two interacting spheres are studied and fully discussed.
The last section focuses on flow-induced alignment of non-colloidal particles in viscoelastic fluids. The phenomenon is treated systematically in order to quantify the alignment of particles and try to correlate it with the rheology of the fluid, the size of the suspending particles, the interactions with the wall. For the first and last section, materials and used methods are presented and obtained results are discussed.

Chapter 1

State of the art

In many industrial processes, materials are formulated that consist of particles dispersed in rheologically complex fluids. In order to control the processing behavior and to tune the end-use properties of formulated products, a study of the rheological properties and generated microstructure is necessary. In this first chapter the state of the art, pertaining to the subject of this thesis, is presented. In particular, the first section focuses on the macroscopic response of suspensions: the suspension rheology. Major contributions, theoretical, experimental and from computer simulation are discussed. Both Newtonian and non-Newtonian suspending media are covered.
The second part of this chapter deals with particle motion and flow induced microstructure in suspensions in shear flow.

1.1 Rheological properties of suspensions

1.1.1 Viscosity of suspensions of spheres in Newtonian media

Viscosity is the most fundamental rheological property in characterizing the structural organization and interaction of constituents within suspensions.
The simplest model suspension is composed of so-called hard spheres in a Newtonian fluid. The addition of a rigid sphere to a liquid alters the flow field, and this influence has been the subject of a vast literature.
If spheres are very small (<1 micron), colloidal forces between particles can become enormous and can also introduce deviations from Newtonian behavior.
For the case of rigid spheres in a Newtonian fluid at very low concentra-

tion hydrodynamic effects were accounted by Einstein [2] 100 years ago. He gave the first prediction for the viscosity of dilute suspensions. The relevant assumptions for the analysis in Einstein's classic paper are the following:

- The surrounding fluid or solvent is incompressible and Newtonian and can be treated as a continuum. This implies that the fluid molecules are much smaller than the suspended particles.
- Creeping, buoyancy-free flow.
- No slip between particles and fluid.
- Particles are rigid and spherical.
- Dilute non-interacting particles are considered.
- The viscometer characteristic length is much greater than that of the suspended particles, so that wall effects neglectable.

All these assumptions lead to Einstein's celebrated formula:

$$\eta = \eta_0(1 + 2.5\phi) \tag{1.1}$$

with η the viscosity of the suspension, η_0 the viscosity of the suspending fluid and ϕ the volume fraction of spheres.
The experimental confirmation of eq. (1.1) is not so trivial, as the assumptions of Einstein's theory are not easily satisfied. Reports on experiments can be found in literature, especially in the 30's, for example by Bachle [3], Blow [4], Eirich et al [1]. In the latter work spherical particles were used and the total absence of agglomeration was observed. Under these conditions, the equation (1.1) was verified up to volume concentrations of 5%.
For more concentrated suspensions it is necessary to consider corrections to the viscosity that are of higher order in the volume fraction. When the flow field around a sphere is influenced by the presence of neighbouring spheres, the hydrodynamic interactions cannot be neglected and they could be treated as a contribution to η that is proportional to ϕ^2 for two bodies, to ϕ^3 for three bodies and so on.
The major contribution to theory comes from Batchelor and Green [5, 6] and Batchelor [7], who performed a fully hydrodynamic calculation using statistical mechanics to account for Brownian forces and hydrodynamic interactions in a semidilute suspension of hard spheres. Interactions between particles determine the presence of terms of order ϕ^2 in the expression for the stress tensor. In particular, it was assumed that [6]:

- The fluid is Newtonian.
- Creeping flow is assumed.
- Inertia of the particles can be neglected.
- No external forces or couples act on the particles.
- The particles are spherical and their spatial distribution throughout the ambient fluid is assumed to be random.

With these assumptions, the suspension has isotropic structure and the stress behaviour can be represented to order ϕ^2 in terms of an effective viscosity:

$$\eta = \eta_0(1 + a\phi + b\phi^2) \tag{1.2}$$

In eq. (1.2), obviously, a=2.5. The second order coefficient b is equal to 7.6 [6]. It becomes equal to 6.2 [7] when Brownian motion is included.
It must be stressed that Batchelor's result is a prediction for purely irrotational flow only, where the particle probability function can be exactly calculated. As a consequence, eq. (1.2) is a prediction for an elongational viscosity, not for a shear viscosity. Exact predictions for the shear viscosity of interacting particles have never been developed. Extensions to the work of Batchelor to higher volume fractions always contained several, arbitrary assumptions [8].
Experimental validations of Batchelor's calculations (assuming that the prediction of (1.2) holds also for shear flow) are very scarce in the literature. A major review of the dependence of the relative viscosity on concentration is due to Rutgers [9], who collected the results of several experimental investigations up to very high concentrations [9, 10, 11, 12, 13, 14]. From these measurements on suspensions of spheres in Newtonian fluids, he found an average curve which represents a new relation valid for all shear rates up to a volume fractions of about 0.25. Fig. (1.1) presents the relative viscosity η_n (the ratio between the viscosity of suspensions and that of pure suspending medium) vs the volume fraction ϕ and also the average curve obtained by Rutgers, whose results are presented in the accompanying table.

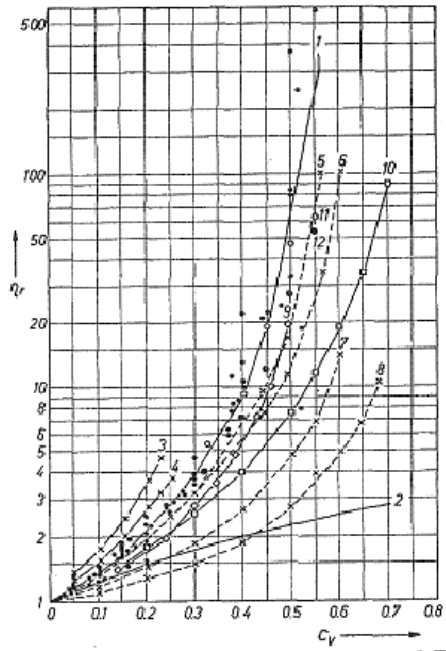

Fig. 1. • ——— 1 Average sphere curve; • ——— 2 *Einstein* formula; × ——— 3 *Oden*, 10 $\mu\mu$; × ——— 4 *Oden* 100 $\mu\mu$; × – – – 5 *Maron*, $\tau = 50$; × – – – 6 *Maron*, $\tau = 800$; × – – – 7 *Robinson*, sucrose, $D = 1860$; × – – – 8 *Robinson*, oil, $D = 1860$; ◇ ——— 9 *Ting-Luebbers*; □ ——— 10 *Eilers*; ⊙ 11 *Sweeney*, 49 μ, η_0, $D = 0$–147; ⊗ 12 *Sweeney*, 49 μ, η_∞, $D = 0$–192

Concentration and Relative Viscosity

c	η_r
0.00	1.00
0.05	1.16
0.10	1.38
0.15	1.67
0.20	2.11
0.25	2.76
0.30	3.8
0.35	5.7
0.40	10
0.45	20
0.50	58
(0.55	250)

Figure 1.1: Data from Rutgers.

From all the investigations on Newtonian suspensions shown in Fig. 1.1, the only relevant contribution for low concentrations is that of Saunders [15], who measured the shear viscosity of sub-micron sized polystyrene lattice suspensions and found that a good agreement with Batchelor's equation for volume

fractions up to about 10%. In Fig. (1.2) Saunders results are shown.

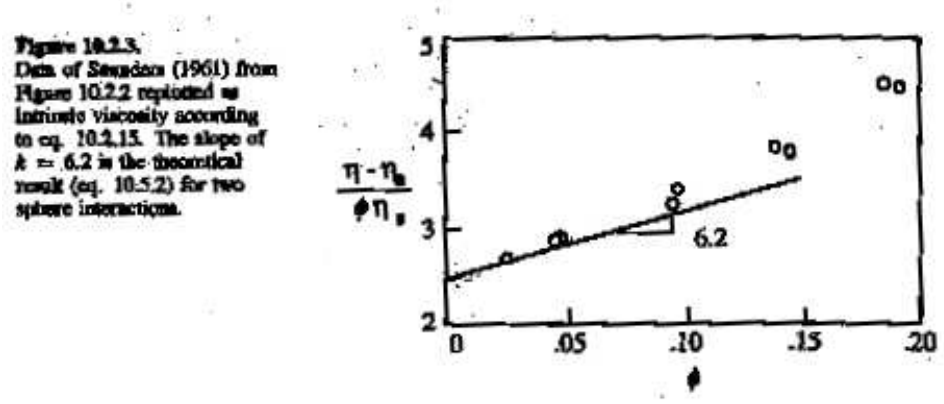

Figure 1.2: Data from Saunders. The slope of 6.2 is in good agreement with Batchelor's prediction

For concentrated suspensions, semi-empirical approaches have been adopted. The coefficients for higher-order terms in the polynomial expansion of viscosity as a function of volume fraction are even more difficult to calculate. Thomas and Muthukumar [16] considered full hydrodynamic interactions between three hard spheres and derived, using the multiple scattering theory:

$$\eta = \eta_0(1 + 2.5\phi + 4.83\phi^2 + 6.4\phi^3) \tag{1.3}$$

However, each successive term extends the equation's applicability to only slightly higher ϕ. By taking into account hydrodynamic interactions of an arbitrary number of hard spheres, Beenakker [17] performed an analysis that is for high volume fractions. However, instead of a formula, Beenakker obtained numerical results for ϕ up to 0.45.
Hence, the value of the second order coefficient, b, for the shear viscosity of suspensions of spheres, becomes contradictory and much dependent on the model assumptions.
The most widely used equation for concentrated suspensions was formulated by Dougherty and Krieger [18, 19] (or equivalent formulas, e.g. Quemada, Maron-Pierce or Mooney):

$$\eta = \eta_0 \left(1 - \frac{\phi}{\phi_m}\right)^{-2.5\phi_c} \tag{1.4}$$

where ϕ_m is an adjustable parameter related to the volume fraction at which spheres become close packed. Typical values for ϕ_m range from 0.6 to 0.7 for monodisperse spheres. The -2.5 used in the exponent is used in order to re-obtain the Einstein's solution when $\phi \to 0$.
Another model to be mentioned for the effective viscosity of Newtonian suspensions of monosized spheres is the one derived by Hsueh and Becher [20]. The derived formula is in a good agreement with Beenakker's numerical simulation. In particular, the power series expansion of the viscosity equation reported in this work is:

$$\eta = \eta_0(1 + 2.5\phi + 6.25\phi^2 + 10\phi^3 + 13.75\phi^4 + 17.5\phi^5 + 21.25\phi^6 + ...) \quad (1.5)$$

In Fig. (1.3), equation (1.5) is compared with existing solutions for the normalized effective viscosity of suspensions of monodisperse hard spheres.

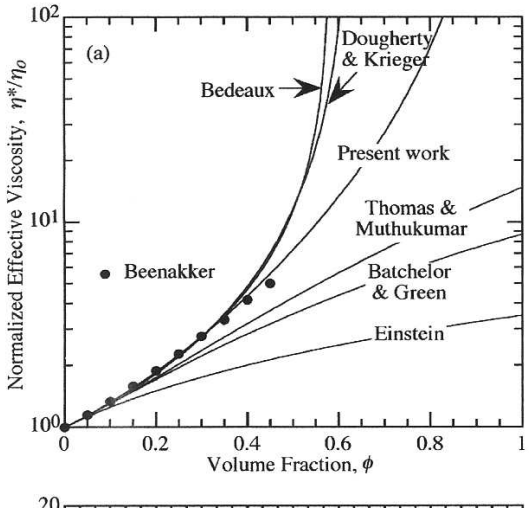

Figure 1.3: Normalized effective viscosity of suspensions as a function of volume fraction of monosized hard spheres showing comparison between Hsueh's work and existing predictions [20].

As can be easily seen, all solutions predict similar results for dilute suspensions in Newtonian fluids, which overlap to the analytical solution deduced by Batchelor and Green for elongational flow [5].

Several investigators considered the rigid particle suspension as a special, limiting case of a liquid-liquid emulsion, when the drop viscosity goes to infinity. Oldroyd [21] derived expressions for the viscosity of emulsions of one Newtonian fluid in another. He used an effective-medium approach to

relax the hypothesis of diluteness. Oldroyd's prediction for the coefficient b in (1.2) was b=2.5, far smaller than Batchelor's exact calculation. Along similar lines Choi and Schowalter [22], using a cell model approach, obtained the prediction b=125/8, an amazingly different result.

A new approach for the study of suspensions is Computational Fluid Dynamics. Its current popularity is rooted in the perception that information implicit in the equations of fluid motion can be extracted without approximation using direct numerical simulation.
Numerical simulations of fluidsolid flow systems can be classified in different categories, as it will be explained later.
For our purpose, in particular, two articles from Hwang *et al* [23, 24] and one from D'Avino *et al* [25] on simulations of circular inertialess disks in a Newtonian fluid have to be mentioned. In their articles, only two-dimensional simple shear and two-dimensional planar elongational flows are simulated.
In the case of simple shear flow, Hwang *et al* calculated the bulk shear viscosity as function of solid area fraction for a wide range of the area fraction, from less than 1% to about 75%. The bulk shear viscosity is plotted as function of ϕ in Fig. 1.4.

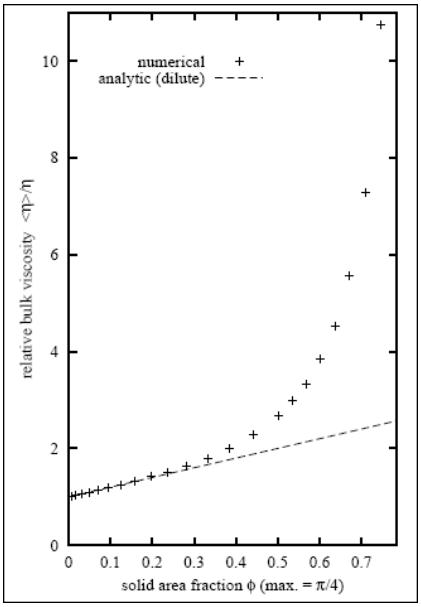

Figure 1.4: Time-averaged bulk shear viscosity as a function of solid area fraction, calculated from the single particle problem [23].

As regards elongational flow, the relative bulk viscosity as a function of the particle area fraction was obtained as in Fig. 1.5.

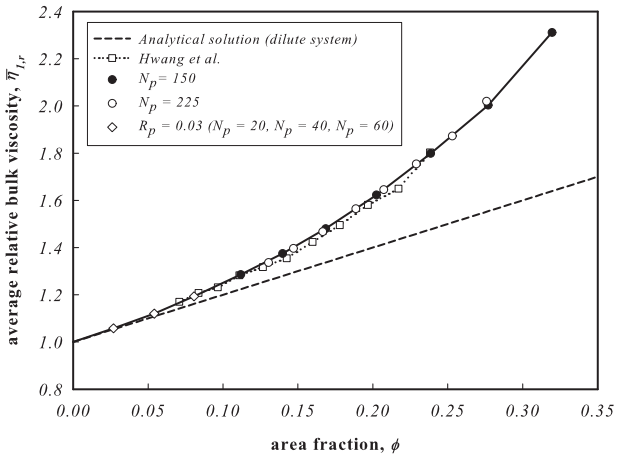

Figure 1.5: Relative bulk shear viscosity as a function of solid area fraction. Hwang and Hulsen results [24] are plotted as well (open squares).

To clarify Fig.(1.4) and 1.5, it has to be stressed that Einstein's classical result for a dilute suspension with circular disk particles is given by [26]:

$$\eta = \eta_0(1 + 2\phi) \tag{1.6}$$

as opposed to the factor 2.5 in three-dimensional flow.
In the dilute concentration limit, Fig. (1.4) and 1.5 show that Einstein's result is recovered. A clear deviation from Einstein's result appears at volume fraction of about 5%. For a volume concentration of 10% there is an increase in the viscosity of about 4% which means a second order factor in the Eq.(1.2) equal to 4.

1.1.2 Viscosity and viscoelastic properties for suspensions of spheres in non-Newtonian Media

If both theoretical and experimental studies for dilute and semi-dilute suspensions in Newtonian matrices are relatively scarce and somewhat contradictory, the situation is even worse for suspensions in viscoelastic fluids. The rheology of suspensions in non Newtonian media is, from a technological point of view, more important than its counterpart in Newtonian media. Important industrial applications are the processing of filled polymers, technical ceramic pastes and drilling muds for oil recovery. In particular, in the last few decades the emergence of filled plastics and composites as high-performance and cost effective materials has attracted considerable attention towards the rheology of polymer suspensions.
Typically, viscoelastic fluids exhibit a shear thinning viscosity, first and second normal stress differences, and memory effects. Suspending solid particles in these fluids leads to an even more complex flow behavior.
Theoretical analysis of suspensions in non-Newtonian media are only available for high volume fractions [27], where lubrication hydrodynamics dominate the interactions (and only for the viscosity function).
Koch *et al.* [28] provide the first reliable theoretical prediction for the stress in a three-dimensional suspension of spherical particles in a viscoelastic fluid. Unfortunately, the result is restricted to a homogeneous, dilute suspension (to order ϕ) and linear velocity field.
It's possible [29, 30, 31, 32], however, following Einstein's and Batchelor's approaches, to express the fluid viscoelastic properties in terms of a series expansion in the solid volume fraction, that is:

$$G^{''} = G_0^{''}\left(1 + a^{''}\phi + b^{''}\phi^2\right) \tag{1.7}$$

$$G' = G_0'\left(1 + a'\phi + b'\phi^2\right) \tag{1.8}$$

Palierne [33, 29] exactly calculated the first order coefficients $a^{'}$ and $a^{''}$ of Eq. (1.7)-(1.8) via direct hydrodynamic calculations. He was able to show that $a' = a^{''} = 2.5$.
There are no exact calculations for the second order coefficient. However, some empirical models have been proposed. Palierne [29], using a cell model approach for emulsions and blends, obtained the following prediction for the limiting case of non Brownian rigid spheres in a viscoelastic medium:

$$G^* = G_0^*\left(\frac{1 + 1.5\phi}{1 - \phi}\right) \tag{1.9}$$

where G^* is the complex modulus of the suspension and G_0^* that of the matrix fluid. When expanded into power series, Eq. (1.9) gives the first order result correctly whereas it predicts $b^{'} = b^{''} = 2.5$ for the quadratic coefficient.
Based on the work of Palierne [29], three different viscoelastic empirical models for suspensions at any concentration were developed using also the maximum packing volume fraction, ϕ_m as parameter. The model predictions for the viscoelastic properties are complex. When expanded in power series of the volume fraction, the three models yield:

$$G^* = G_0^* \left(1 + 2.5\phi + 4.4\phi^2\right) \tag{1.10}$$

$$G^* = G_0^* \left(1 + 2.5\phi + 7\phi^2\right) \tag{1.11}$$

$$G^* = G_0^* \left(1 + 2.5\phi + 5.1\phi^2\right) \tag{1.12}$$

where the value ϕ_m=0.64 has been used.
It should be noted that, like the purely Newtonian models for the viscosity, the viscoelastic models presented above show contradictory predictions for the second order coefficient. They share, however, the common feature that $G^{'}$ and $G^{''}$ have the same dependence upon the solid volume fraction.
Guth [31, 32] introduced a new quadratic term to explain the reinforcing effect of elastomers and found the following equations for the viscosity and modulus of Young E:

$$\eta = \eta_0 \left(1 + 2.5\phi + 14.1\phi^2\right) \tag{1.13}$$

$$E = E_0 \left(1 + 2.5\phi + 14.1\phi^2\right) \tag{1.14}$$

valid with concentrations up to 10% of spherical particles.
Guth's work deals with a "solid" suspending medium, it can however still useful to understand that changing the properties of the suspending medium could bring about a change (and, specifically, an increase) in the quadratic term of polynomial functions both for viscosity and viscoelastic moduli.
Elucidating a quantitative value for the quadratic term of the polynomial is one of the major objectives of this work.

Concerning the study of normal stress differences, the work by Koch *et al* [28] gives the first theoretical result on the first normal stress difference for a dilute (at order ϕ) suspension of spherical particles in a viscoelastic fluid. At

a given shear rate the first normal stress difference is increased by the same factor, 1+2.5ϕ, as the shear stress. The second normal stress difference, instead, is increased by a larger factor.
The first normal stress difference, N_1, has been experimentally characterized for various viscoelastic suspensions. The first normal stress difference is positive but usually decreases with filler amount when compared at constant shear stress [34, 35]. The second normal stress difference of viscoelastic suspensions has been recently investigated for solid fraction up to 0.25 [34]. In contrast to N_1, N_2 is negative with a magnitude that increases with volume fraction of the filler. The variations of the first and second normal stress differences are represented by power law functions of the imposed shear stress with an exponent that appears to depend on the specific matrix fluid used in preparing the suspensions and independent of the particle volume fraction [36].

Concerning numerical simulations, there are some interesting calculations on the relative shear viscosity as function of solid area fraction in two-dimensional flow for viscoelastic suspensions:

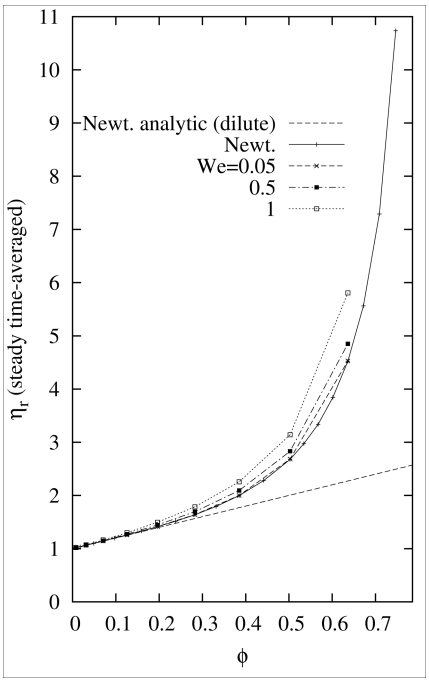

Figure 1.6: Relative shear viscosity as a function of solid area fraction for different Weissenberg numbers [37].

As shown in Fig.(1.6), the bulk shear viscosity increases with the Weissenberg number as well as with the solid area fraction. The Weissenberg number is a measure for the degree of viscoelastic behavior and is a dimensionless number, defined as the ratio of the first normal stress difference over the shear stress at a certain rate:

$$Wi = \frac{N_1}{\sigma} \tag{1.15}$$

The higher the Weissenberg number, the more elastic the fluid; the lower the Weissenberg number the more Newtonian the fluid. For small values of ϕ, the shear viscosity of the viscoelastic system converges to Einstein's analytical result for a dilute suspension in a Newtonian fluid (Fig.1.6) [26]. However, limited information about the comparable three-dimensional flow for one or two particles was presented.
To our knowledge, no simulations are performed in order to check the dependence of the viscoelastic moduli on volume fraction.

Many experimental results on the rheology of viscoelastic suspensions can be found in the literature.
In the case of filled polymeric systems, Kitano *et al* [38] proposed that the dynamic data may be reduced relative to the data of the matrix polymer at the same frequency, in the hope that the relative properties would be functions of the volume fractions of particulates and their properties but independent of the frequency. Kitano *et al* showed that these functions for composite systems filled with glass fibers are dependent on the volume fractions and the frequency.
Highgate and Whorlow [39] measured the steady shear viscosity of PMMA beads suspended in several fluids, for volume concentrations up to 10%. They focused, however, on the flow curve behavior and did not systematically study the zero-shear rate concentration dependence.
In general the literature focuses on high solid concentrations (typically above 10%)and this is beyond the scope of the present work.

Faulkner and Schmidt [40] studied polypropylenes filled with glass beads for concentrations up to about 30%. They found that the relative loss modulus grows with the square of volume fraction and the relative storage modulus (moduli of filled material normalized with respect to the moduli of pure polymer) grows linearly with volume fraction as follows.

$$G_n' = 1 + 1.8\phi \tag{1.16}$$

$$G_n'' = 1 + 2\phi + 3.3\phi^2 \tag{1.17}$$

The calculation of these polynomial functions was made at a fixed frequency and for a wide range of volume fractions up to about 30%. This means that the ratio $G_n^{''}/G_n^{'}$ should be a decreasing function of volume fraction. No discussion is provided for the choice of the frequency.
Poslinsky *et al.* [41] studied thermoplastics filled with glass beads for concentrations up to 60% and found that the relative loss modulus grows more than linearly with the filler volume fraction. See *et al.* [42] studied Separan polymer solutions filled with PE particles for concentrations up to 40% and found in contrast to Faulkner and Schimdt [40], that the relative storage and loss moduli follow similar scaling. They also reported an equation for the relative elastic modulus:

$$G_n' = [1 + \frac{\phi}{\phi_m}]^{-2} \tag{1.18}$$

where ϕ_m is the maximum packing volume fraction. Aral and Kalyon [43] studied dynamic properties, relaxation modulus and first normal stress difference for a polydimethylsiloxane matrix loaded with glass beads for concentrations up to 60%. They found that the increase of solid concentration increases the elasticity.
Walberer and McHugh [44] studied the frequency moduli of glass bead filled polydimethyl siloxanes (PDMS). They examined the influence of molecular weight on the ratio $G^{''}/G^{'}$ frequency and volume fraction and found that, as the molecular weight increases, the difference between $G^{''}/G^{'}$ of unfilled and filled materials at low frequencies is progressively smaller until it nearly disappears for the highest molecular weights.
Le Meins *et al* [45] reported experimental results on suspensions of monodisperse spheres dispersed in a liquid polymer for volume concentrations up to 31%. The measurements included steady-state viscosity, dynamic moduli and non linear stress relaxation. They found that in the hydrodynamic limit, particles increases in the same way both storage and loss moduli and similar to the Newtonian steady viscosity.

1.2 Hydrodynamics and interaction forces

1.2.1 Newtonian media

Rotation, interactions and migration of particles

The motion of isolated particles suspended in Newtonian fluids is well understood. Particles rotate with a rate equal to half the shear rate and translate with the local velocity of the fluid. An important conclusion is that the rotation speed of the particle is independent of a particle radius and the viscosity of the fluid.

When moving to higher volume fractions, instead, hydrodynamic interactions between particles become relevant. Other interparticle interaction (like Brownian motion, other colloidal forces) are only relevant for smaller particles.

Hydrodynamic forces are proportional to the viscosity of the medium.

Balance between Brownian and hydrodynamic forces can be expressed by a Peclet number defined as:

$$Pe = \frac{\eta_0 \dot{\gamma} R^3}{K_B T} \tag{1.19}$$

For large particles, hydrodynamic forces for shear flow dominate Brownian motion. Hence, neglecting particle inertia, the Pe number is the only relevant parameter.

At relatively low concentrations only binary hydrodynamic interactions are important.

Two-body interactions of rigid spheres in Newtonian fluid were investigated experimentally by Mason [46] and coworkers. The interaction is symmetric and reversible. The particles approach along curvilinear paths and, after contact, they rotate as rigid dumbbells until they separate.

The interaction between two spheres is well described by Joseph [47]. The nature of the particle particle interaction in a Newtonian fluid is displayed during the sedimentation process of spheres. In particular, the principal interactions between spheres can be described as *drafting, kissing and tumbling.*

The drafting of spheres in a Newtonian fluid is governed by the same mechanism by which a cyclist is aided by the low pressure in the wake of another. If a part of one sphere enters the wake of another sphere there will be a pressure difference to impel the second sphere all the way into the wake where it experiences a reduced pressure at its front and a less reduced pressure at the rear. This pressure difference impels the trailing sphere into kissing contact with the leading sphere.

Some information about the mobilities near contact can be obtained from lubrication theory. The mobility seems to go to zero at contact because of

the increased lubrication stresses required to expel the fluid.

Particle migration in concentrated suspensions of Newtonian suspending fluids has received considerable attention since it was first observed by Gadalamaria and Acrivos [48]. In Newtonian media migration may occur even in dilute systems, when inertia plays an important role [49, 50]. Migration has been studied in different works and with different flow geometries; in particular, spheres in a Couette geometry are observed to move towards the center line of the flow, while in Poiseuille flow particles will concentrate about midway between the wall and the center-line. With smaller spheres and slower flow, migration will become smaller because Brownian motion can keep the particles uniformly distributed.

1.2.2 Non-Newtonian media

Rotation and particle-particle interactions
The motion of isolated particles suspended in non-Newtonian fluids is far from being understood, even for non-Brownian, spherical particles at low concentrations, and under shear flow.
Mason and coworkers made some preliminary experimental studies [51, 52, 53] in the very low elasticity limit; no difference with the Newtonian case was found, but in the limit of slow flows, no differences are expected to occur. More recently, simulation results [23] and experimental studies [54, 55] have been published on particle rotation in viscoelastic media. As a general conclusion from these studies, one can qualitatively say that particles tend to slow down in viscoelastic fluids as compared to the Newtonian and second order fluid cases, and the higher the elasticity, the more the particles slow down. The only relevant parameter seems to be the Weissenberg number.

When moving from isolated spheres to non-dilute suspensions, particle-particle interactions become important and the complex nature of these interactions is dramatically displayed during the sedimentation process [56].
There are only few reports on two body interactions in non-Newtonian fluids [57, 58]. In general, two-body interactions of particles in viscoelastic and shear thinning fluids are not symmetric and irreversible. The irreversibility comes from the nonlinear constitutive properties of the suspending fluid. The paths of approach and recession of the particles are still curvilinear, but the angle of recession is smaller than the angle of approach, resulting in an increased separation between the particle centers.
Whereas in Newtonian fluids the interactions between sedimenting spheres

can be described as *drafting, kissing and tumbling*, in non-Newtonian fluid the mechanism changes in *drafting, kissing and chaining* [47]. Moreover, it seems that elasticity is a necessary (but not sufficient) condition for chaining to occur.

Particle alignment

Flow induced changes are expected in the microstructure of non-Newtonian suspensions due to the non symmetric nature of the hydrodynamic interactions.
The first study of flow induced structures in viscoelastic suspensions of non colloidal spheres is from Michele *et al* [59]. They subjected dilute and semi dilute suspensions (2% and 10%) of spherical particles (glass spheres) in highly viscoelastic suspending media (0.5% polyacrylamide in deionized water or poly-isobutylene solutions). Alignment and aggregation effects of spheres in viscoelastic media were presented in the case for oscillatory shear flows (see Fig. 1.7). The spheres line up and come into contact producing long string-like structures oriented in the flow direction.

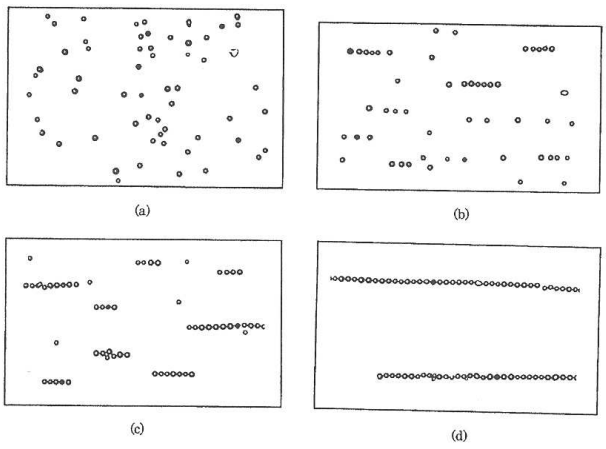

Figure 1.7: Alignment and aggregation effects in suspension of spheres in non Newtonian fluid (a) after loading (b)with few oscillations of the plate (c)after several oscillations (d)after long oscillatory times

In the work of Michele *et al* [59], the ratio of the first normal stress difference over the shear stress which is the Weissenberg number (eq. 1.15), seems to be the determining factor for the alignment process. In particular, string formation seems to occur only if the Weissenberg number exceeds the value of 10. Some aspects of the article are however not clear; e.g. the choice of a 100 micron gap with particles of 60-70 micron and the subsequent assumption that "the spheres don't touch the glass plates".
Giesekus [60, 61] showed that in a bidisperse suspension, the particles segregate and form separate strings according to the size (see Fig. 1.8).

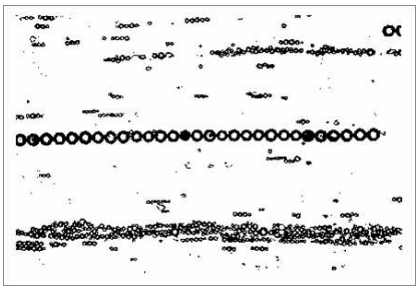

Figure 1.8: Alignment of a bidisperse suspension in a non-Newtonian liquids [61].

Giesekus also linked the physical origin of string formation to normal forces, thus rationalizing the existence of a critical value for the Weissenberg number.
Petit and Noetinger [62] observed particle clusters whose major axis was aligned in the direction of the applied strain for oscillatory flow.
Lyon *et al* [63] reported experimental results on the evolution of the particle microstructure for non colloidal particles suspended in viscoelastic fluids. In particular they performed monolayer experiments on concentrated suspensions (up to 40%) with monodisperse and bidisperse particle size distributions for both steady and oscillatory flows.
More recently, Scirocco *et al* [64] investigated the effect of the suspending fluid on flow-induced alignment by means of microscopy and light scattering on non colloidal suspensions. They found that the alignment was not governed only by the Weissenberg number. For example, no alignment could be observed in constant viscosity, highly elastic Boger fluids, and in slightly shear thinning Boger fluids the critical Weissenberg number was one order of magnitude larger than in polymer solutions. Moreover, Scirocco *et al* [64] studied the kinetics of string formation and the role of the presence of the walls. They found that the walls seem to hinder rather than promote the alignment and that the alignment can be considered as a bulk phenomenon.

Still recently, Kim *et al* [65] performed monolayer experiments on alignment and chaining of non-colloidal spherical particles (300 μm) in viscoelastic fluids (concentration 10%). As for Scirocco *et al* [64], particles form string-like structures even when the normal stress difference is less than the shear stress, proving the hypothesis of the existence of a critical value for the Weissenberg number for alignment wrong [59].
The mechanism for alignment and chaining is not clearly understood. The mechanism proposed by Jung *et al* [66] is the most convincing and can be explained as follows. Before the particles chain, they need to be aligned along the flow direction in a flowing suspension. First, alignment was explained for the case of two cylinders in a viscoelastic fluid. When the distance between two cylinders is large enough there is no hydrodynamic interactions and nothing happens. If the two cylinders are placed obliquely and are near to each other, there is an imbalance due to the fact that the fluid between the cylinders is hindered. In particular, as shown in Fig. (1.9), for the left cylinder the imbalance will push the left cylinder to the right. For the right cylinder the reverse is true.

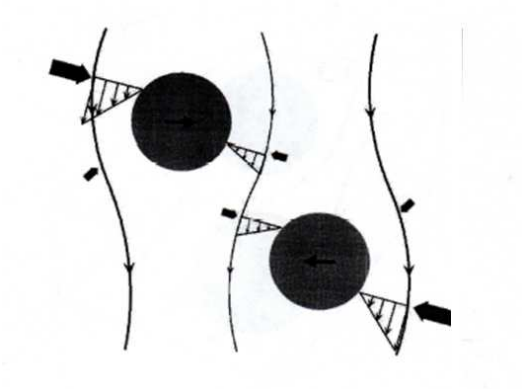

Figure 1.9: Imbalance of shear rate for two cylinders.

This lateral movement will result in the alignment of the two cylinders along the flow direction. In the case of a shear thinning fluid the flow between the two cylinders will become even weaker due to an increased viscosity caused by the reduced shear rate. This will result in an even smaller shear rates and in a very small value of the normal stress difference. Therefore, in a shear thinning fluid, particles will align more strongly. This mechanism agrees with the results of Joseph and Feng [56]. They showed that, in case of flow past two spherical particles of the same size along the line connecting their centers, the pressure pushes the particle along the line of centers towards each other. The alignment of two spheres seems to be very similar to that for two

cylinders.

Migration of particles

In addition to alignment and segregation, particle migration occurs in non-dilute systems. While the reason for migration in Newtonian fluids is inertia, there are several reasons for migration in viscoelastic suspensions and the situation becomes more complex. The term migration refers to lateral migration to the wall, promoted by normal stress differences and shear thinning. The role of normal stress differences on particle migration was elucidated in a theoretical calculation by Brunn [67] and Ho and Leal [68] and in simulations by Morris and Brady [69]. Migration of particles in non homogeneous shear flow occurs because of a spatially varying shear rate, entailing variations in the first normal stress difference. The variations in N_1 result in a force in the direction of decreasing shear rate.

Numerous papers concern the cases of Poiseuille and of Couette flows. Especially in the 60's Mason and coworkers worked on the microrheology of dispersions both in Newtonian and in non Newtonian media [52, 53]. Various particle shapes were considered. These papers provided a precise analysis, both theoretical and experimental, of the trajectories of two or several particles and their hydrodynamic interactions in shear flows.
Mason and Karnis [70] found that rigid particles (also not spherical) migrate in the direction of decreasing shear rate in Couette and Poiseuille flows for fully viscoelastic fluids. They suggested that this behavior was due to the normal stress effects of the medium, since migration didn't occur in Newtonian fluids.
During the same period, Highgate [71] did experiments in a cone plate geometry.
Circular rings of high particle concentration that moved outward were observed.
A series of experiments on particle migration in a plate-plate geometry were performed at the Carnegie-Mellon University [72, 73, 74] in Pennsylvania. The migration was observed to be in the direction of decreasing shear rate (inward). Later [72, 74, 75], lateral migration in a Boger fluid was also studied. In these fluids the existence of a critical radius in the plate-plate geometry was found; if the distance between the particle and the midpoint of the geometry was smaller than this critical radius, migration was directed toward the axis while there was outward migration when the particle was initially located at a distance further from the axis than the critical radius. Along with lateral migration observations were also done for vertical migra-

tion: the particles seemed to migrate towards a plane midway between the plates, regardless of the radial migration.
Jefri and Zahed [76] observed a chain structure in planar Poiseuille flow of viscoelastic suspensions of 10%. Experiments were done on three different media, a Newtonian fluid, a Boger fluid and a shear thinning elastic medium. They found that:

- In Newtonian suspensions the particles were uniformly distributed in both the transverse and axial directions.
- In the shear thinning fluid an immediate migration of particles toward the upper and lower walls took place. Alignment on the walls was also observed. The minimum concentration of particles was at the centre-line.
- In the constant viscosity elastic fluid (Boger fluid) the particles mostly stationed along the tube axis with very few particles near the upper and lower walls.

The results obtained in this study indicate two important points; first they confirm that migration is a consequence of normal stresses and second that migration is connected with alignment.
Tehrani [77] studied the migration of near spherical particles in pipe flow. In the case of a shear thinning fluid with measurable elasticity rapid migration to regions of lower shear was observed. The highly elastic fluids showed severe wall slip with no appreciable migration.
Feng and Joseph [78] studied the migration of spheres for torsional plate plate flows in viscoelastic fluids. They found that particles migrated outward and towards the midplane in the vertical direction.

Chapter 2

Suspension Rheology

2.1 Materials and Methods

2.1.1 Materials

Three different types of suspending fluids are used in this work. Polyisobutylene (PIB, Parapol 1300 from Exxon) is used as a Newtonian suspending fluid. Two Polydimethilsiloxanes (PDMS) and an atactic polypropylene are, instead, used as viscoelastic carrier fluids. Sylicon Fluid 60000 CST from Dow Corning (PDMS-A) has a zero shear viscosity at ambient temperature that nearly matches that of PIB. Rhodorsil 50000 CST from Caldic (PDMS-B) is characterized by a viscosity one order of magnitude larger. Both PIB and PDMS have a specific gravity of about 0.98 at 25°C.The atactic polypropylene (a-PP), instead, has a viscosity of one order larger than PDMS-B at T=120°C and a density of about $1 g/cm^3$ at 120°C. The zero shear viscosities of the suspending fluids is reported in Table 2.1.

Fluid	$\eta_0[Pas]$	**T** $[°C]$
PIB	64	25
PDMS-A	53	25
PDMS-B	460	25
a-PP	4000	120

Table 2.1: Zero shear viscosities of the suspending fluids

Polymethylmethacrylate (PMMA) spheres have been used as filler (Spheromers CA15, Microbeads) for the PIB and the two PDMS suspending media. They have a volume average particle diameter of about 14 μm and a density of 1.3 g/cm^3 at 20°C. The small density mismatch with the suspending media

did not give rise to sedimentation effects on the time scale of the experiments. Details of the bead size distribution, measured with a Mastersizer 2000 particle size analyzer, are shown in Fig. 2.1.

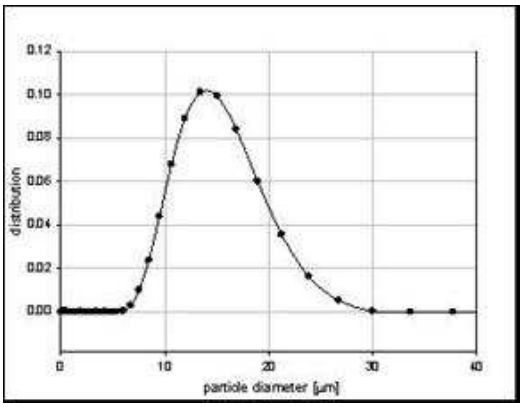

Figure 2.1: Particle size distribution for PMMA spheres.

As a dispersed phase for the a-PP based suspensions glass spheres have been used (Spheriglass 5000, Potters Industries Inc) with a volume average particle diameter of about 9 μm and a density of 2.5 g/cm^3 at ambient temperature. Glass beads are preferred in this case because the experiments are carried out at high temperatures. The high viscosity of the suspending medium is a guarantee to avoid sedimentation.
Details of the size distribution are shown in the Fig. 2.2.

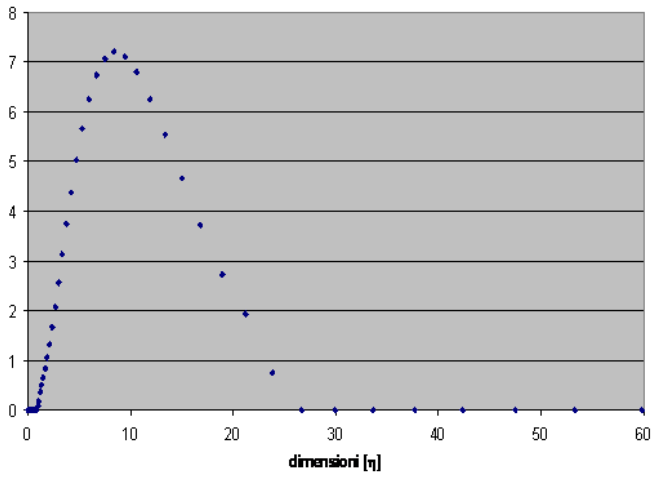

Figure 2.2: Particle size distribution for glass beads.

2.1.2 Preparation of the suspensions

Preparation of the suspensions was done with care as homogeneous dispersions of non agglomerated particles are difficult to obtain especially for low solid concentrations.
To avoid confusion, in this chapter each part contains two sections: in the first one, PIB and PDMS based suspensions will be discussed. For these fluids it is easier to control the volume fraction accurately and the dispersion has been hand made; in the second section B the a-PP based suspensions that requires the use of an extruder to mix particles with fluid will be discussed.

Preparation of suspensions - A

First, the PMMA beads were placed in a vacuum oven pump to remove moisture. The polymer and the beads were then weighted and hand mixed in a beaker for 10 minutes in the desired proportion. The air incorporated during mixing was removed by letting the sample rest for 12 hours. Homogeneous, and at least kinetically stable suspensions, could be obtained using this procedure. Optical microscopy confirmed that the particles were well dispersed and did not form aggregates over long times.
In addition, it was checked that in all cases the time scale associated with sedimentation was much larger than the time scale of both sample preparation and experiment. Indeed, Stokes' law indicates a maximum settling velocity (for the least viscous fluid) of about 2μm/hr. The time for PMMA particles to sediment in the gap of h tickness h= 10^{-3}m of the measurement device can be estimated by [18]:

$$t = \frac{0.45\eta_0 h}{(\rho_p - \rho_0)R^2 g} \tag{2.1}$$

in which η_0 is the viscosity of the pure matrix, R the particle radius and g the gravity constant. ρ_p and ρ_0 are respectively the densities of the suspended particles and the suspending medium. In all cases, the time scale associated with sedimentation (about 12 h for the lowest viscosity suspending medium and about 5 days for the more viscous of viscoelastic fluids) was much larger than the time scale of the experiments. In laminar shear flow the particle Reynolds number is defined as follows:

$$Re_p = \frac{\rho_0 R^2 \dot{\gamma}}{\eta_0} \tag{2.2}$$

As $Re_p \ll 1$, in all cases particle inertia can be neglected. The particle size was sufficiently large to be able to ignore Brownian forces ($Pe > 10^5$).

Preparation of suspensions - B

The high viscosity requires that the suspensions are prepared by mixing the polymer with the beads in an extruder (Haake) at $100°C$ for about half an hour. Mixing glass particles with the polymer matrix is not trivial and there is a significative error on the volume fraction.
In order to check the volume fraction of these suspensions, TGA (thermo-gravimetric-analysis) was used.

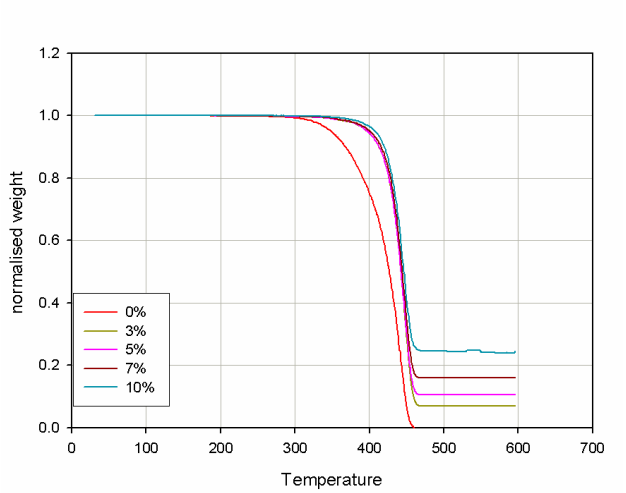

Figure 2.3: TGA for aPP suspensions.

In Fig. 2.3, the normalized weight is shown as function of temperature. Using these data, one can easily calculate the relative volume fraction and make a comparison with the expected volume fraction, as shown in Table 2.2.

Table 2.2: Comparison between required and effective volume fractions

from TGA	*required*
2.9	3
4.5	5
7.1	7
11.5	10

2.1.3 Rheological measurements

Rheological measurements - A

Rheological measurements were carried out in a controlled stress rheometer (Rheometric DSR 200) using a 25 mm parallel plate with gaps significantly larger than the particle size (typically 1 mm). Temperature ($30°C$ for the experiments under section A) was controlled by means of a Peltier element, which guaranteed a thermal stability within $0.1°C$.
Steady shear flow tests were done to measure the steady-state viscosity of the suspension. Linear oscillatory tests (upon verification of the linearity limit) were also performed to determine the viscoelastic frequency response.
The fluids and suspensions were loaded by carefully pouring a sample into the lower plate. The upper geometry was loaded until it touched the sample at the bottom plate. After contact, the upper geometry was lowered further while it was slowly rotated to promote homogeneous spreading of the sample. Any excess sample was scraped off around the geometry with a spatula. Then, the upper geometry was lowered further until the measurement gap was reached.
When particles are suspended in a carrier fluid, an increase of both viscosity and viscoelasticity with respect to the pure fluid is generally observed. When solid volume fractions below 10% are used, however, the increase in such properties is relatively low. As shown for example in fig. 2.8, maximum variations in G'' of about 30% over the whole frequency range are typically observed for the highest solid concentration (10%). For lower concentrations, the variations are obviously even lower.
This makes the issue of measurement reproducibility particularly important and as such all measurements were repeated three times for each volume fraction, each time using a fresh sample. Experimental conditions for each test were identical. They included the choice of the plate diameter and gap, but also the characteristic experimental times (such as the time between sample preparation and loading, delay time between sample loading and actual measurement,...). Measurements for the pure fluids were also repeated three times using fresh samples.

Rheological measurements - B

For the a-PP based suspensions, rheological measurements were obtained with a strain controlled rheometer (ARES, TA Instruments). Steady state and oscillatory flow experiments were performed on this device using a 2000 g/g cm transducer. Temperature was controlled using a convection oven.

Parallel plate geometries have been used (r=12.5 mm, gap$\sim$1 mm). Temperature was set at 120°C. A waiting time of about 20 minutes after loading was used to eliminate the effects of loading history. This waiting time was a compromise between the time of the sample to "anneal", the effects of loading and the limitations set by the thermal stability of the material.

2.2 Experimental results-A

2.2.1 Rheology of suspending fluids

The shear viscosity of suspending fluids is measured using stress sweeps in the low stress range. All fluids have a constant viscosity in this region. The values are reported in Table 2.1.
The linear viscoelastic response of the pure fluids is reported in Figs 2.4 2.5 and 2.6. For the Newtonian PIB the loss modulus, G'', shows a linear dependence upon frequency for the whole frequency range investigated (0.1-100 rad/s).
The elastic modulus, G', of the PIB shows an erratic behavior. In particular, the values for G' were negative at the lowest frequencies, indicating that the elastic modulus was non measurable, within the sensitivity limits of the rheometer. Moreover, the Newtonian plateau behavior is observed at all frequencies. Therefore, we consider PIB as a Newtonian fluid.
Both PDMS, on the contrary, show viscoelastic behavior. For them the Newtonian plateau extends up to a frequency of about 1 rad/s.
Below these frequencies the typical behavior of the terminal region is observed for the viscoelastic fluids, with G' and G'' characterized by the +2 and +1 slopes, respectively.

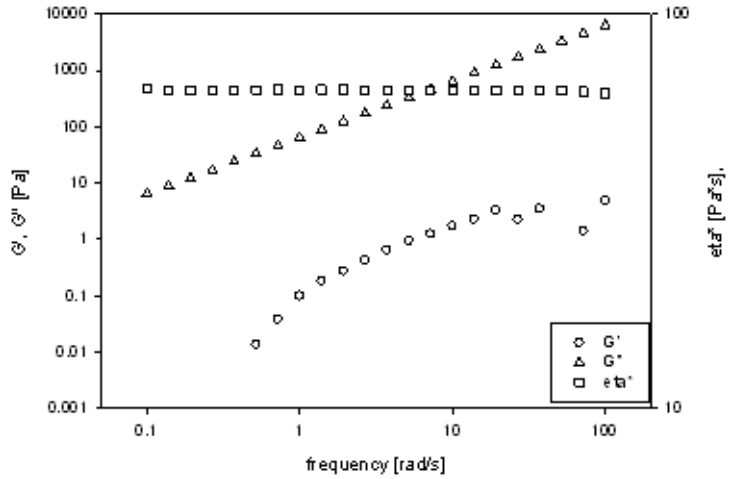

Figure 2.4: DFST for Newtonian Polyisobutylene, at 30°C.

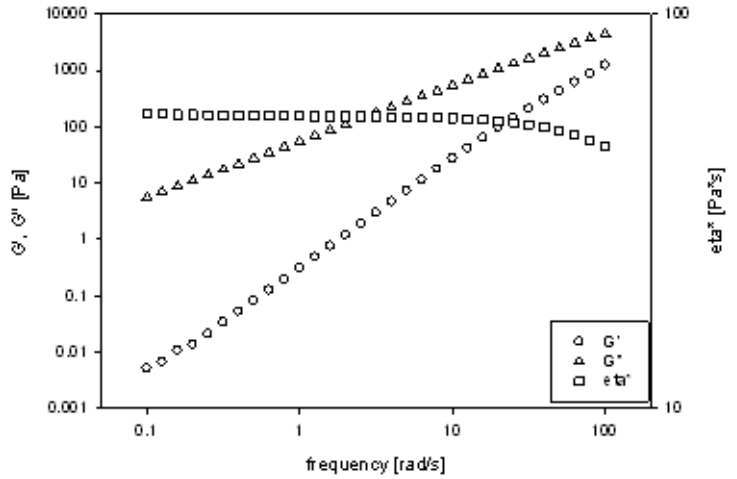

Figure 2.5: DFST for the Dow Silicone Fluid, at 30°C.

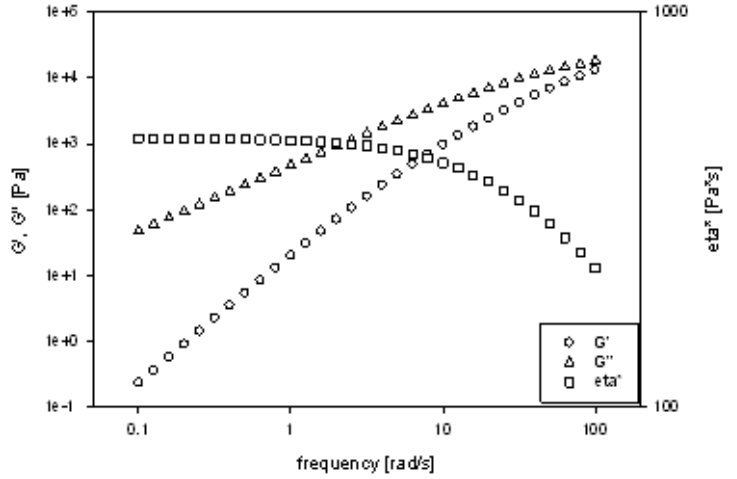

Figure 2.6: DFST for the Rhodorsil fluid, at 30°C.

2.2.2 Rheology of suspensions

As it is generally observed, the additive of particles increased both viscosity and viscoelastic moduli over those of the pure matrix. This increase can be attributed to the hydrodynamic disturbance of the flow, full caused by the presence of solid particles.
In Figs 2.7 and 2.8 typical experimental steady (2.7) and oscillatory (2.8) results are shown. The steady shear viscosities for all fluids follow the same

trend reported in Fig. 2.7, where the results for the PIB-based suspensions are shown. In particular, the viscosity increases with the filler concentration. At the same time, the Newtonian plateau at low shear rates is preserved.

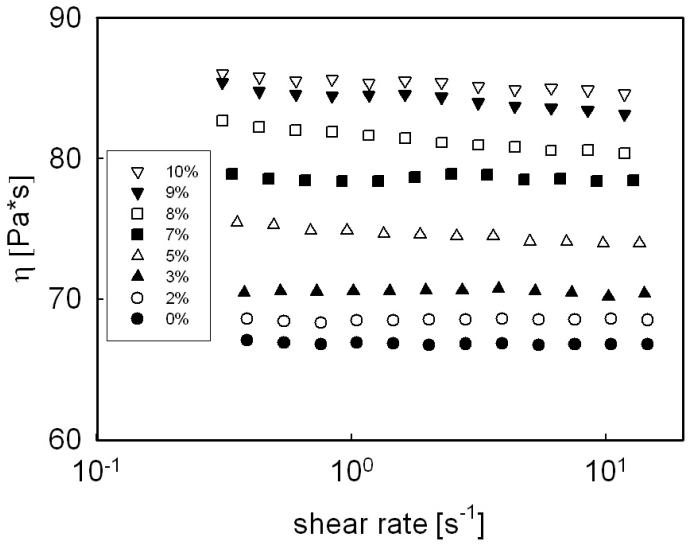

Figure 2.7: The steady shear viscosity of PIB based suspensions as function of shear rate at various filler concentrations.

Similarly (see fig. 2.8 where the results for the PDMS-B based suspensions are shown) the loss modulus increases with the concentration. Furthermore, the curves keep the same shape similar with that of the matrix fluid.
Fig. 2.8 (b) is a close-up of 2.8 (a) in the low frequency region (0.1-1 rad/s). All data fall on straight lines confirming the terminal behavior of G'' in this frequency region. It should be noted that the lines in fig. 2.8 (b) represent actual linear regressions of the experimental data. The excellent fit and the fact that all lines converge to the origin confirm the good quality and reliability of the measurements.

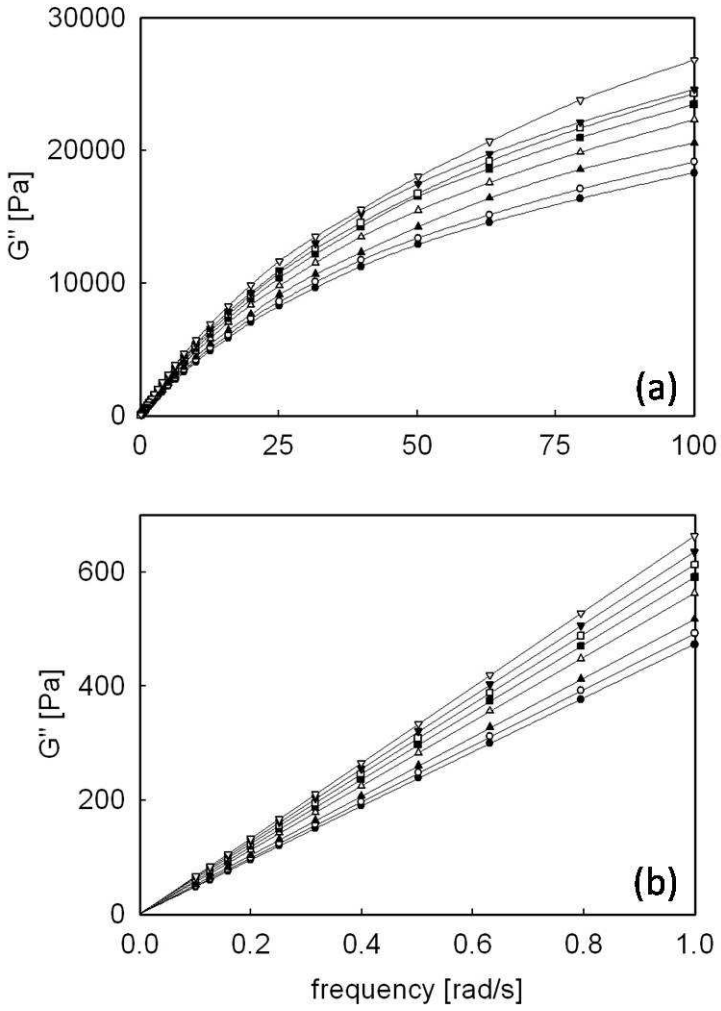

Figure 2.8: Loss modulus for PDMS-B based suspensions as function of frequency at various filler concentrations; (a) for all measured frequencies (lines are guides to the eye); (b) in the low frequency range: lines are linear regressions of the data). Symbols as in the Fig. 2.7.

The trends in Fig. 2.8 are similar in all fluids and indicate that in the low frequency range (0.1÷1rad/s) the relative increment in rheological properties only depends on the filler concentration. This implies that, in this range, the concentration dependence of the viscous properties can be robustly checked in terms of the normalized quantities:

$$\eta_n = \frac{\eta}{\eta_0} \tag{2.3}$$

$$G_n'' = \frac{G''}{G_0''} \tag{2.4}$$

in which η is the suspension's viscosity in the zero-shear plateau at a given stress and η_0 the viscosity of the pure suspending fluid at the same stress; conversely, in equation 2.4, G'' is the suspension's loss modulus at a given frequency and G_0'' the value of the pure matrix at the same frequency.

Dissipative response of suspensions

Figs 2.9-2.11 show the normalized viscosity and loss modulus of the suspensions as function of the volume fraction. The error bars in the figure summarize the statistical information related to the experimental data. Each point in the figure represents a large number of measurements. All measurements for all concentrations have been repeated on three fresh samples. Furthermore, all measurements taken in the above mentioned ranges of shear rate and frequency have been considered. As a consequence, about 45 (for viscosity) and 30 (for loss modulus) independent measurements are lumped into each data point and its corresponding error bar. In Figs. 2.9 the results for the PIB Newtonian suspensions are reported. Both the viscosity and the loss modulus increase non linearly with concentration. It is also confirmed that for relatively low concentrations (in this case, for ϕ<5%), the limiting viscosity law of Einstein is well obeyed. Furthermore, the loss modulus follows quantitatively the same behavior as the steady shear viscosity.

Figs 2.10 and 2.11 show the results for the two viscoelastic samples. The qualitative behavior does not differ from that already observed in Figs. 2.9 for the Newtonian suspensions. Quantitatively, however, the deviation from Einstein's viscosity law can be seen at lower concentrations with respect to the Newtonian case. The difference is further enhanced when the solid concentration increases. On the contrary, when comparing, η_n and G_n'' to each other, they show a similar behavior.

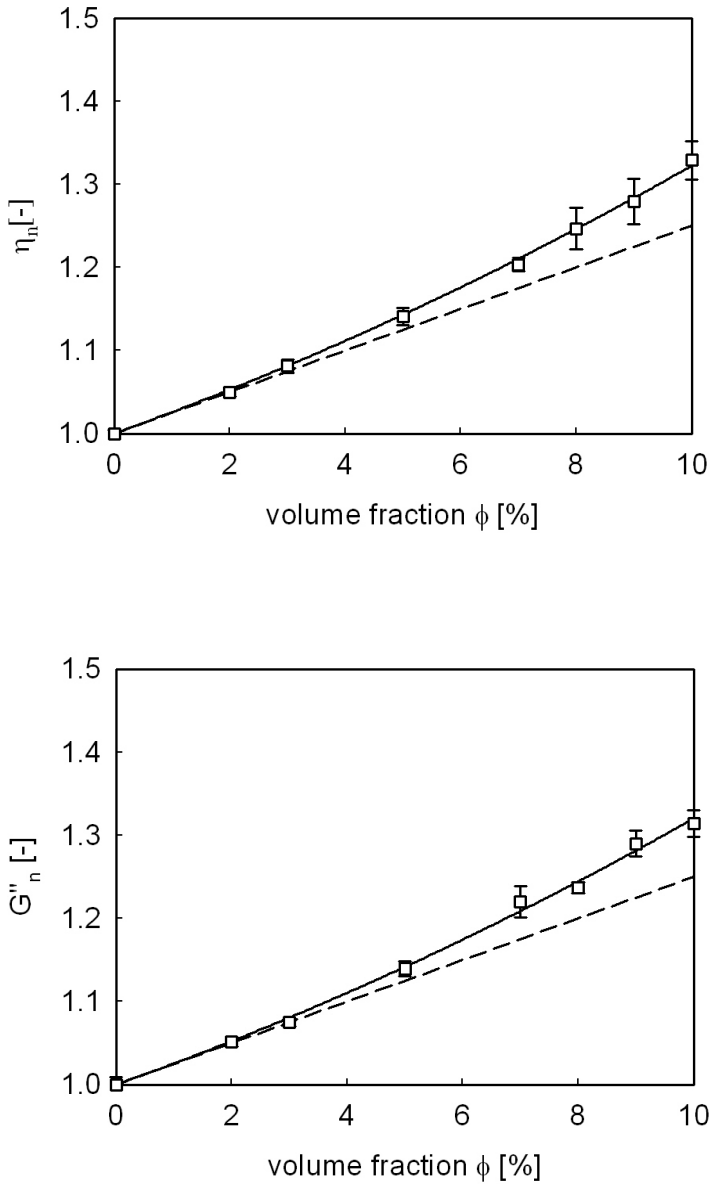

Figure 2.9: Normalized steady shear viscosity (top) and viscous modulus (bottom) for the PIB suspensions as function of volume fraction. Dashed line: Einstein's viscosity law; solid line: quadratic fit.

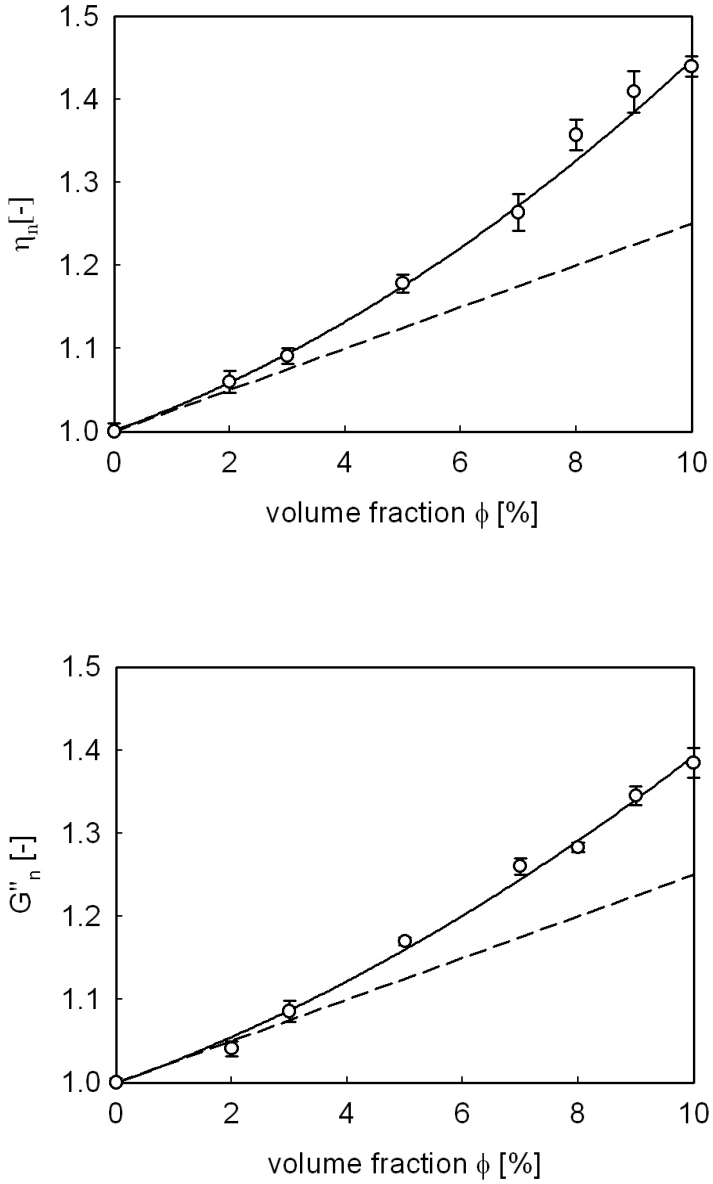

Figure 2.10: Normalized steady shear viscosity (top) and viscous modulus (bottom) for the PDMS-A suspensions as function of volume fraction. Dashed line: Einstein's prediction; solid line: quadratic fit.

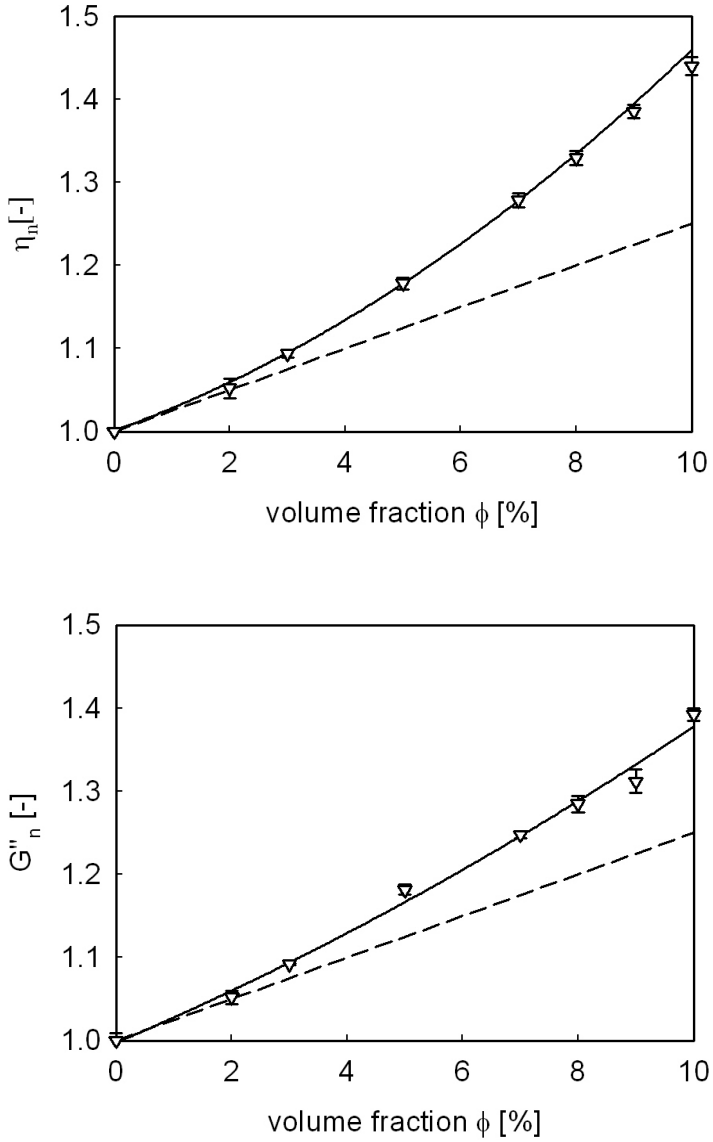

Figure 2.11: Normalized steady shear viscosity (top) and viscous modulus (bottom) for the PDMS-B suspensions as function of volume fraction. Dashed line: Einstein's prediction; solid line: quadratic fit.

Following the approach already outlined in the state of the art it is possible to express the normalized viscosity and both moduli in terms of second order polynomials in the volume fraction, according to Eqs. 1.2 and 1.7. The results of the linear regression fits are summarized in Table 2.3. It must be noted that two regression procedures have been applied. In the first one,

both first and second order coefficients are free parameters and calculated by the regression. In the second one, only the second order coefficients (b for the viscosity and b$''$ for the loss modulus) are calculated using the best fit procedure, the first order coefficients (a and a$''$) are kept fixed and equal to 2.5 as predicted by Einstein.

Table 2.3: Fit values of the polynomial coefficients of Eqs. 1.2 and 1.7. Standard deviations are also shown.

Fluid	Fit	a	b	a''	b''
PIB	a and b	2.34±0.07	8.82±0.82	2.47±0.17	7.39±0.85
	b only	2.5	7.00±0.18	2.5	6.99±0.18
PDMS-A	a and b	2.63±0.09	19.5±1.11	2.63±0.07	12.8±0.77
	b only	2.5	20.9±0.24	2.5	14.5±0.13
PDMS-B	a and b	2.67±0.04	17.9±0.51	2.80±0.05	11.1±0.58
	b only	2.5	19.7±0.15	2.5	14.3±0.13

The polynomial quadratic fits of the experimental data are shown as solid lines in the figures 2.9-2.11. The curves corresponding to the two fit procedures are virtually indistinguishable and in excellent agreement with the experimental data.
It can be noticed that the fit on the first order coefficient is quite robust and always in good agreement with Einstein's prediction for dilute suspensions. In fact, even when a and a$''$ are calculated through regression, the maximum deviation from the theoretical value of 2.5 is 11%. The 2.5 value is confirmed for both the Newtonian and viscoelastic suspensions, as theoretical demonstrated [29].
As far as the second order coefficients are concerned, Table 2.3 shows the substantial difference in behavior between the Newtonian and viscoelastic suspensions.

The b and b'' values for the Newtonian PIB fluid are in excellent quantitative agreement with Batchelor's exact calculations (which is valid for elongational viscosity). The results for the Newtonian PIB matrix are also in good quantitative agreement with the experimental results of Saunders [15], who measured the shear viscosity of sub-micron size polystyrene latex suspensions. The results are also consistent with those of Highgate and Whorlow [39] for PMMA beads (average diameter of 100 μm) suspended in a Newtonian synthetic oil. The results also agree with the simulations of particles in both Newtonian and non-Newtonian fluids by Hwang et al [23] and Hwang and Hulsen [24]. In these simulations of circular inertialess disks in New-

tonian fluids a deviation from the limiting linear behavior appear when the area fraction exceeds about 5%; moreover a deviation of about 4% is shown for an area fraction of about 10%, that is our highest solid concentration. This implies a second order factor equal to about 4 (not far from Bacthelor's result even if the simulation is 2D). Moreover, our results confirm that the bulk shear viscosity increases with elasticity [23] [24]. The second order polynomial coefficients of the two viscoelastic suspensions are, indeed, significantly larger.
Significantly larger values of the second order coefficient of the viscoelastic suspensions are obtained either leaving the first order coefficient as a free regression parameter or keeping it fixed to 2.5. The effect seems somewhat less pronounced for the loss modulus than for the viscosity. It can be concluded that, out of possible experimental error, the viscoelastic suspensions show larger deviations from linearity in the semidilute regime than those of the Newtonian suspensions. An overall comparison between the polynomial predictions and the experimental data is presented in Fig. 2.12. Here, data have been replotted in terms of $(\eta-\eta_0)/(\eta_0\phi)$ and $(G''-G_0'')/(G_0''\phi)$, as done for example by Saunders [15], in order to single out the deviations from linearity due to the quadratic term. The different behavior between Newtonian and viscoelastic suspensions can be again clearly appreciated, as well as the good quantitative agreement between the experimental data and the second order polynomial fit.

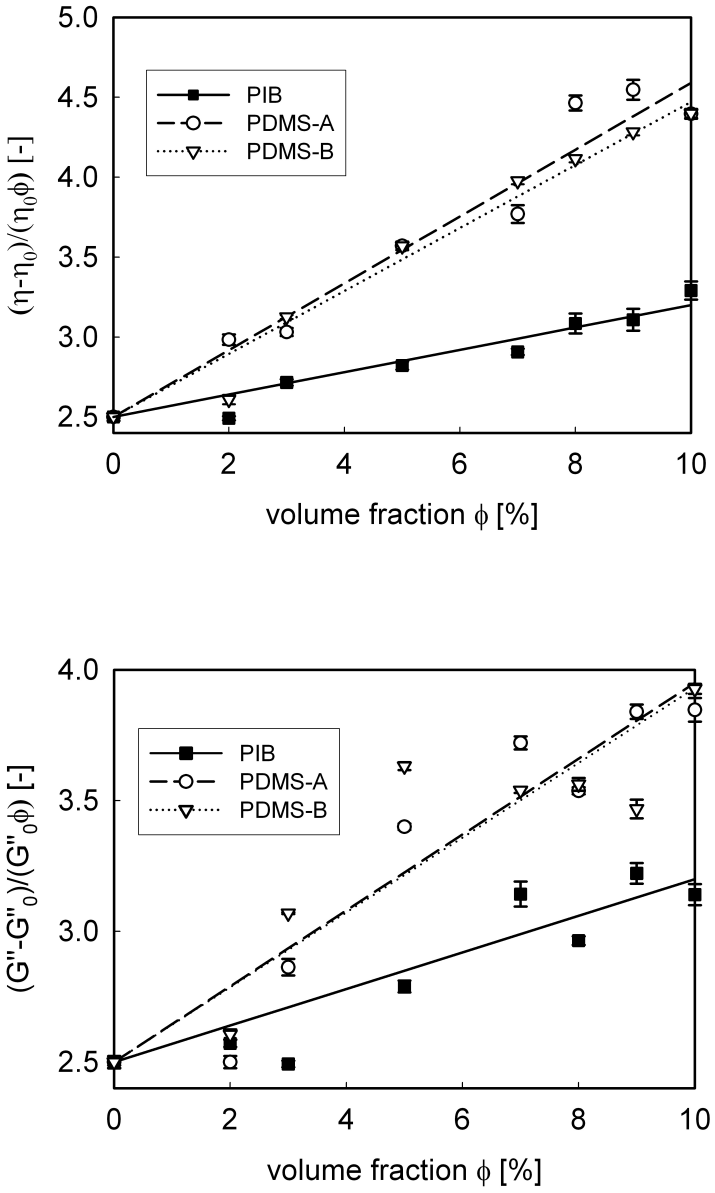

Figure 2.12: Intrinsic steady shear viscosity (top) and intrinsic loss modulus (bottom) for the three suspensions as function of volume fraction

Elastic behavior of suspensions

The elastic moduli for the two PDMS viscoelastic fluids are much smaller than the corresponding loss moduli, as can be seen in Figs 2.5 and 2.6. As a consequence, the experimental data for $G^{'}$ and their dependence upon solid concentration are much less reliable and reproducible than the corresponding results for $G^{''}$. Hence, the dependence of the storage modulus on volume fraction is not so easy to determine with the same accuracy in particular in the low frequency range. At low frequencies, indeed, the stress signal leads phase angle shift by $\pi/2$; the ratio of the viscous modulus to the elastic modulus (the tangent of the phase angle shift between stress and strain) turns into ∞ and the determination of storage modulus is more affected by errors. This is shown in Fig. 2.13. With a Dynamic Point Test, ten points are taken sequentially at a certain frequency, and this for different frequencies. The Fig. 2.13 shows that the experimental error which is the standard deviation on the mean value increases with decreasing frequency. Whereas the error on the loss modulus is quite the same in the whole frequency range, the error on the storage modulus increases with decreasing frequency with more than one order of magnitude.

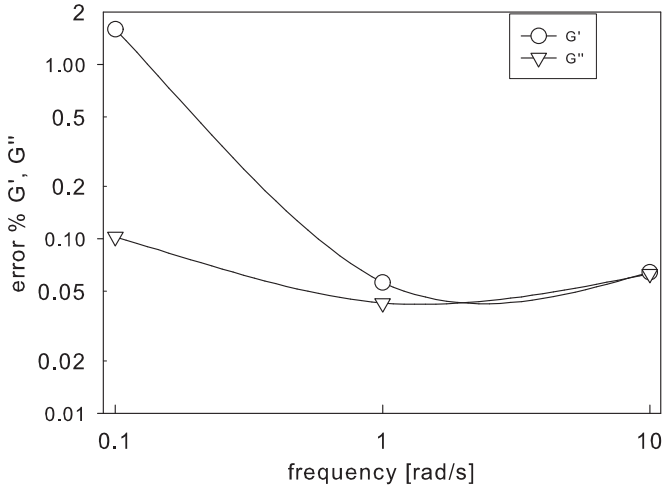

Figure 2.13: The percent error for three different frequencies (0.1, 1 and 10 rad/s), for both the calculation of $G^{'}(\circ)$ and $G^{''}(\bigtriangledown)$

To examine the influence of frequency and polymer molecular weight on the relative behavior of $G^{'}$ and $G^{''}$ as filler volume fraction is increased, we plot the ratio of $\frac{G^{''}}{G^{'}}$, versus frequency.

In fig. 2.14, trends of tanδ=G$''$/G$'$ is shown as function of frequency for our viscoelastic suspensions.

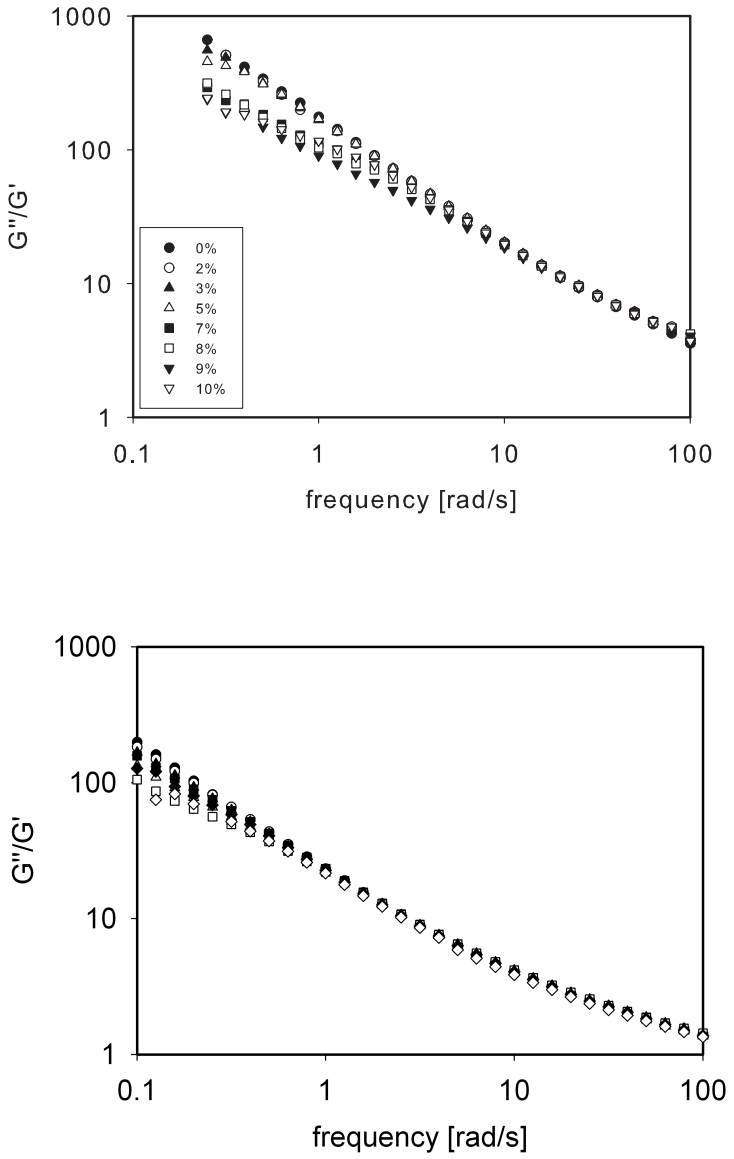

Figure 2.14: The ratio of the loss over the storage modulus versus frequency for filled and unfilled PDMS fluids.

As the molecular weight of the polymer increases, the magnitude of G''/G' decreases at all frequencies and shows a monotonic decrease with increasing frequency at all volume fractions.
As shown by Walberer and McHugh [44], the decrease in G''/G' at a given frequency indicates that material elasticity (as quantified by G') grows more rapidly with molecular weight than the material dissipative behavior (as quantified by G''). Furthermore, as frequency increases, the materials become more elastic and $\tan(\delta)$ decreases. Fig. 2.14 demonstrates that G''/G' for different molecular weight PDMS is identical for all filler amounts in the frequency range 1-100 rad/s. Moreover, with increasing the molecular weight PDMS systems, the presence of the filler seems to have no influence on the G''/G' ratio both in the high and low frequency range.
This behavior was explained by Walberer and McHugh [44] in terms of the relative effect of the filler on the Deborah number of the system: "The effect of an increase in filler amount is to increase the elasticity of the material and therefore increase the average relaxation time of the material. At high frequencies, the Deborah number is quite large and the unfilled material exhibits elastic dominated behavior. Therefore the addition of more elasticity to the material with the addition of filler has relatively little effect on the Deborah number. The behavior is quite different at low frequencies however."
Our results agree with those of Walberer and McHugh [44] with regards to the dependence on molecular weight. Our findings are however different from their generic trend in which the value of G''/G' is shown to decrease as filler amount is increased.
This is ensured by a random sequence of data of $\tan(\delta)$ in the low frequency range, with no obeying to a specific law in the volume fraction.
Moreover, if viscoelastic moduli are an increasing function of volume fraction, the constant value of $\tan(\delta)$ at each frequency suggests the possibility of an overlap of $G''(\phi)$ and $G'(\phi)$, in contrast with at least two works in literature [40, 42].
The possibility to use the same functions for the viscoelastic moduli suggests that:

- by adding particles G'' and G' shift only vertically.
- One can calculate a polynomial function of normalized values, useful for both G'' and G', that represents the dependence of viscoelastic moduli on frequency at least in the high frequency range.

In fig. 2.15, comparison between data in the low frequency range and data in the whole frequency range is shown. Fits in both cases have been made.

In the low frequency range, the result are those reported in tab 2.3; for the whole frequency range (100-0.1 rad/s), the regression line for the PDMS-B based suspensions is plotted in fig. 2.15. The difference between the fit in the low frequency range and in the whole frequency range is neglectable. The error bars are calculated as explained before.

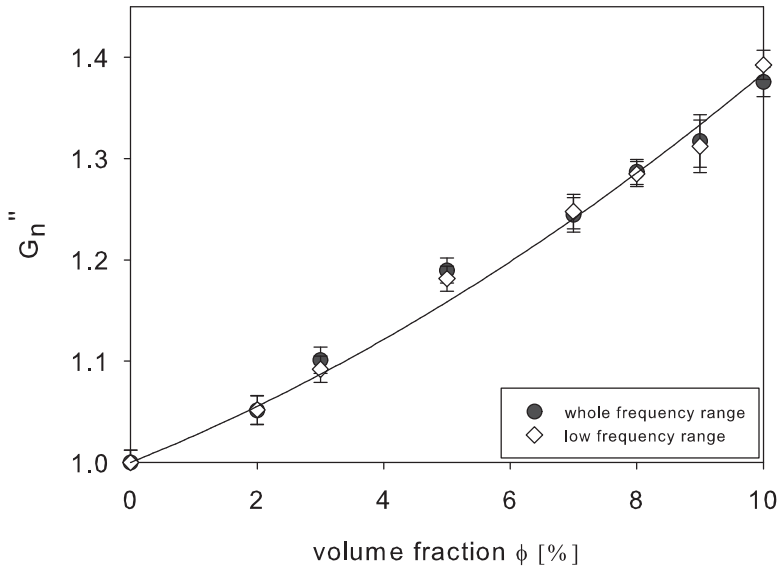

Figure 2.15: Comparison between normalized viscous modulus for PDMS based suspensions in the low frequency range and in the whole frequency range. Line is the best fit to data.

By quantitatively calculating both fits, one can conclude the following:

- The fit on the first order coefficient is quite robust and always in good agreement with Einstein's prediction for dilute suspensions.
- The curves corresponding to the two fit procedures are virtually indistinguishable and in excellent agreement with the experimental data, meaning that the curve of G'' shifts only vertically when particles are added to the pure suspending fluids.
- The possibility to use also the high frequency range suggests to fit data of storage modulus in the range [1-100] rad/s. In this way, it is possible to avoid the problem of sensitivity of the instrument and confirm the same scaling with volume fraction for storage and loss moduli.

Following the lines of the previous discussion, the normalized storage in the frequency range [1-100] rad/s is shown in Fig. 2.16. When going from the PDMS-A (top) to PDMS-B (bottom) based suspensions, the molecular weight of the suspending medium increases.

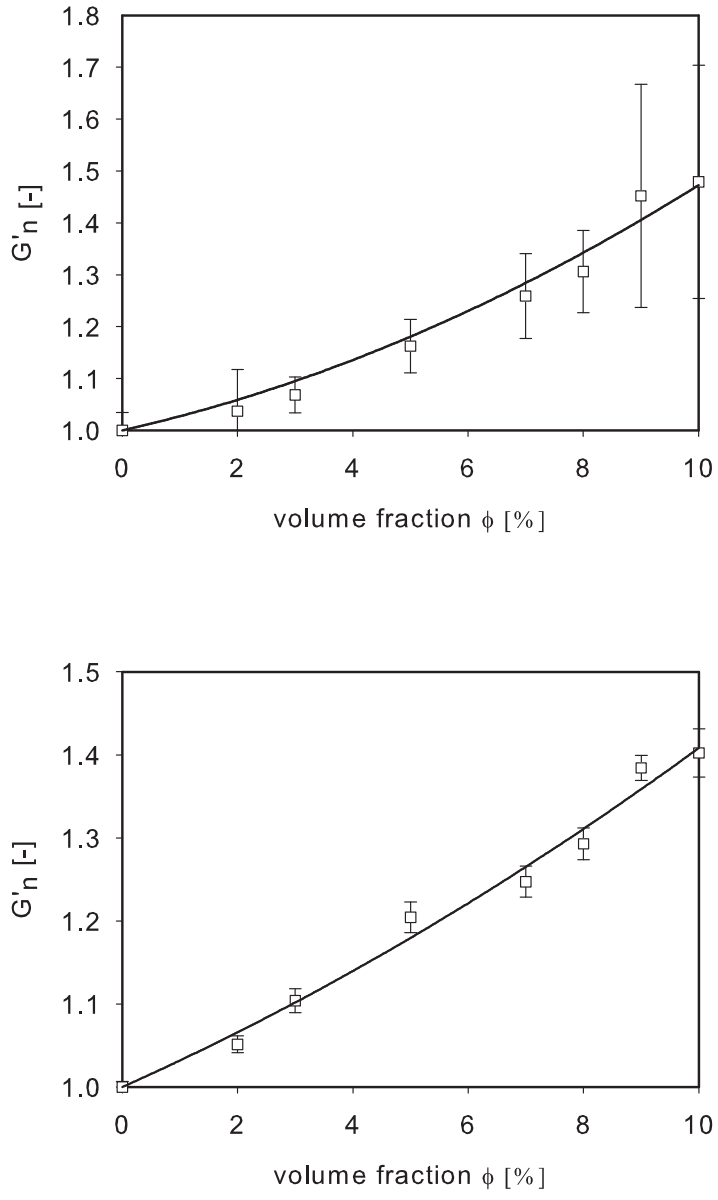

Figure 2.16: Relative storage modulus as function of volume fraction for the suspending media. The lines are best fits to the data.

As the molecular weight increases there is an increase in elasticity, consequently, the errors bars are smaller. Following the approach as before, the experimental results are fitted with second order polynomials eq. 1.7. The results of the linear regression's are summarized in table 2.4.

Table 2.4: Best fit values for b$'$ of eq. 1.8 and comparison with b'' of eq. 1.7 with the assumption that $a' = a'' = 2.5$. Standard deviations are also reported to appreciate the statistical error.

Fluid	b'	b''
PDMS-A	22.28±0.60	14.5±0.13
PDMS-B	16.76±0.55	14.3±0.13

Even if the values of b' are somewhat larger than those of b'', we believe that the polynomial function for G'' can be used for G', at least as a first approximation. The experimental error is, indeed, larger for the storage modulus than the loss modulus and in particular it decreases with increasing the molecular weight, as explained before.

Temperature dependence of the rheology of suspensions-A

The same tests of previous subsection have been performed at $70°C$. The temperature was chosen in order to have a significant decrease in viscosity. In particular, e.g. the viscous modulus at $70°C$ is only half as big as at $30°C$. In fig. 2.17 the viscous moduli of the PDMS-B based suspensions for both temperatures are plotted as a function of the volume fraction. No appreciable difference is detected with the fit of the data by changing the temperature. In table 2.5, results for the fitted parameters at $70°C$ are shown and compared with those at $30°C$.

Table 2.5: Parameters of eq. 1.7 and 1.8 for PDMS-B based suspensions at $30°C$ and $70°C$.

	b	b''
$30°C$	19.7±0.15	14.3±0.13
$70°C$	20.8±0.55	13.0±0.45

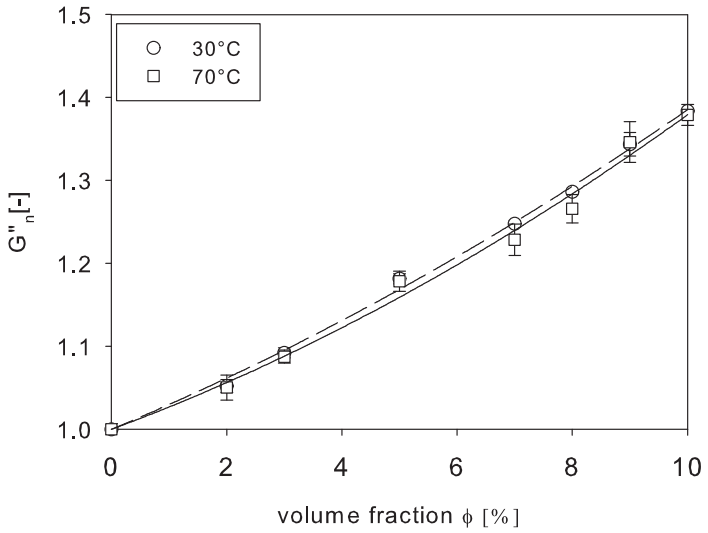

Figure 2.17: Comparison between data of viscous modulus for PDMS-B based suspensions at $70°C$ with those at $30°C$.

There is a good agreement between the fitting parameters at the two temperatures.
The temperature affects only the properties of the pure suspending media, meaning that, when considering normalized values, the dependence of the rheological properties on temperature is not relevant anymore.
Moreover, the data at $70°C$ have larger error bars. This can be explained with a worse sensitivity rheometer, due to the decreasing of measured torques, as well as to the decreasing of the viscosity, which means faster sedimentation of the particles (eq.4.1) and, as such, less stable suspensions.

2.3 Experimental results-B

2.3.1 Rheology of atactic-polypropylene

Fig. 2.18 shows the viscoelastic behavior for the a-PP suspending medium. The Newtonian plateau extends only until 0.1 rad/s. The terminal region is observed, with $G^{'}$ and $G^{''}$ characterized by the +1 and +2 slopes, respectively.

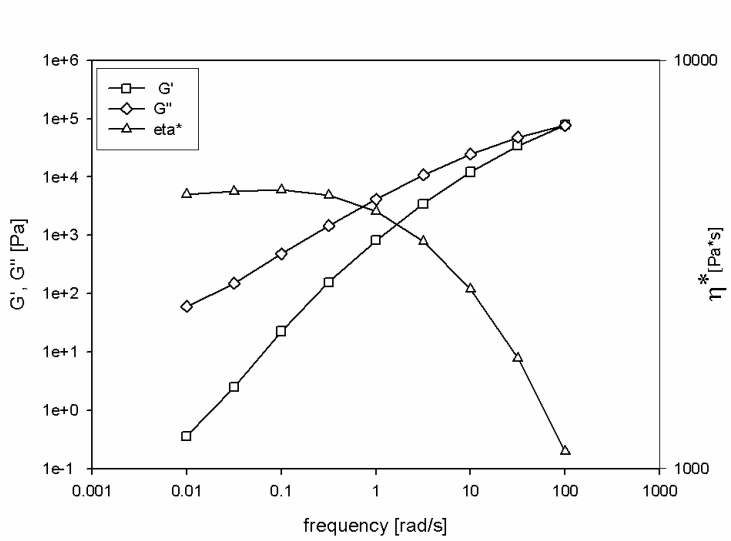

Figure 2.18: DFST for pure suspending atactic polypropylene

2.3.2 Rheology of the suspensions

As already said, the values of b that we found are different for Newtonian and viscoelastic suspending liquids. We attributed this to the elasticity of the suspending media.
However, the visco-elastic suspending fluids used before are both PDMS liquids and are chemically as well as rheologically not very different. That is why the coefficients $b^{''}$ (and b) are almost equal for these fluids.
The question is: how does $b^{''}$ (and b and $b^{'}$) depend on the rheological properties of the suspending matrix? In order to answer this question, the dependence of the viscoelastic moduli on volume fraction was studied for atactic polypropylene based suspensions, as shown in fig. 2.19.

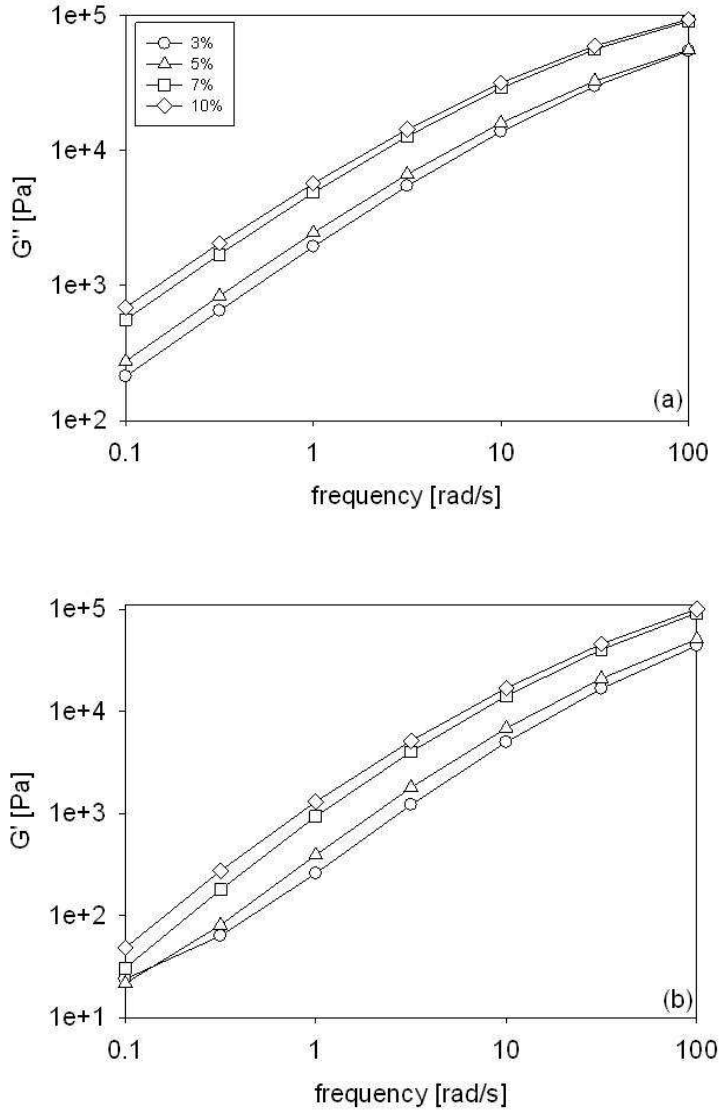

Figure 2.19: Loss (a) and storage (b) moduli for a-PP based suspensions as function of frequency at various filler concentrations.

As for the previous suspending media, G'' and G' increase with increasing volume fraction. It is impossible to perform experiments with the same accuracy as before, because on one hand the accuracy on volume fraction is lower (see section 2.1.2) and, on the other hand, the rheology tests are performed at high temperature, with more difficulties to check and control the test conditions.

The normalized viscous and storage moduli are plotted as function of the real volume fraction in figs. 2.20 and 2.21.

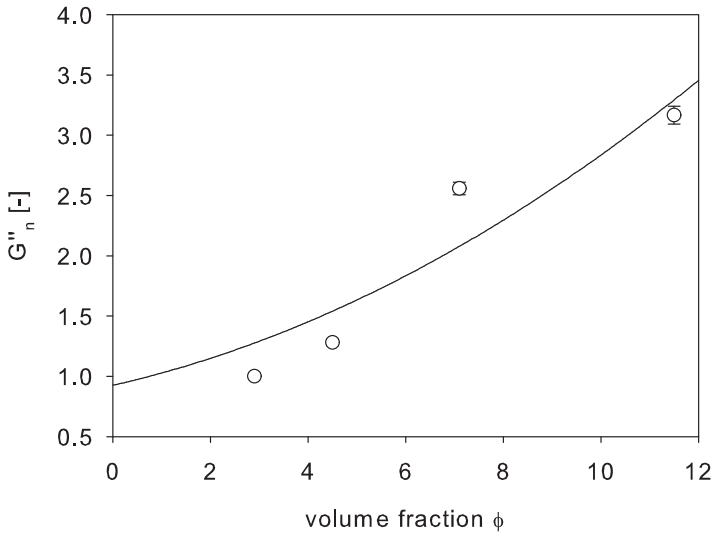

Figure 2.20: Normalized viscous modulus for the a-PP suspension as function of bead volume fraction.

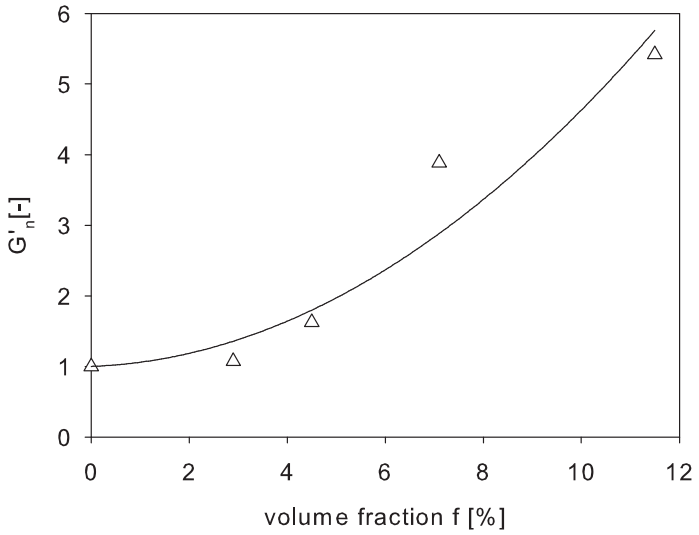

Figure 2.21: Normalized storage modulus for the a-PP suspension as function of bead volume fraction.

Even without the high accuracy, it can be easily seen that the increase in G'' and in G' with increasing volume fraction is larger for the atactic polypropylene based suspensions than PDMS based suspensions, and definitely larger than the Newtonian case.
For example, in fig. 2.20, at a frequency of 1 rad/s, the increase in G$''$ when volume fraction changes from 3% to 10% is about 300%, in comparison to about 30% for the same volume fractions for the PDMS suspensions.
The normalized complex viscosity seems to have the same dependence of the viscous modulus.
This behavior can be explained again with the higher elasticity of the suspending medium and, perhaps, with a different chemical structure of the fluid.
The elastic modulus seems to have a stronger dependence on volume fraction than the viscous modulus as shown in fig. 2.21 in contrast with results obtained for PDMS based suspensions.
Some experiments on the first normal stresses difference (N_1) have been performed on the a-PP based suspensions. Results for N_1 as a function of shear rate are shown in fig. 2.22 for different volume fractions.

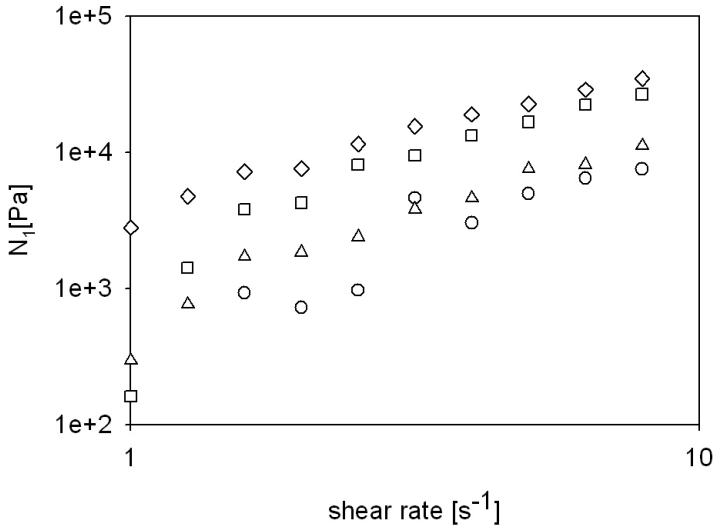

Figure 2.22: N_1 as function of shear rates for different volume fractions. Symbols as in Fig. 2.20.

In agreement with previous literature [34] [79] [80] [36] [28] [23], using viscoelastic suspending fluids at moderate volume fractions, we find that the first normal stress difference increases with increasing solid content, when

compared at a certain fixed shear rate.
In fig. 2.23, the normalized value of the first normal stress difference (that is the ratio between the first normal stress difference of the suspension and that of the pure suspending fluid) is plotted as function of the volume fraction.

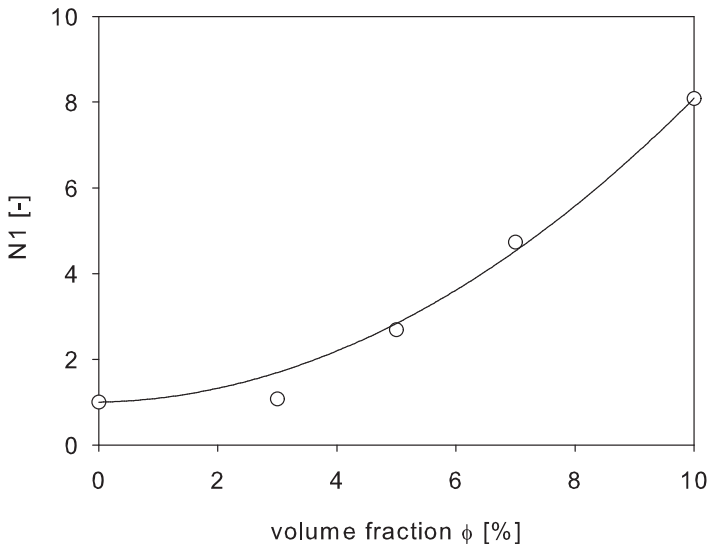

Figure 2.23: Normalized value of N_1 as function of volume fraction.

One can see that also the first normal stress difference can be expressed as a polynomial function of the volume fraction.
When comparing fig. 2.23 with figs. 2.20 and 2.21, it is clear that N_1 for the a-PP suspensions has a stronger dependence on volume fraction than the viscoelastic moduli. This means that, since the first order coefficient in the polynomial equation is equal for both properties [28] [29], the second order coefficient is larger for the first normal stress difference than for the viscous modulus.

2.4 Conclusions

In this chapter the rheology of suspensions of particles in different suspending media has been studied. The influence of the medium on the rheological response of the suspensions has been investigated in the dilute and semi-dilute regions.
To our knowledge, this is the first experimental study comparing the rheological behavior of Newtonian and viscoelastic suspensions in the semidilute concentration range as function of volume fraction. In this range, particle/particle hydrodynamic interactions are relevant and determine a substantial deviation from the limiting dilute behavior.
The experimental measurements show that in the semi-dilute regime the dependence of the linear viscoelastic properties of the suspensions can be well described with a quadratic polynomial.
For Newtonian suspensions, the experimental data agree quantitatively well with the analytical hydrodynamic calculations performed by Batchelor [5]. However, Batchelor's results are for irrotational flows. The limiting behavior in the dilute regime predicted by the exact equation of Einstein [2] for Newtonian fluids and Palierne [29] for viscoelastic fluids is well obeyed by the investigated suspensions.
In the semidilute regime, viscoelastic suspensions display substantial deviations with respect to the Newtonian case. In particular, the deviation from linearity of the dissipative properties in the semi-dilute regime is found to be larger when compared to that of the Newtonian-based suspensions. This was verified at two different temperatures, $30°C$ and $70°C$.
For the viscoelastic fluids, the dependence on volume fraction seems to be valid for the whole frequency range: adding particles only shifts the curves vertically.
Furthermore, $tan(\delta)$ confirms that the storage and loss moduli have the same dependence on volume fraction.
Finally, the study of the first normal stress difference shows that the dependence on volume fraction is stronger (a larger deviation from linearity) than the dependence of the viscous modulus.
The most important result of this chapter is that the nature of the suspending fluid is responsible for changes in the rheological response of suspensions, in shear and oscillatory tests, at second order in ϕ.
Moreover, in order to compare with existing simulations on viscoelastic suspensions, we calculated the Weissenberg number as the product of the shear rate and the longest relaxation time [81]. Herein, the longest relaxation time was considered the inverse of the frequency at which the viscous modulus deviates from its terminal region behavior (slope 2).

The longest relaxation time for the different viscoelastic suspending media, calculated with this method, are shown in tab. 2.6.

Table 2.6: Longest relaxation time λ_{max} for the suspending media.

Fluid	λ_{max}
PDMS-A	0.03
PDMS-B	0.2
a-PP	3.00

In fig. 2.24 the intrinsic viscous modulus is shown as function of the longest relaxation time, for different volume fractions.

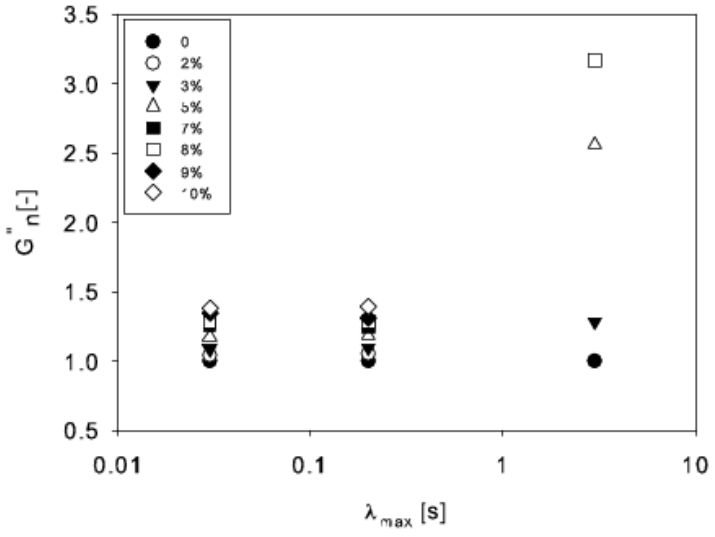

Figure 2.24: Normalized viscous modulus as function of the longest relaxation time λ_{max} for the three suspending media, for different volume fractions.

The increase of the viscous modulus at a certain volume fraction is much higher for the suspending media with a larger relaxation time (or Weissenberg number). This result is in agreement with simulations [23].
At this moment, there is no definite explanation for the observed difference between Newtonian and viscoelastic suspensions. Certainly, this difference originates from the complex, time dependent flow in the viscoelastic fluid between two nearby particles. Efforts are needed to elucidate the hydrodynamic interactions between two particles and their consequent effect on the rheological response of viscoelastic suspensions.

Chapter 3

Simulation of circular disks in a Newtonian fluid under 2-D oscillatory flow

Computational fluid dynamics is currently very popular because information implicit in the equations of fluid motion can in principle be extracted without approximation using numerical simulations. The potential for solid-liquid flows is very big and has yet to be fully realized.
In the last two decades the rheological behavior of suspensions has been intensively investigated using computer simulations. However, literature focuses mainly on flow simulations of Brownian (colloidal) systems [82], and not so much on non-Brownian suspensions.
For simulations of fluid-solid systems at finite Reynolds number, quite same numerical methods have been developed in recent years. One of the most used methods is the ALE (Arbitrary Lagrangian Eulerian) particle mover. The ALE particle mover uses a technique based on a combined formulation of the fluid and particle momentum equations, together with an arbitrary LagrangianEulerian (ALE) moving, unstructured, finite-element mesh technique to deal with the movement of the particles. It was developed by Hu and co-workers [83], [84]. The method has been used to solve particle motions under flow in both Newtonian and viscoelastic fluids in two and three dimensions flow geometries. It can describe particles of different size, shape, and material.
Recently, Hwang *et al* [23] [24] simulated the motion of circular inertialess disks under flow particles in Newtonian and viscoelastic fluid. The bulk shear and elongational viscosity as function of solid area fraction and Weissenberg number for a wide range of area fractions were calculated. For small solid area fractions, the shear viscosity was found to converge to Einstein's ana-

lytical result for a dilute suspension of circular disks [26] [85]. For larger area fractions, both the elongational and shear viscosity show the same quantitative deviation from the dilute case. Furthermore, the viscosity was found to be an increasing function of the Weissenberg number, implying a shear thickening behavior of the suspension.
As far as we know, no simulations have been done to investigate the dependence of the viscoelastic moduli on volume fraction.
In this section, we describe simulation for non Brownian hard particle suspensions formulated with a Newtonian fluid under *oscillatory shear flow* in a well defined domain. Concentrating on circular disks in two-dimensional flows of a Newtonian fluid, we will demonstrate the feasibility of our scheme for the single sphere as well as the two particle problem.
This chapter is organized as follows: first, the governing equations and the boundary conditions are stated. Next, the assumptions are discussed. Finally, the two different example problems will be discussed along with the evaluation of bulk rheological properties.

3.1 Modeling aspects

Consider an incompressible fluid occupying a bounded region Ω with boundaries Γ_i, i=1,...4. There are one or two particles freely moving in the fluid.
We are interested in the motion of both the fluid and the individual solid particles and, in particular, the dependence of viscosity on volume fraction.
The model consists of a fluid part, solved with the Navier-Stokes equations in the flow channel, and a structural mechanics part, which it is solved across the particle. Moving Mesh (ALE) application mode makes sure that the flow domain is deformed along with the particle. Transient effects are taken into account in both fluid and structure.
The particles move because of the imposed flow and hydrodynamic interactions: their rigid-body motion is completely defined by their translational velocity, U_i and their angular velocity, $w_i = w_i\underline{k}$, where $\underline{k}$ is the unit vector in the normal direction to the xy plane.
We restricted the calculations to 2-D systems composed of circular disks in a Newtonian fluid. However, the present scheme can be probably extended to viscoelastic fluids without too much further effort [23]. However, extending to three-dimensional flow seems more difficult and only limited information about this is available.
The motion of the fluid satisfies the conservation of mass equation:

$$\nabla \cdot u = 0 \tag{3.1}$$

and the conservation of momentum equation:

$$\rho\frac{\partial u}{\partial t} - \nabla\sigma + \rho(u \cdot \nabla)u = \rho f \tag{3.2}$$

where u is the velocity vector, ρ the density of the fluid, f the body force and σ the stress tensor.
For a Newtonian fluid the stress tensor is given by the simple constitutive equation:

$$\sigma = -pI + \eta_0[\nabla u + (\nabla u)^T] \tag{3.3}$$

where I is the unit diagonal matrix, p the pressure and η_0 the viscosity of the fluid. We assume that gravitation nor other body forces are working on the fluid, so $f = 0$.
The fluid boundary condition are given by:

$$u = U_i + w_i \times (x - X_i) \tag{3.4}$$

$$u = \gamma_0 \omega y cos(\omega t) \quad v = 0 \tag{3.5}$$

Eq. 3.4 describes the rigid-body condition, x are the coordinates of the points on the particle surface, X_i=(X_i, Y_i) are the coordinates of the particle center and $U_i = (U_i, V_i)$ are the components of the translational velocity. Eq. 3.5 describes the oscillatory flow boundary condition, with ω the frequency, γ_0 the deformation and y the distance from the center of the square. The Cartesian x and y coordinates are selected such that the origin is at the center of the domain, so everything is oscillating.
In absence of inertia, no initial conditions are needed for the velocity field of the fluid and the motion of particles.
Usually the particle is considered as a rigid ring, filled with the same fluid as the fluid domain so that the rigid-body condition is imposed on the particle boundary only. This rigid-ring description is possible when inertia is negligible and is particularly useful because it saves memory.
We decided to consider the particle as a structural mechanics part [86], but, as inertia is neglected, the evaluation of the stress can be carried out with the same procedure as in the rigid-ring description.
The motion of solid objects satisfies Newton's law, in which the force that makes the particles move is that imposed by the fluid. The movement of particles is given by the following kinematic equations:

$$\frac{dX_i}{dt} = U_i \tag{3.6}$$

$$\frac{d\Theta_i}{dt} = w_i \tag{3.7}$$

(with the corresponding initial values) where X_i=(X_i, Y_i) are the coordinates of the particle center and Θ_i is the angular velocity.
To determine the unknown rigid motions of the particles, one needs to balance the drag forces and torques on the particle boundaries. Neglecting inertia and other external forces and torques, the particles are force-free and torque-free and the balance equations can be written as:

$$F_i = \int_{Ap_i} \sigma \cdot n ds = 0 \tag{3.8}$$

$$T_i = \int_{Ap_i} (x - X_i) \times \sigma n ds = 0 \tag{3.9}$$

In these equations, F_i and T_i are the total force and torque on the particle boundaries and n is the outward directed unit normal vector on each part of the boundary Ap_i of the particle.

The model geometry consists of a square box in which a Newtonian fluid is forced to move in an oscillatory way and in which one or at maximum two particles are dispersed.
The non-dimensional parameters governing this flow problem are:

- the relative channel width and length normalized using the particle size L/D, which have to be large enough to avoid wall effects (minimum 10 for 0.25% calculation error).
- the solid area fraction $\phi_a = \frac{N\pi D^2}{4L^2}$ with N the number of particles present in the fluid 1 or 2.

In our system the box in which the fluid and particles are forced to move is square (L in fig. 3.1). The fluid is assumed to be Newtonian, having a density equal to zero and a viscosity of η_0=1 Pa·s.
The particles are assumed to be rigid with a density equal to zero. The particle size (D in fig. 3.1) is changed in order to have L/D ratios from 10.4 to 26.

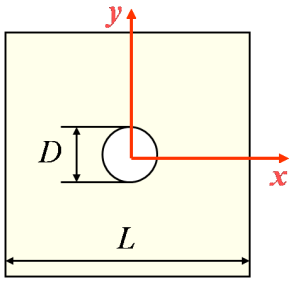

Figure 3.1: The geometry used in the simulation technique.

3.2 Bulk stress

As previously discussed, we are interested in the rheological properties of dilute and semi-dilute suspensions in oscillatory flow, such as the viscous modulus.
The flow and stress fields obtained from the equations just presented are local. Local values of pressure and velocity are directly related to the stress distribution around the particles and provide information about the hydrodynamic interaction between the particles.
However, it is also important to evaluate global properties (bulk properties) to be able to make predictions for the global behavior of the material.
To be able to evaluate global properties, we have to calculate the bulk stress from the local quantities. The bulk stress, which is the average stress over the domain, can be expressed, for a volume V, as the sum of the fluid contribution and the particle contribution. We will consider Batchelor's formula [87]. For 2D, the bulk stress tensor can be calculated as follows:

$$< \sigma >=< \sigma >_f + < \sigma >_p = \frac{1}{A}\int_{A_f} \sigma dA + \frac{1}{A}\int_{A_p} \sigma dA \tag{3.10}$$

where the symbol <> means an average over an area A, A_f and A_p are respectively the area occupied by the fluid and the particles.
For a Newtonian fluid, the fluid contribution is given by Eq. 3.3 and the shear stress can be easily calculated. Concerning the particle contribution it can be shown that the integral over the total particle area for the stress can be written as follows:

$$< \sigma >_p = (\sigma_{xx} n_x + \sigma_{xy} n_y) n_y \frac{D}{2} \tag{3.11}$$

n being the outward directed unit normal vector on the particle boundary (in the x or in the y direction) and σ_{xx} and σ_{xy} components of the stress in the designated directions.

3.3 The single particle problem

The first test problem is a single particle of diameter D suspended freely at the center of the described domain. As mentioned earlier, the reference velocity is zero at the center of the domain. As such the upper boundary translates with a velocity $L/2\dot{\gamma}$ and the lower one translates at the velocity $-L/2\dot{\gamma}$, $\dot{\gamma}$ being the externally imposed shear rate. As such the particle will not translate relative to the domain but rotates with an angular velocity w(t).
The externally imposed oscillatory deformation is given by:

$$\gamma = \gamma_0 \omega cos(\omega t) \tag{3.12}$$

with γ_0 being the amplitude of deformation (set equal to 10%) and ω the oscillation frequency.
By changing the L/D ratios from 10.4 to 26, the maximum available volume fraction ranges from 0.1% to 0.8%.
The problem of the dynamics of a single sphere immersed in a linear flow field imposed at infinity, in the absence of both fluid and particle inertia, was first addressed by Einstein [88] for the case of a Newtonian suspending medium. Under shear flow, the sphere translates in the flow direction, while rotating around the vorticity axis. Einstein demonstrated that, with no-slip boundary conditions at the particle surface, the rotation rate of the sphere is $w = \dot{\gamma}/2$. This simple result stems from a torque balance at the sphere surface, whereby the torque on the sphere is only due to the flow field (the so called torque-free condition presented before).
To check our model, we measured the rotation rate of one particle in the case L/D=26 (see fig. 3.1) changing the frequency from 0.1 to 100 rad/s. Because the suspending fluid is Newtonian, the rotation rate should not change with frequency (see fig. 3.2).

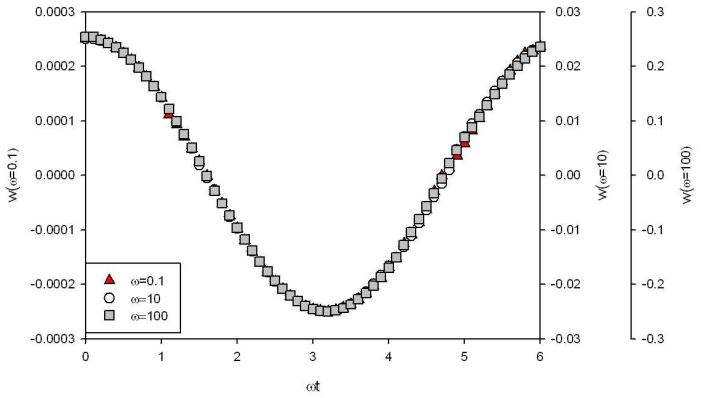

Figure 3.2: The angular velocity as function of ωt.

The fluid and particle contribution to the bulk stress can be calculated as previously discussed; in fig. 3.3, the result for a frequency of $0.1 rad/s$ is shown. The Newtonian fluid contribution obviously does not depend on the particle size. The particle contribution to the stress, instead, increases with increasing particle size. Both contributions are plotted as a function of time in fig. 3.3.

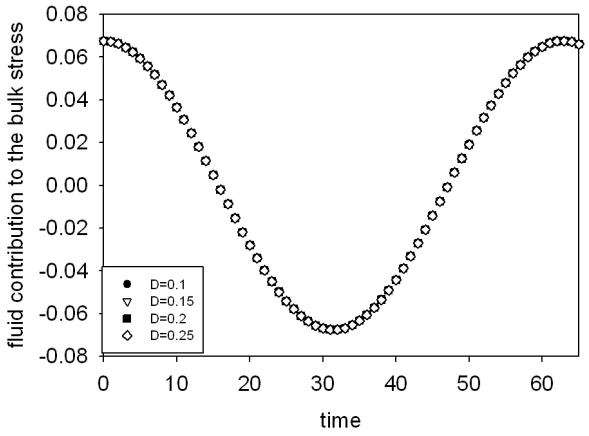

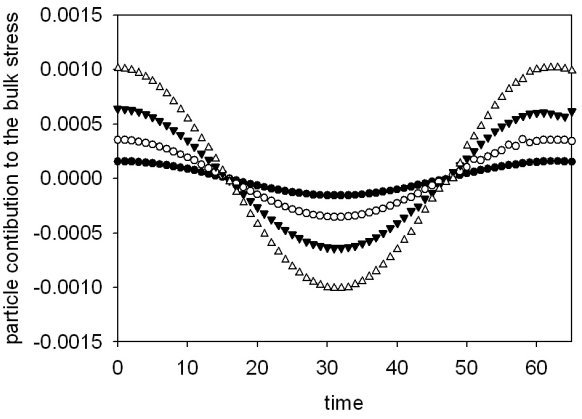

Figure 3.3: Fluid (top) and particle (bottom) contributions to the shear bulk stress as function of particle size.

In sinusoidal oscillatory shearing flow, the bulk shear stress is also sinusoidal, making it possible to model the results with a waveform. Therefore, the phase angle can be used to calculate the loss modulus as a function of solid area fraction, as shown in fig. 3.4.

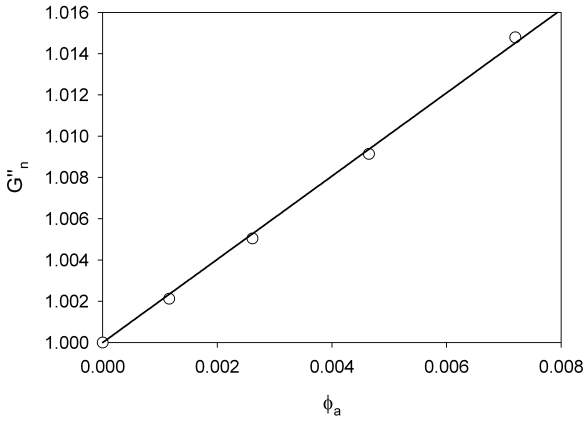

Figure 3.4: Viscous modulus as function of solid area fraction. The line is the best fit to the data.

A linear regression to the data results in $G_n^{"} = 1 + 2.02\phi_a$.
As expected, the viscous modulus, for small values of solid area fraction ϕ_a, converges to Einstein's analytical result for a dilute Newtonian system with the coefficient 2 [26], [85] (and references therein).

3.4 The two particles problem

The two-particle problem is simulated to investigate the effect of the hydrodynamic interactions between two particles. Two identical particles, with diameter D, are suspended freely in the domain.
Again, the reference velocity is zero at the center of the domain. We divided the domain in four sub-domains and investigated the approach between the particles only in one of them by changing the interparticle distance. One can discard the other subdomains for symmetry reasons.
Hence, the distance between the particles can be seen as the strength of the hydrodynamic interactions between the particles.

One particle is placed in the center of the domain, as before. As such, it can rotate freely but it will not translate. The other particle is placed in one of the four sub-domains and its initial position is changed randomly. In particular, as shown in fig. 3.5, the red particle will start moving to the right and then moving to the left, following the sinusoidal strain. To increase the volume fraction while avoiding influences of the walls, one can translate the chosen sub-domain towards the center.
For each particle size, about twenty initial configurations are studied, changing the distance between the two spheres both horizontally and vertically.

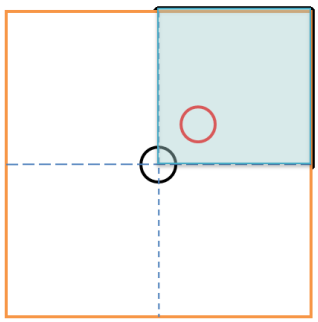

Figure 3.5: The division of the domain box in four sub-domains; one particle is in the center of the box; the initial position of the other particle is changed.

The bulk stress is always larger than one; it goes through a maximum when the particles are very close together and becomes minimum when they are far apart.
The bulk stresses, and consequently the viscous moduli, are calculated for all configurations; the final value for the viscous modulus at a certain solid area fraction is the mean of all configurations.
The result is shown in fig. 3.6.

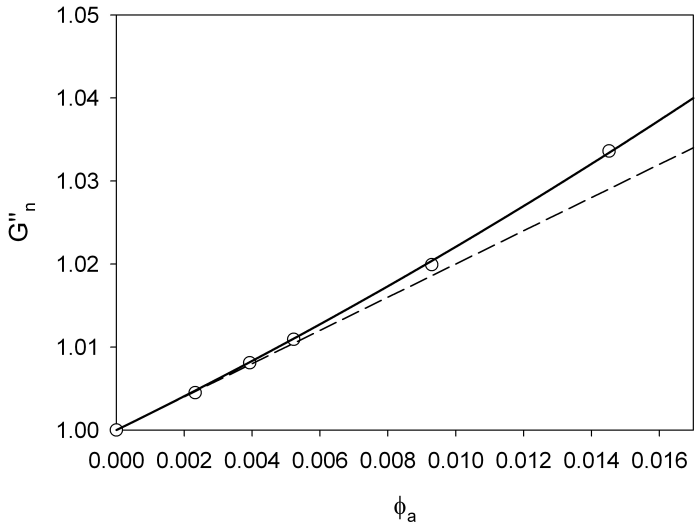

Figure 3.6: The viscous modulus as function of solid area fraction. The dashed line is Einstein's result for 2-D flow [26]. The solid line is a quadratic regression to the data.

As shown in the first chapter, the contribution of two particle hydrodynamic interactions to the rheological properties can be treated mathematically as a quadratic term ϕ^2 (or ϕ_a^2 for 2-D flows) in the expression for the stress tensor. As such, the data plotted in fig. 3.6 is fitted with a quadratic polynomial function. The best fit to the data is given by the following equation:

$$G_n^{"} = 1 + 2.02\phi_a + 19.2\phi_a^2 \tag{3.13}$$

The first coefficient in this expansion was set to 2.02, as found in the single particle problem. It must be stressed that these are only preliminary results. The second coefficient 19.2 cannot be easily rationalized. First, there is currently no theory relating the 2-D results to 3-D; as such, it is not possible to associate the 19.2 to any existing theory.
Second, it's not possible to compare these results with those on elongational and steady shear viscosities from some recent simulations [25] [23] [24]; indeed, these studies are on higher volume fractions and no quadratic regressions have been used to fit the data.

3.5 Conclusions

In this chapter, simulations for non Brownian hard disks dispersed in a Newtonian fluid under oscillatory shear flow in a well defined domain were presented. As far as we know, there are currently no simulations that investigate the dependence of the viscoelastic moduli on volume fraction.
We investigated the case of a single particle and of two particles. The stress tensor was calculated in both cases.
We focused on the dependence of the viscous modulus on solid area fraction. For the single particle problem, the viscous modulus approaches Einstein′s analytical solution for 2D [26], showing the feasibility of our scheme.
For the two particle problem, the contribution of the hydrodynamic interactions to the rheological properties was treated mathematically as a quadratic term ϕ^2 in the polynomial expansion of the viscous modulus. We found that the coefficient is equal to 19. At this moment, this value cannot be easily rationalized: there is no theory relating the 2-D results to 3-D and the existing numerical results on elongational and steady shear viscosities are for higher concentrations.

Chapter 4

Flow-induced structure formation of spheres in viscoelastic fluids

This chapter focuses on the flow induced microstructure of non-colloidal suspensions of spherical particles in viscoelastic fluids. First, the used materials and methods are presented.
Then, the characterization of the suspending fluids, both rheologically and rheo-optically, is shown.
In the last part of the chapter, the experimental results are presented and the effect of the viscoelasticity of the suspending fluid on the structure formation is discussed.

4.1 Materials

4.1.1 Polystyrene particles

Monodisperse polystyrene (PS) spheres have been used as the dispersed phase. The polystyrene particles were found to behave as hard spheres in dilute suspensions [89]. They were synthesized by a dispersion polymerisation process, similar to the one described by Almog *et al.* [90]. The method is a dispersion polymerisation process in an organic phase. The synthesis relies on the differences in the solubility of styrene and polystyrene in ethanol: styrene is soluble in anhydrous ethanol whereas high molecular weight polystyrene is not. The method depends on incipient aggregation that takes place at the very early stages of the polymerisation. This determines the number of formed nuclei. When a critical value molecular weight is reached, short

polystyrene chains precipitate and form nucleation seeds. The reaction, then, proceeds inside the particles, the latter being swollen by short polystyrene chains and by the monomer itself. These nuclei will subsequently grow to large size spheres according to the amount of monomer used. The integrity of the particles is ensured by a protective agent, Polyvinylpyrrolidone. This agent controls the growth of the particles by decreasing the surface tension. This avoids second step nucleation by enabling short chains of polystyrene to penetrate inside the formed spheres.
The size of the resulting polymeric spheres strongly depends on the limit of the solubility of the polymer in the solvent. The better the solubility, the larger the particle size; the solubility of polystyrene was increased as much as possible using water-free ethanol. Different dimensions of spheres can be produced by adding different amounts of water to the ethanol.
In particular, three different sizes are synthesized: 2.8, 1.9 and 1.2 μm ($\pm$ 0.1) (see Fig. 4.1).
To obtain the largest dimension of 2.8μm the subsequent recipe was used:
40g Polyvinylpyrrolidone was dissolved in 1300ml of anhydrous ethanol and introduced in the reactor. The mixture was stirred at 200 rev/min and heated up to 71°C. Subsequently, 1.76 g of an initiator, AIBN, was dissolved in 300ml of styrene and quickly added to the reactor. The reaction then starts and the Temperature of 71°C was maintened during 21 hours; after while heating was stopped and the reactor cooled down to room temperature. After the synthesis, the PVP was removed from the surface of the particles by successive centrifugations, while redispersing the particles in bidistillated water.
Scanning electron microscopy (SEM) was carried out to check monodispersity and dimension of the produced spheres, as shown in Fig 4.1.

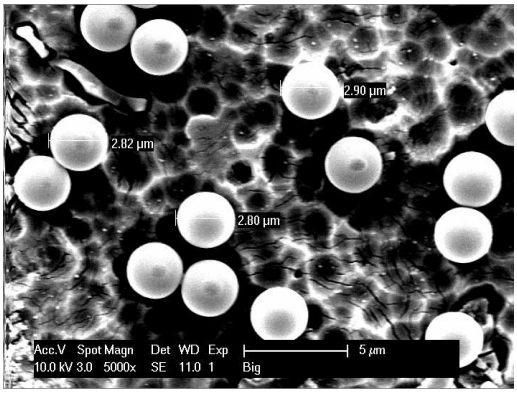

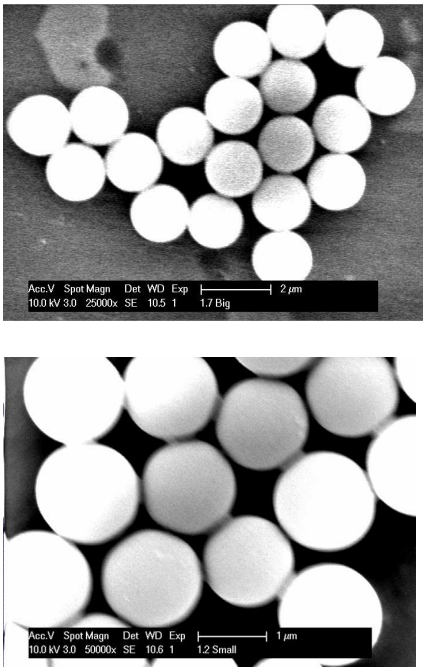

Figure 4.1: SEM micrographs of Polystyrene spheres. From the top to the bottom, 2.8 μm, 1.9 μm and 1.2 μm respectively.

The density of particles was measured to be about 1050 Kg/m^3 [91].
Suspensions containing a volume fraction of 0.008 have been prepared.
Charged polysterene particles of 1.6 μm were also used in order to check the importance of charges in string formation.
For the counterrotating rheometer with microscopy devices, PMMA particles (see chapter II) have been used.

4.1.2 Polymer solutions

The suspending fluids were selected to be able to investigate the effects of viscoelasticity and shear thinning on the particle microstructure under shear flow. Aqueous solutions of hydroxypropylcellulose and polyoxyethyleneoxide were prepared by adding the right amount of polymer to a suspensions of PS particles in water. the molecular weights of the polymers and an overwiew of the composition of the suspending fluids are given in tab. 4.1.
The densities of the suspending media are about 1100 kg/m^3. The small density mismatch between suspending media will not give rise to sedimentation effects on the time scale of experiments. In particular, using Stokes law, the sedimentation time for polystyrene particles over 10% of the gap for a gap

Table 4.1: Molecular weights of the polymers and composition of the suspending media.

Polymer	**Molecular weight** (Dalton)	**%w/w**
HPC (Klucel LF Hercules)	9500	30%
PEO (Union Carbide)	$4 \cdot 10^6$	3%

of h=100 μm can be calculated as follows:

$$t_{0.1h} = \frac{0.45\eta_0 h}{(\rho_p - \rho_0)R^2 g} \tag{4.1}$$

with g the acceleration gravity, ρ_0 and η_0 the density and the viscosity for the pure suspending medium, R the particle radius and ρ_p the density of the particles. In all cases, $t_{0.1h} > 3000h$.
In the performed experiments, the effects of particle inertia can be neglected. In laminar shear flow, the particle Reynolds number is defined as:

$$Re_p = \frac{\rho_0 R^2 \dot{\gamma}}{\eta_0} \tag{4.2}$$

The Re_p value is always smaller than 10^{-10} in the shear rate range investigated.
The particle size is sufficiently large to be able to neglect Brownian forces. Indeed, the Peclet number (eq. 1.19 the ratio between the hydrodynamic forces and Brownian motion) is high enough (10^4 to 10^8) to state that the hydrodynamic effects will be dominant over Brownian motion.

4.2 Experimental techniques

Rheological measurements on the unfilled suspending media were carried out on two rheometers, a stress controlled rheometer (Rheometric DSR 200) and a strain controlled rheometer (ARES, Rheometric scientific). In both cases cone and plate geometry of 25 mm diameter and a cone angle of 0.1 rad were used. All measurements were carried out at 20°C. Temperature was controlled by means of Peltier elements, which guaranteed a thermal stability within $\pm$ 0.1°C.

Microscopy and small angle light scattering experiments (SALS) were performed on suspensions of PS in the discussed suspending media.

A parallel plate flow cell (CSS 450, Linkam) has been used for all the optical experiments, enabling views in the velocity vorticity plane.
The system is composed of two parallel quartz windows. The bottom window is controlled by a motor. Temperature can be changed from ambient temperature to about $450°C$. Observations are made 7.5 mm from the center of the geometry and the viewing area is 2.5 mm in diameter. The rotational speeds vary from 0.0001 to 10 rad/s and it is possible to change the gap from 50 to 2500 μm.
The optical setup consists of a He/Ne laser with a wavelength $\lambda = 632.8nm$; it is followed by a pinhole, the shearing cell, a semi transparent screen and a CCD camera to record the images (see Fig. 4.2).
Microscopy images and SALS patterns are collected by means of a digital, progressive scan, high resolution 10-bit CCD camera. The camera was connected to a digital frame grabber (CORECO, TCI).
In order to check the microstructure during flow, light scattering experiments were used. Using an in-house developed software (SALS software, K.U.Leuven) time-resolved images were collected at preset time intervals. The scattering images are later treated with an image processing software, Fit2d. The measurements were performed at 20°C (±2°C).

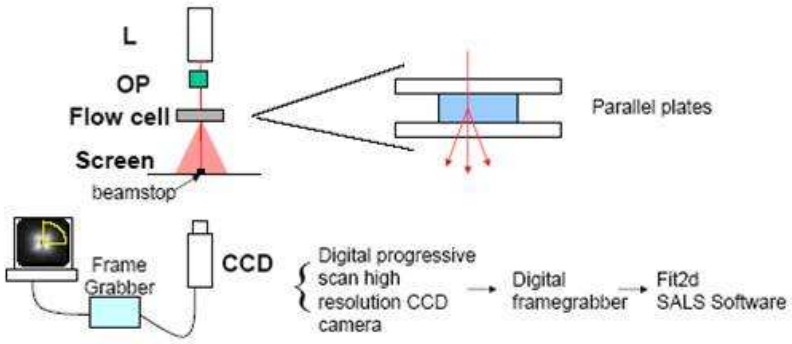

Figure 4.2: Schematic diagram of SALS setup

Principles of light scattering

Before showing the experimental results, it is important to outline the principles of light scattering essential to understand SALS experiments.
Reviews and books of general applications on scattering methods are available [92] [93] as well as a wide body of literature in which rheology and SALS/SAXS experiments are studied and discussed [94] [95] [96].
The basic formalism of small angle scattering is similar for light, neutrons and X-rays. The important difference is in the interaction of the radiation with the scattering medium. As a result, these scattering techniques are very similar and some basic definitions are common to all scattering methods.
For SALS, light is scattered from regions or volumes with different refractive index within the sample.
Fig 4.3 depicts a typical SALS experimental setup.

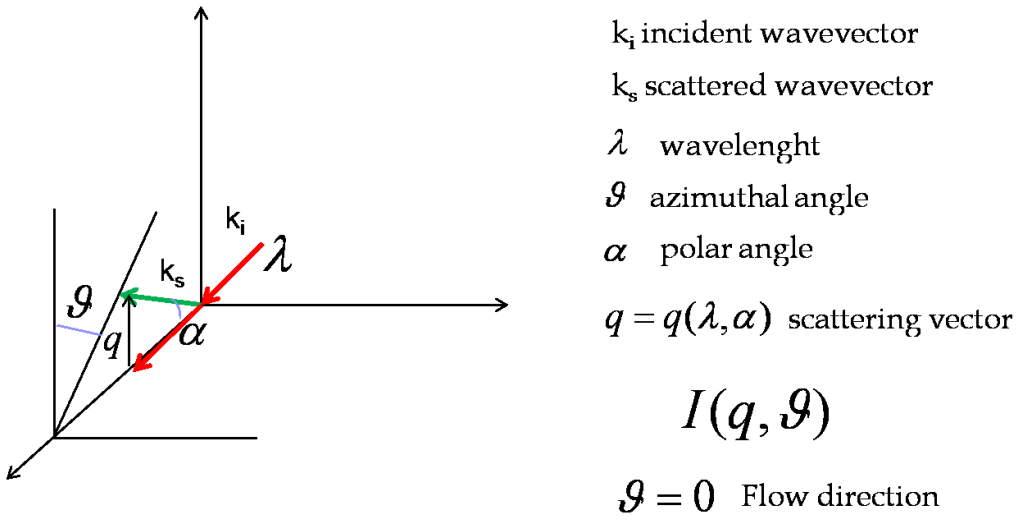

Figure 4.3: Schematic layout of a SALS setup dipicting the incident and scattered beams, the 2-D detector and the definition of the scattered vector (q).

A He/Ne laser impinges on a sample and the scattered intensity in the forward direction is recorded by a two dimensional detector (screen). The transmitted primary beam is fully absorbed by the beamstop placed in front of the detector. The incident wave vector k_i will be deviated by the presence of particles with a polar angle α, becoming k_s. The scattering at small angles is fully elastic because of the high energy of the radiation, so the magnitudes of the incident and scattered wave vectors are equal, $|k_i| = |k_s| = \frac{2\pi}{\lambda}$. In SALS

experiments the intensity of scattering is usually measured as a function of the momentum transfer or scattering vector, $\underline{q} = \underline{k_s} - \underline{k_i}$ and its magnitude:

$$q = \frac{4\pi}{\lambda} \sin \frac{\alpha}{2} \tag{4.3}$$

where λ is the wavelenght and α is the scattering angle (or polar angle).
For a dilute system containing N uniform particles per unit volume, the inter particle interactions can be neglected and I(q,θ), that is the intensity at any scattered vector and azimuthal angle, mainly depends on the shape and size of the particles. It can be calculated by summing the scattered amplitudes, F(q,θ), that arise from all parts of the sample as:

$$I(q,\theta) = \sum F(q,\theta)F^*(q,\theta) \tag{4.4}$$

where the sum is taken over the entire sample and $F^*(q,\theta)$ is the complex conjugate of F(q,θ). If the summation is replaced by an integral, the form of the eq. 4.4 closely resembles a Fourier transform of the distribution of scatteries in the sample. This recognition of the scattered intensity as a Fourier transform leads to several simplifications in the interpretation of data. For example, the convolution theorem allows eq. 4.4, for the case of interacting particles, to be written as:

$$I(q,\theta) = cP(q,\theta)S(q,\theta) \tag{4.5}$$

where P(q) is the form factor of a particle and S(q) is the structure factor, related to the microstructure through the pair correlation function. In other words, P(q) is related to the correlation within a single particle and S(q), instead, describes the correlations between different particles.
The constant c depends on other characteristics of the suspensions (volume fraction, difference in the refractive indeces,...).
The quantity P(q) is calculated for many simple shapes.
If the particle in a suspension are solid, P(q) will be constant and any change in scattered intensities during shear will arise from in a change in the microstructure (S(q)). Although eq. 4.5 might suggest that it is easy to extract the structure factor from measurements of the intensity by calculating the form factor, in practice several difficulties are not easily resolvable (discussed in more detail elsewhere [97]).
Anyway, the study of the intensity can be useful to understand microstructural changes. The two-dimensional SALS patterns provide information about the suspensions microstructure in reciprocal space. Fig. 4.4 shows on the left a schematic diagram of the anisotropic structure before shearing

and its pattern in the reciprocal space; on the right an aligned structure and the corresponding image in reciprocal space: particles aligned in the flow direction result in a scattering pattern displaying a pronounced streak in the vorticity direction.

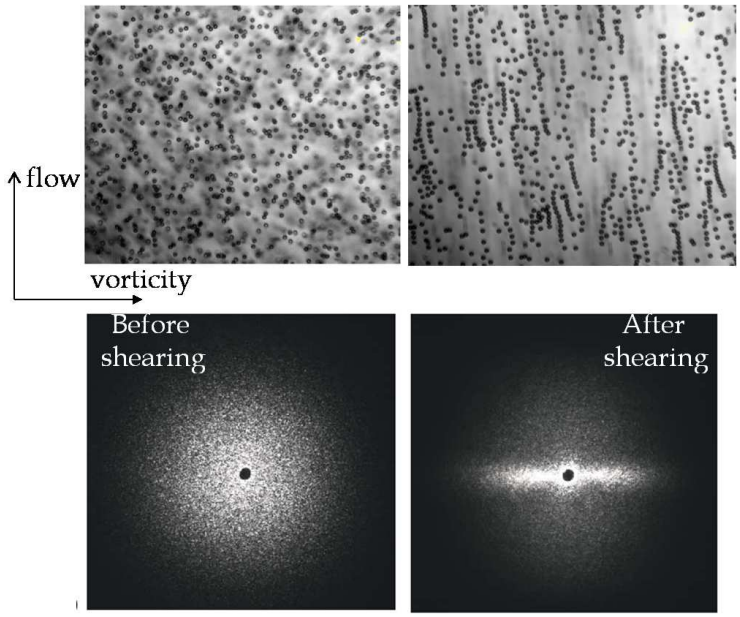

Figure 4.4: Real space image of a flow aligned structure and the corresponding image in the SALS pattern (respectively top left and top right). Scattering pattern before shearing and after shearing for PS suspensions in HPC.

To get a quantitative measure for the alignment from these patterns, it is necessary to weight the I(q,θ) by a spherical harmonic. In this way, the asymmetry in the pattern can be studied using an alignment factor.
In the works of Walker *et al.* [98] and Scirocco *et al.* [64] the definition is as:

$$A_f(q) = \frac{\int_0^{2\pi} I(q,\theta)\cos(2\theta)d(\theta)}{\int_0^{2\pi} I(q,\theta)d(\theta)} \tag{4.6}$$

with θ=0 the flow direction.
Another way to define the alignment factor is to substract the pattern without flow and to weight the subtracted image by a spherical harmonic:

$$A_f(q) = \int_0^{2\pi} [I(q,\theta)_{\dot{\gamma}} - I(q,\theta)_0]\cos(2\theta)d(\theta) \tag{4.7}$$

where $I(q,\theta)_{\dot{\gamma}}$ is the scattering intensity at a generic shear rate and $I(q,\theta)_0$ is that at shear rate equal to zero.

The counterrotating rheometer combined with microscopy

Another device is used to quantify the migration. A special designed counterrotating rheometer is combined with an optical microscopy setup, as in fig. 4.5. The counterrotating rheometer is composed of two stress controlled rheometers: a Physica MCR-300 for the top geometry, and a Physica DSR-300 for the bottom geometry (Paar Physica, Austria). These rheometers can be independently controlled.
A BK7 glass parallel plate geometry with a plain diameter of 50mm in combination with an in-house developed glass cup that surrounds the bottom plate to keep the sample in place is used as flow geometry.
Since the rheometer is counter-rotating, there is a stagnation plane with velocity zero in between the glass plates. This zero-velocity plane can be shifted up and down using a potentiometer which adjusts the rotation speed of the bottom and top plate, while keeping the shear rate constant. As such it is readily possible to capture a particle and keep it in view of the optical setup while all effects of the shear flow are working on the particle, although the mean particle velocity is zero.
The optical setup is composed of a Wild M5A stereomicroscope (Heerbrugg, Switzerland) connected to a Basler A301-fc digital camera (80 frames/s, 8 bit, resolution 658x494, progressive scan). This enables one to record sequences of images on a computer using Streampix software (Norpix, Canada).
A prism in between the microscope and the top parallel plate is used, and, as condenser, a energy saving lamp in conjunction with a small mirror. This setup enables one to record images of strings in the zero shear velocity plane. A schematic representation of the counterrotating Physica and the optical setup is shown in fig. 4.5
To locate the radial position of the particle in the geometry (to be able to get a value for the shear rate on the particle) we look with the microscope at a plastic "grid", which is placed between the cup and the bottom plate. Using this method one can measure the radial position of the particle in the geometry with an accuracy better then 200μm, with an error on the shear rate of about 1%. All measurements on the particles are done at radial positions between 15 and 19mm, the first limit is due to the geometry itself which is opaque in the middle, the upper one comes from the quality of the flow field. Usually, the gap is about 500 μm; at smaller gaps a small misalignment of the parallel plates affects the measurements. Higher gaps don't allow a good study of the migration phenomenon. Only one shear rate of $10s^{-1}$ has been studied.

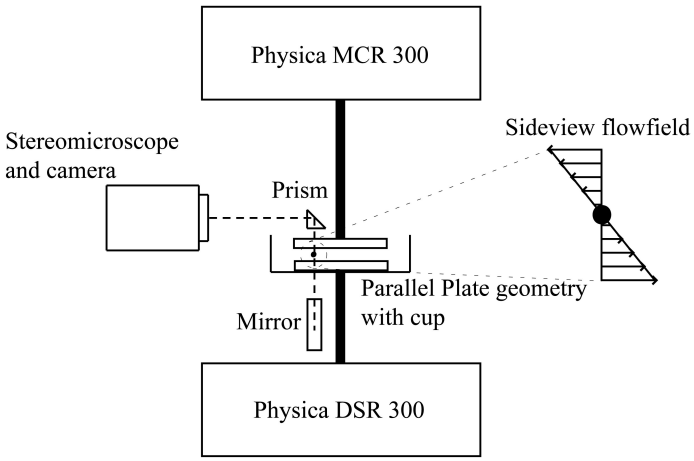

Figure 4.5: The counterrotating rheometer combined with microscopy from [55].

The recorded sequences of pictures were analyzed using Streampix and ImageJ software [99].

4.3 Experimental results

4.3.1 Rheology of suspending fluids

The steady state material functions for the HPC and PEO suspending media are presented in figs. 4.6 and 4.7.

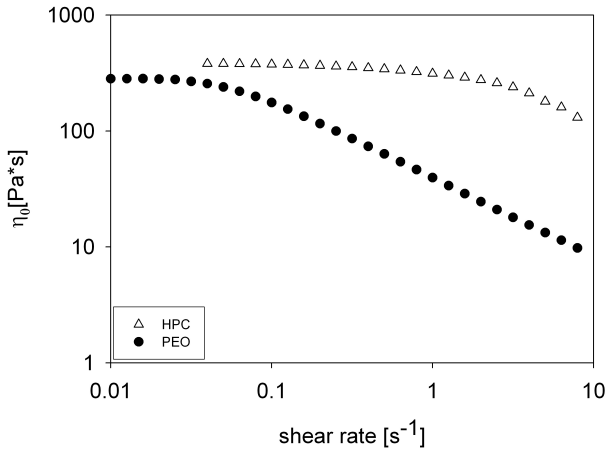

Figure 4.6: Viscosity of the fluids as function of shear rate.

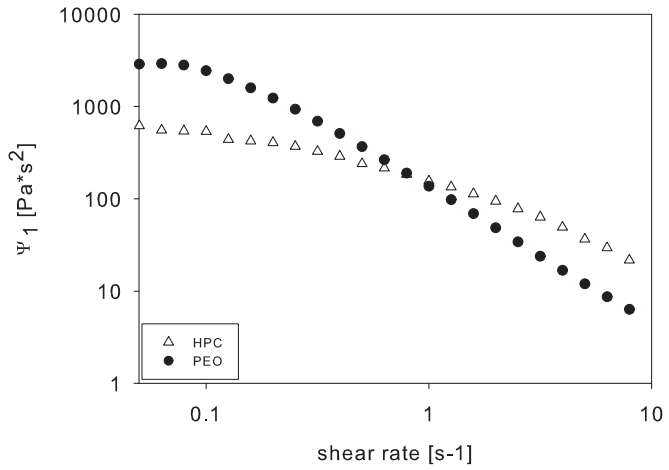

Figure 4.7: First normal stress coefficients of the fluids as function of shear rate.

The viscosity η_0 (and the first normal stress coefficent ψ_1) show weak shear thinning for the HPC suspending medium and stronger for the PEO suspending fluid. A dimensionless number which is used a lot in the study of viscoelastic fluids is the Weissenberg number defined as in eq. 1.15 as the ratio of the first normal stress difference over the imposed shear stress.
The evolution of the Weissenberg number with shear rate is shown in fig. 4.8 for both fluids.

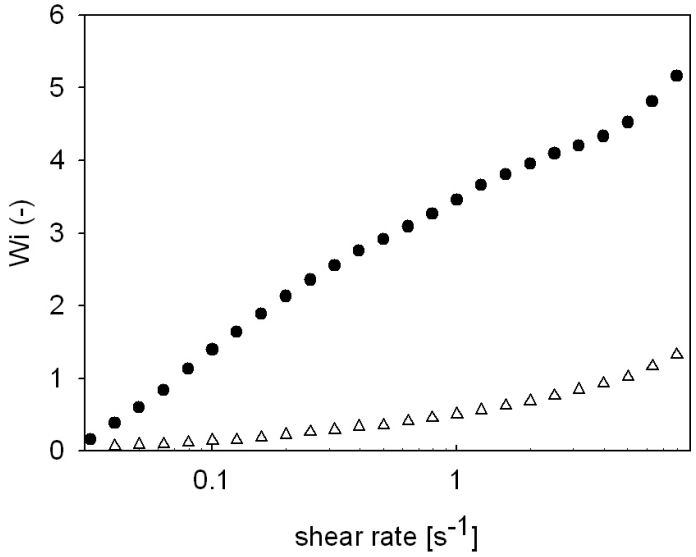

Figure 4.8: Weissenberg numbers of the fluids as function of shear rate.

Linear dynamic tests have also been performed. The moduli are shown in fig. 4.9. As shown, the two suspending media have different relaxation behavior. For example, when defining the relaxation time as the inverse of the cross-over frequency, one can appreciate the difference between the media: 80 rad/s for HPC suspending medium and 0.11 rad/s for PEO suspending fluid. Dilute suspensions of polystyrene particles with volume fraction of 0.8%, with different filler sizes were observed microscopically both during and after cessation of flow.
The PEO suspensions could not be made homogeneous. The particles are aggregated in rest, as shows in fig. 4.10.
When shearing, no flow alignment could be detected after one hour. Probably, waiting more time could be useful to detect some string formations. In any case, the presence of the clusters did not allow for accurate and reproducible experiments. Hence, we focused our attention only on the HPC based suspensions.

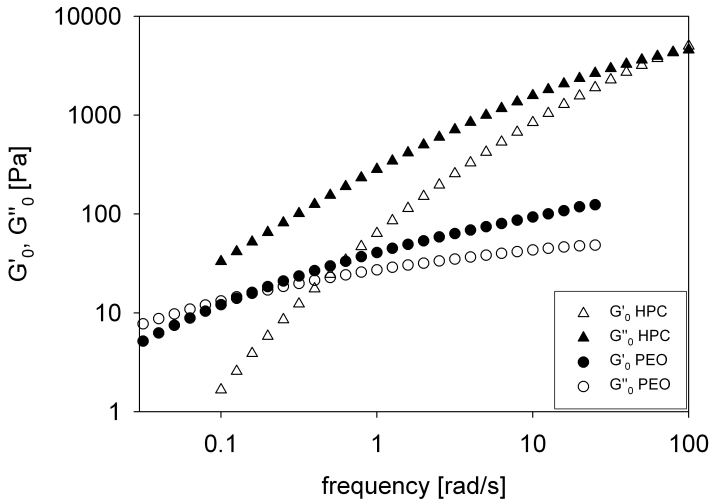

Figure 4.9: Viscoelastic moduli for the suspending media as function of frequency.

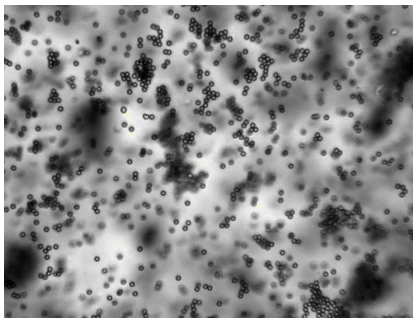

Figure 4.10: Microscopy image of PEO's suspension with 3μm diameter spheres.

4.3.2 Microscopy

The particles in the HPC suspensions were initially randomly dispersed. Differences in the microstructure have been studied for different particle sizes. Dilute suspensions, ϕ=0.8%, of polystyrene particles(with diameters 2.8μm, 1.9μm, 1.2μm $\pm$0.1), were sheared and observed microscopically both during flow and after cessation of flow.
When shearing the suspensions for a sufficiently long time, string-like structures were observed to develop. Differences and similarities can be studied for the different particle sizes.

In all cases, alignment and migration were coupled: first migration towards the plates took place, then the particles aligned. Alignment in the bulk of the fluid was never detected.

Migration effects, as clearly demonstrated before (see first chapter), are promoted by the fluid normal stress difference and shear thinning.
Migration and the consequent alignment are stronger when the shear rate is increased.
To examine the relation between migration velocity and the normal stresses, it is possible to write a simple force balance for a neutrally buoyant particle, following the work of Tehrani *et al* [77]:

$$6\pi R\eta_0 v_z \propto R^3 \frac{N_1 - N_2}{z} \tag{4.8}$$

where z is the coordinate in the vorticity direction, R the particle radius, v_z the velocity of the migration towards the walls and N_1 and N_2 the first and second normal stress differences. Neglecting N_2, the equation can be re-written in terms of the migration velocity:

$$v_z \propto \frac{N_1 R^2}{6\pi\eta_0 z} \tag{4.9}$$

Using $\eta_0 = \frac{\sigma}{\dot{\gamma}}$ for the viscosity and $\frac{N_1}{\sigma}$ for the Weissenberg number, one obtains:

$$v_z \propto \frac{Wi\dot{\gamma}R^2}{6\pi z} \tag{4.10}$$

According to eq. 4.10, the migration velocity is proportional to the square of the particle and to the product of the Weissenberg number and shear rate.
Increasing the gap results (not so clear because of the turbidity of the sample) in less alignment of the particles at the plate compared to the smaller gaps for the same shear rates. In any case, alignment in the bulk was never observed (see fig. 4.11).

Another possibility is to increase the volume fraction: probably the alignment is due only to a local increase of the volume fraction on the wall; the increasing of the volume fraction could bring to stronger hydrodynamic interactions between particles that could definitively "win" the migration forces towards the walls and align in the bulk.
Also this hypothesis does not give any result: particles go towards the wall more easily with increasing volume fraction [100] and inside the bulk any string formation in the direction of the flow was not detected.
The evolution of the microstructure under shear for particles of 3 μm is shown in fig. 4.12. The top left picture is the microstructure at shear rate zero.

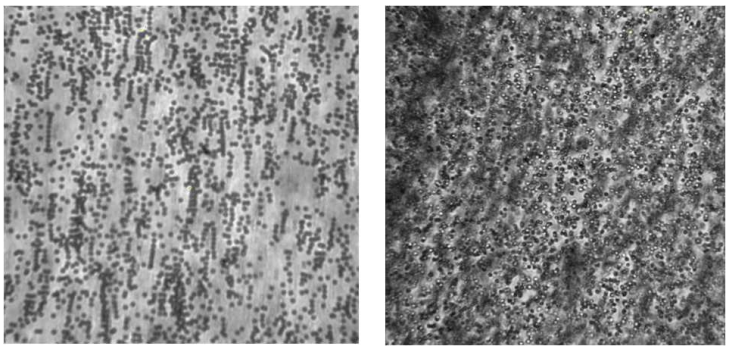

Figure 4.11: Microscopy images of a HPC suspension at $30s^{-1}$ and 200μm gap (diameter spheres=1.9 μm). After 1h: on the left side the microstructure on the plate; on the right side in the bulk.

The right top picture is after shearing the suspension for one hour at $30s^{-1}$. The bottom picture is, finally, the bulk after shearing: no alignment could be detected inside the sample. One can clearly see that the concentration in the bulk is lower than on the plates, this because the particles migrated towards the plates.

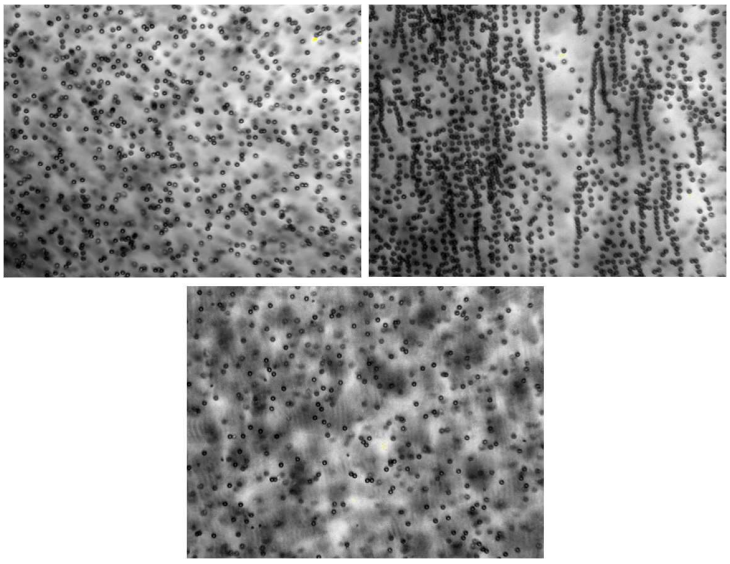

Figure 4.12: Microscopy image of a HPC suspension at $30s^{-1}$, 100μm gap (diameter spheres=3μm). Top left: before shearing. Top right: on the plate after shearing 1h. Bottom: in the bulk after shearing 1h.

The time for forming the strings decreases with increasing shear rate. For

very high shear rates the migration and subsequent flow alignment on the walls of the flow cell can be seen after few seconds.
Moreover, at very low shear rates (1 and 5 s^{-1}), for the two larger particle sizes, the transversal migration did not take place and no alignment was observed. Fig. 4.13 shows the influence of shear rate on the microstructure for 1.9 μm spheres in HPC based suspensions. At high shear rate, as shown in

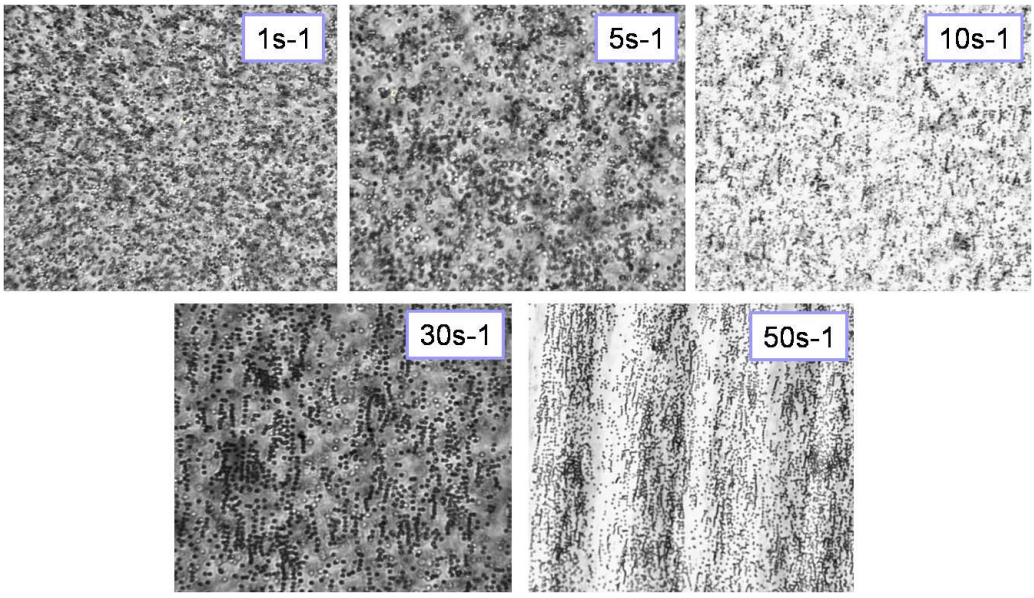

Figure 4.13: Microscopy image of a HPC suspension at different shear rates (diameter spheres: 1.9μm) after shearing 1h at 100μm gap.

the last picture of fig. 4.13, the particles regroup in bands. The bands are separated by particle-free zones. This phenomenon was already observed in different flow geometries [101], [78].
The particles of 1.2 μm aligned in the vorticity direction at low shear rate, as shown in fig. 4.14.
In this case the vorticity string formation takes place in the bulk of the sample (in the middle of the gap of the flow cell).
The vorticity alignment probably results from the hydrophobicity of the polystyrene spheres and the Van der Waals forces. An explanation can be found in the fact that the particles, by aggregating, form equivalent ellipsoidal shapes and, for ellipsoids, vorticity alignment has been observed before [102]: "As the shear rate is increased further, the fraction of vorticity-oriented particles decreases progressively until all particles become flow oriented."
The critical Weissenberg number [59, 64] for the onset of alignment of the particles has been determined for the different particle sizes and seems to

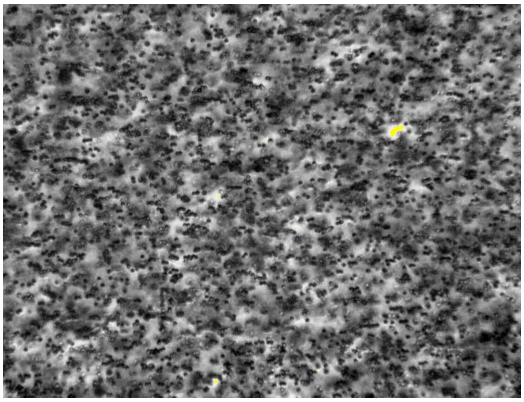

Figure 4.14: Microscopic image of HPC suspension with 1.2μm spheres in the bulk of the liquid after shearing at 1 s^{-1}.

be nearby independent on particle size. It can be said that $0.5 < Wi_{cr} < 1$ for this fluid, where the first number refers to high shear rates at which no alignment could be detected, whereas the second one corresponds to the next shear rate, at which alignment could be seen. We consider a string as a structure with at least three particles, chained and aligned in the flow direction. The Weissenberg number and the onset of flow alignment (at the walls) corresponding to various shear rates are determined by microscopy and shown in table 4.2.

Table 4.2: Weissenberg number and onset of alignment as function of shear rate.

$shearrate$	$flowalignment?$	Wi
1	no	0.5
5	yes	1
10	yes	1.35
30	yes	1.5
50	yes	1.6

The last two values of the Weissenberg number are extrapolated from the plot in fig. 4.8.

4.3.3 Small angle light scattering

SALS experiments have the advantage that the pattern stems from the whole sample, while microscopy, instead, yields more local information.
To analyze the patterns in a quantitative way, an alignment factor, as already defined (eq. 4.6), was calculated.
The suspensions were sheared at different shear rates and SALS patterns were recorded at fixed time intervals. For each image the alignment factor was calculated.
Strings oriented in the flow direction cause a pronounced streak in the vorticity direction. The alignment factor is positive for such a structure and negative for a vorticity oriented structure. One can understand this, by considering fig. 4.15 and eq. 4.7.

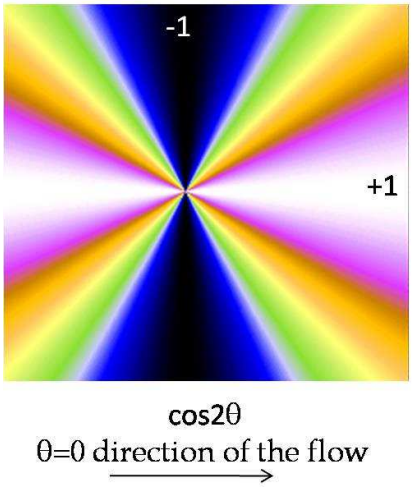

Figure 4.15: The sign evaluation of $\cos 2\vartheta$ for the alignment factor.

Before presenting data, the reproducibility of the experiments is discussed. Experiments ($30s^{-1}$, 100gap, $1.9\mu m$) are repeated three times each time renewing the sample. The error, defined as the ratio of the mean of the difference between the three tests and the mean value of the alignment factor, is calculated and plotted in fig. 4.16. As one can easily see, the error decreases at higher scattering vectors, and remains close to about 7% at high q. This means practically that we have to be careful when choosing a single value of the scattering vector to compare data.

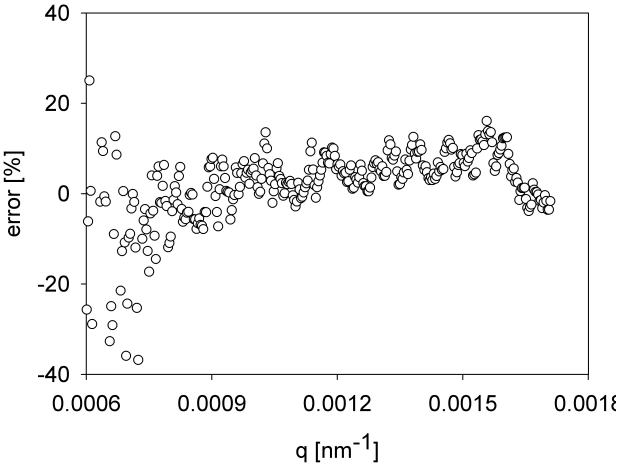

Figure 4.16: Evaluation of percent error in a meaningful q range for 1.9 μm based suspension.

Alignment factor dependence on shear rate

Under steady state conditions the patterns change with shear rate as shown in fig. 4.17. At first stage, we use eq. 4.7 to calculate A_f.

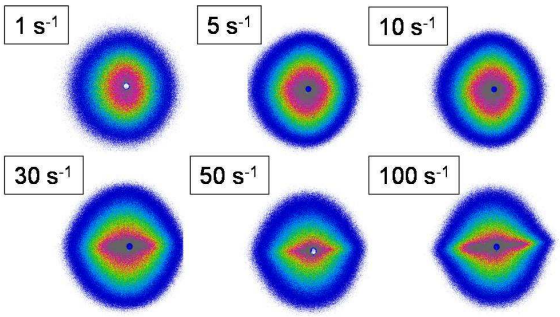

Figure 4.17: SALS patterns as function of shear rate for 1.2 μm size particle. At low shear rates, a weak vorticity alignment can be see. Increasing the shear rate reorients the strings in the flow direction.

In order to understand the evolution of the alignment factor as a function of shear rate, it is necessary to compare the patterns at the same deformation ($\gamma = \dot{\gamma}\Delta t$) or at the same time. The results for the 1.2 μm size suspensions are shown in figs 4.18 and 4.19. The behavior is however qualitatively the same for all sizes (except for the vorticity alignment phenomenon at lower

shear rates).
In Fig. 4.18, the alignment factor as function of the scattering vector is shown for different shear rates at fixed deformation. We are not able to show the lowest shear rates, for which such a high deformation was not reached in our experiments.

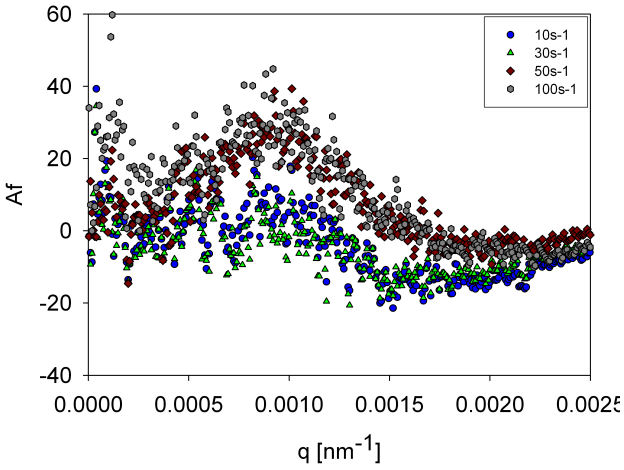

Figure 4.18: Alignment factor as function of scattering vector at 360% strain for the 1.2 μm size suspension.

Another way to compare the data of different shear rates is at the same shearing time; the result is shown in fig. 4.19. In this case it is possible to compare the alignment factor for all experimental shear rates.

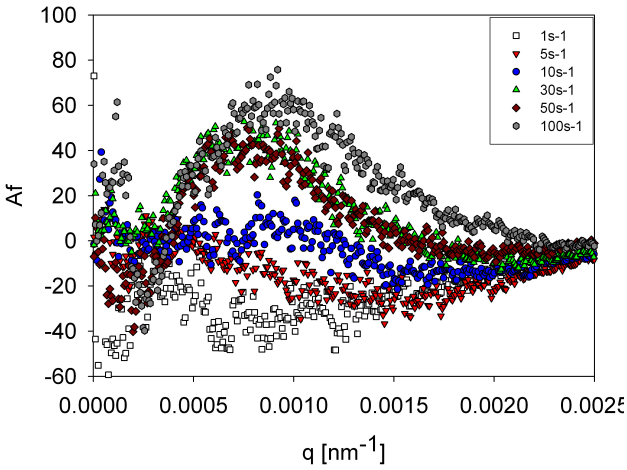

Figure 4.19: Alignment factor as function of scattering vector after 1h for 1.2 μm size spheres.

It is clear from figs. 4.18 and 4.19 that, at a fixed q, or for a range of q values, the alignment factor increases with increasing shear rate.
For the 1.2 μm spheres the alignment factor observed under steady state conditions for a fixed scattering vector q=1[μm^{-1}] is plotted in Fig. 4.20. The alignment factor is negative, indicating vorticity alignment, for shear rate below $10s^{-1}$.

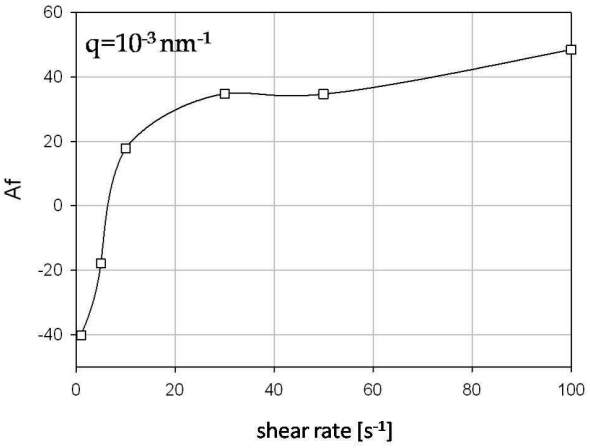

Figure 4.20: Alignment factor as function of shear rate at a scattering vector of $1\mu m^{-1}$.

To be able to compare these results with those obtained of Scirocco *et al* [103, 91] it is necessary to define the alignment factor in the same way [98]. This is why the alignment factor is also calculated according to the eq. 4.6. The alignment factor as function of the scattering vector at steady state (1h) for the suspensions with 1.2 μm size particles is plotted in fig. 4.21 (A_f has a subscript "s" to indicate the use of the eq. 4.6 as definition for the alignment factor).

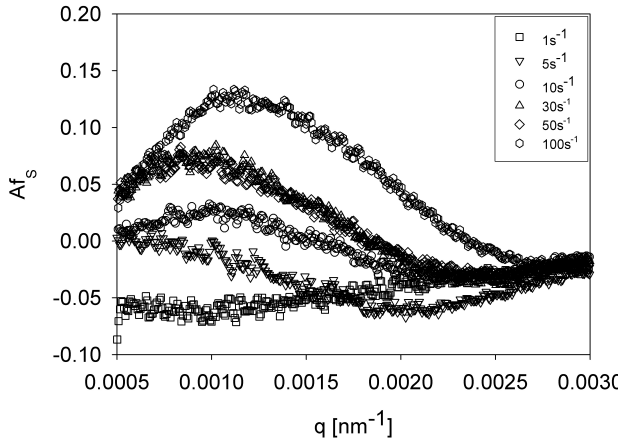

Figure 4.21: Alignment factor (eq. 4.6) as function of scattering vector for the suspensions with 1.2μm particles at different shear rates after 1h of shearing.

The trend in fig. 4.21 is the same as in fig. 4.19, only the values are scaled. Calculations have been done for all sizes.
At high shear rates, where migration and the consequent alignment are strong the alignment factor scales with the spheres size as shown in fig. 4.22.
For suspensions sheared at the same conditions of shear rate, gap and temperature, the alignment factor decreases with decreasing size of the spheres. This is in line with the fact that alignment is a consequence of migration because migration decreases with sphere size: this means that to check the same value of the alignment for This suggests that one probably has to wait longer for smaller spheres to get the same alignment factor.

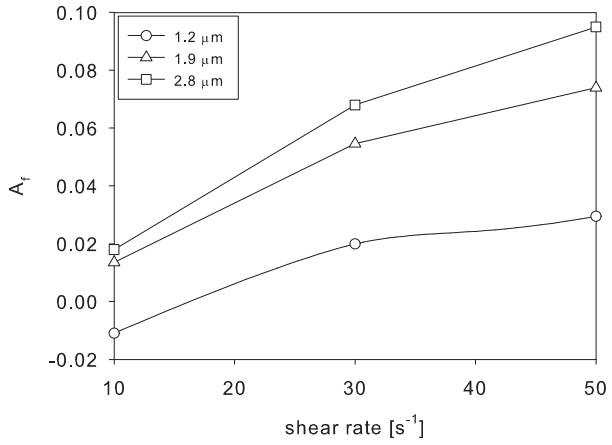

Figure 4.22: Alignment factor at steady state as function of shear rate for suspensions with spheres of different sizes. Data for suspensions with 2.8μm spheres are from Scirocco *et al* [91].

Influence of the walls and kinetics of string formation

The alignment factor was determined for a dispersion of 1.9μm particles in the HPC suspending medium at different gap spacings and for different shear rates, to evaluate the influence of the walls.
Multiple scattering makes the comparison difficult. Therefore, the definition of the alignment factor has to take the difference between the generic intensity at a fixed shear rate and that at shear rate equal to zero into account. This assures a meaningful comparison between the different gap spacings.
In fig. 4.23, the alignment factor observed under steady state conditions is plotted as function of shear rate for different gap spacings, ranging from 50 μm to 400 μm, meaning 26-200 times the particle diameter.
The graph shows A_f for a q value of $1\mu m^{-1}$ after shearing for one hour; the comparison at fixed q is meaningful possible because the alignment factor always decreases with increasing gap for each value of the scattering vector and time.
The alignment factor changes significantly with gap. In particular, it increases with decreasing gap sizes. This means that wall effects promote rather than hinder the alignment. This is in agreement with the results obtained using microscopy and counterrotating rheometer and in disagreement with the results of Scirocco *et al* [64].
With the SALS experiments one can also study the temporal evolution of the alignment.

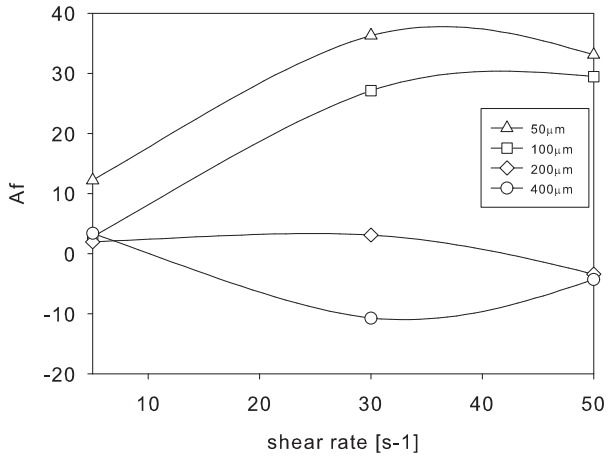

Figure 4.23: Effect of the gap width on the alignment factor for a dispersion of 1.9μm spheres in the HPC based suspending medium. Steady state at q=1μm^{-1}.

In fig. 4.24, the alignment factor is plotted as a function of time for different gaps for a shear rate of 30s^{-1}.
The kinetics of string formation are different for different gaps; for the smallest gap, there are two things to look at: the smaller number of the particles that have to align and the smaller distance between the particle in the bulk and the plate of the flow cell. The result is in an alignment that saturates very fast, meaning that the plateau is easily reached.
The first derivative of the alignment factor can be calculated from fig. 4.24 and, at least in first approximation, is a measure of migration. At start of the flow, the alignment is mainly dependent on migration. The first derivative is shown in fig. 4.25 as function of gap. According to eq. 4.10:

$$v_z \propto \frac{dA_f}{dt} \propto \frac{1}{gap} \tag{4.11}$$

the migration velocity depends hyperbolically on gap, as clearly shown in fig. 4.25.
To understand the role of the shearing time on the migration and, hence, the alignment, an experiment is performed at 30s^{-1} for about three hours, the limit being imposed by the device. To avoid confusion, in fig. 4.26 the result is shown for a mean of the alignment factor in a certain scattering vector range (3*10^{-4}-2*10$^{-3}nm^{-1}$); therefore, it is not possible to directly compare these values with data in fig. 4.24 at the same gap.

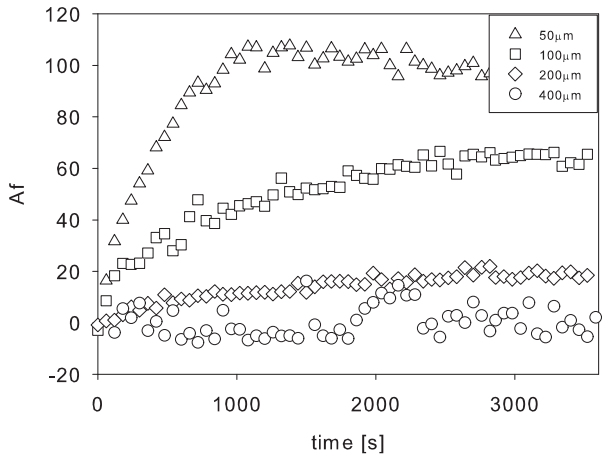

Figure 4.24: Alignment factor as function of the time for different gap sizes.

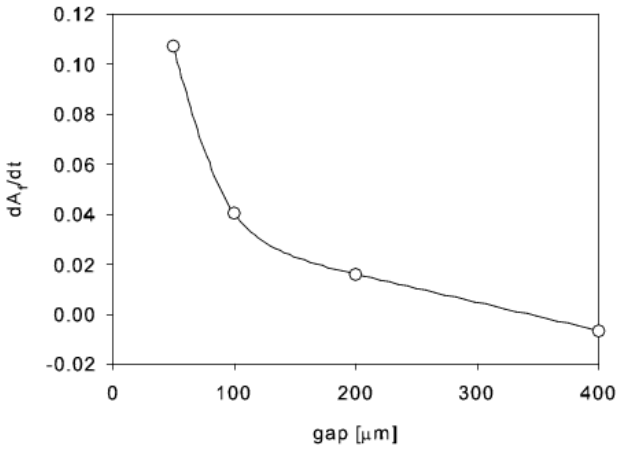

Figure 4.25: First derivative of the alignment factor in fig. 4.23 in the range 0-600s.

Fig. 4.26 shows that the alignment factor reaches a plateau after shearing the sample for 1h. Then it decreases and eventually increases again later on. In conclusion, migration and alignment are definitely connected, as demonstrated by the agreement between the results from microscopy and SALS. In any case, trying to understand the kinetics of both migration and string formation is not an easy task. Indeed, even if the alignment factor provides a useful tool to quantify alignment, it depends in a complex manner on several features of the suspension in 3D.

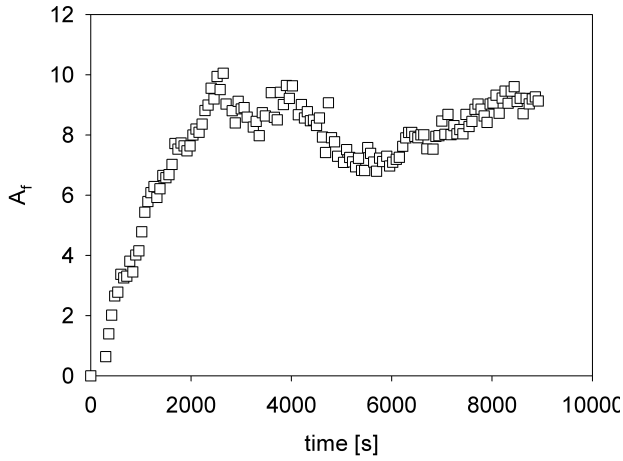

Figure 4.26: Alignment factor as function of time for a gap of 100μm at 30s^{-1}.

Polystyrene charged particles

In order to get a better understanding of vorticity alignment we also studied charged particles. The size dimension of the spheres is nearby the same, so most colloidal and hydrodynamic forces are of the same order. The presence of the charge on the surface of the spheres is the only relevant difference.
The vorticity alignment for the charged particles is less clear and flow alignment appeared always on the walls of the cell. The migration to the walls is higher for this case than previous cases. Moreover, the strings of particles form crystalline patches on the plates at high shear rates, see fig. 4.27.

Figure 4.27: Bands of particles at high shear rates.

Under steady state conditions the patterns change with shear rate as in fig.

4.28. As said before, except weakly for the shear rate of $1s^{-1}$, vorticity alignment is not observed.

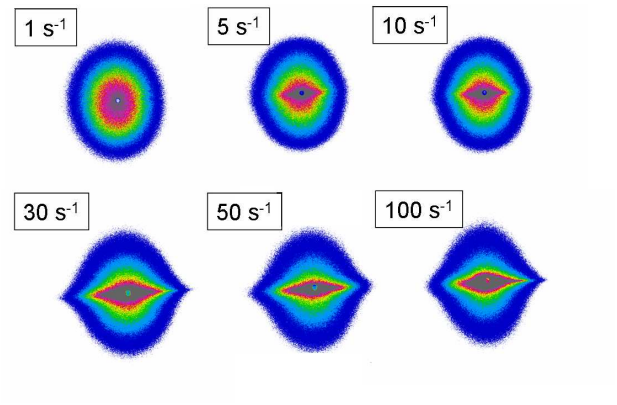

Figure 4.28: SALS patterns as function of shear rate for 1.6 μm size charged particle.

4.3.4 Counterrotating device

The velocity of a particle in a string can be determined taking into consideration the ratio pixel/μm (=0.63 for an image of 654×494 and magnification of 50×) and the time for a particle in a string to travel the length of the image. As the shear rate on the particle and the position of the zero-velocity plane are known, it is possible to calculate the position of the particle with respect to the position of the plates.
To get an accurate measurement of the velocity of the particle in a string, many particles were considered, both of the bottom and of the top plate. The final velocity is an average of all velocities calculated.
In this device, different suspending media filled with PMMA particles of 15μm diameter (0.8% by volume) were used: Newtonian PIB, as a reference, and a shear thinning elastic polymer solution of HPC in water (used before in all the other experiments).

First of all, the Newtonian based suspension was checked and string formation was found to be absent. This agrees with the hypothesis that migration and alignment are strictly connected. Migration is absent in the Newtonian fluid [103, 59], at least when inertia can be neglected, as in this case; consequently the string formation cannot take place. This is, of course, not the only reason why alignment is absent in the Newtonian fluid: alignment is also connected to time effects of the fluid and to the non-symmetric nature of the hydrodynamic interactions in viscoelastic fluids.

Then, the HPC based suspensions were studied (Fig 4.29). Even if the migration and the alignment on the walls of the flow cell have been already studied optically, the counterrotating device is very useful, as said before, to check the distance of the strings from the plates. In particular, it was calculated that the distance of the center of the sphere in a string from both the plates was about 5μm...that's impossible for the PMMA particles which have 15μm as mean diameter! This means that, considering the sum of the errors for the measuring of all the measurements, the particles are sticky to the plates and align on the plate itself.

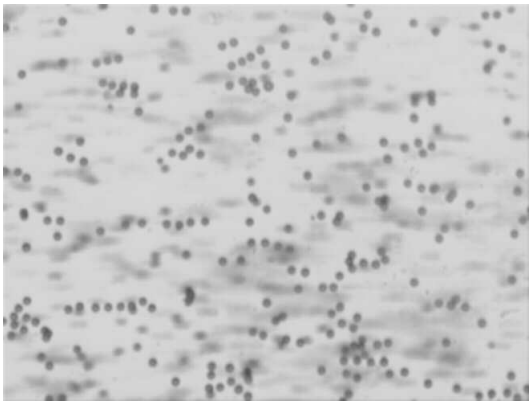

Figure 4.29: Counterrotating image for HPC based suspensions.

4.4 Conclusions

The effect of particle size and presence of the wall on flow alignment have been studied in HPC based suspensions, by means of video microscopy and with small angle light scattering. Alignment factor were derived from the SALS patterns.
The critical Weissenberg number for the onset of alignment found using microscopy is indipendent of particle size. A new phenomenon was found for our smallest spheres: a vorticity aligned structure was observed at low shear rates, never seen before for spherical particles [103, 65]. This probably comes from a competition between different forces, hydrodynamic interactions, colloidal forces (such as Van der Waals forces) etc. Decreasing the diameter of the spheres results in more particles and more surface area at a certain volume fraction. This could explain, together with the hydrophobicity of the polystyrene spheres, the vorticity alignment: at low shear rates, the spheres aggregate and form ellipsoidal shapes; the number of strings oriented in the vorticity direction increases with longer shearing. Moreover, as the shear rate is increased further, the fraction of vorticity-oriented particles decreases progressively until all particles migrate to the walls and flow orient. This phenomenon for non-spherical particles has been studied before [102] [104].
With SALS, we found that the alignment factor increases with particle size. The best way to compare the alignment factors for different particle sizes is to average its values for a range of scattering vectors: $0.9q^* < q < 1.1q^*$, where q^* is the scattering vector value corresponding to a real space distance of five times the particle radius R ($q*5R = \pi$). Fig. 4.30 shows the alignment factor at steady state as function of shear rate for different particle sizes.

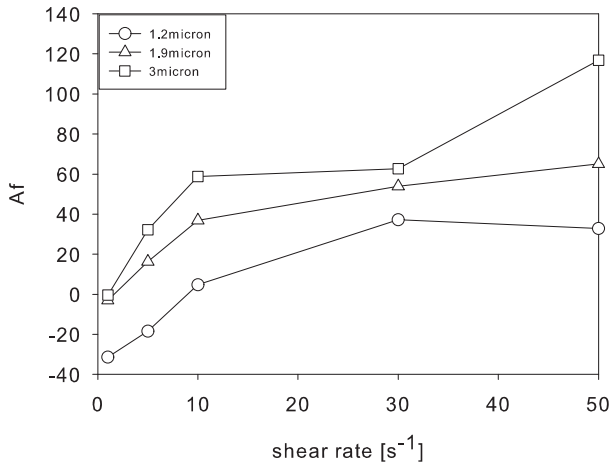

Figure 4.30: Alignment factor as defined by eq. 4.7 at steady state as function of shear rate for suspensions of spheres with different sizes.

The vorticity alignment is only visible (negative values for the alignment factor) for the smaller spheres of 1.2 μm.
The alignment factor has also been studied as function of gap and time. The alignment factor increases significantly for smaller gaps meaning that flow alignment follows the migration to the walls: particles migrate first and then align in the flow direction. This means that, at least for HPC based suspensions, wall effects promote rather than hinder the alignment in strong constant with literature [91, 59]. The bigger the particles, the faster the migration and consequently the alignment.
At the moment we cannot deduce if this behavior is general for all viscoelastic fluids. Other experimentalists [91] reported alignment in the bulk, meaning that the rheological properties of the fluid can affect both migration and alignment separately. In our investigated suspensions migration to the walls is stronger and is strictly connected with flow alignment. In this case it is not simple to understand the kinetics of migration and its bond to string formation (both kinetically and hydrodynamically).

List of publications

Publication in International Journals

- R. Pasquino, N. Grizzuti, P.L. Maffettone, F. Greco, Rheology of dilute and semi-dilute non colloidal hard sphere suspensions, Journal of Rheology, 52(6), 1369-1384 (2008).

- S. Acierno, R. Pasquino, N. Grizzuti, Rheological techniques for the determination of the crystallization kinetics of a rubber filled polypropylene, Journal of Thermal Analysis and Calorimetry, JTAC Special Issue "Rheology as Thermoanalytical Method for Polymers", (2008)

Congress Contributions

- C. Carotenuto, N. Grizzuti, R.Pasquino, Phase transition of cellulosic biopolymer solutions, 77th Annual Meeting of Rheology, Vancouver, Canada (2005).

- R. Pasquino, N. Grizzuti, P. L. Maffettone, F. Greco, Rheology of dilute viscoelastic suspensions, 4th Annual European Rheology Conference, Naples, Italy, (2007).

- R. Pasquino, N. Grizzuti, P. L. Maffettone, F. Greco, Rheology of dilute viscoelastic suspensions, European Polymer Congress, Portoroz, Slovenia, (2007).

- R. Pasquino, N. Grizzuti, P. L. Maffettone, F. Greco, Reologia di sospensioni viscoelastiche, INSTM, Perugia, Italy, (2007).

- N. Grizzuti, R. Pasquino, Effects of matrix viscoelasticity on the rheology of dilute and semi dilute suspensions of non Brownian rigid spheres, XVth International Congress on Rheology, Monterey, California, (2008).

Curriculum vitae

Rossana Pasquino was born in 1982, Avellino, Italy.
In 2000 she got her scientific diploma (Benevento, G. Rummo).
She studied Chemical Engineering at University Federico II, Naples, where she obtained a degree cum laude in 2005; the thesis was performed in rheology of biopolymer solutions and in their phase transitions by heating.
In November 2005 she started a Ph.D. at the laboratory of the Department of chemical engineering in the University Federico II in Naples. In August 2007 she moved to Belgium to do a part of the Ph.D. project at the Laboratory of Applied Rheology, K.U. Leuven.

Bibliography

[1] Eirich, Bunzle, and Margaretha. The viscosity of suspensions and solutions; the viscosity of suspensions of spheres. *Kolloid Z*, 74:276, 1936.

[2] A. Einstein. Berichtigung zu Meiner Arbeiten: Eine Neue Bestimmung der Molekul Dimensionen. *Annalen der Physik Berlin*, 34:591, 1911.

[3] O. Bachle. The viscosity of latex and latex mixtures. *Rubber Chem. Tech.*, 10:675, 1937.

[4] C.M. Blow. The viscosity of rubber solution. *Trans. Faraday Soc.*, 25:458, 1929.

[5] G.K. Batchelor and J.T. Green. The determination of the bulk stress in a suspension of spherical particles to order c^2. *J. Fluid Mech.*, 56:401, 1972.

[6] G.K. Batchelor and J.T. Green. The hydrodynamic interaction of two small freely-moving spheres in a linear flow field. *J. Fluid Mech.*, 56:375, 1972.

[7] G.K. Batchelor. The effect of brownian motion on the bulk stress in a suspension of spherical particles. *J. Fluid Mech.*, 83:97, 1977.

[8] W. B. Russel and A. P. Gast. *Non equilibrium statistical mechanics of concentrated colloidal dispersions: Hard spheres in weak flows*, volume 84. 1985.

[9] I.R. Rutgers. Relative viscosity of suspensions of rigid spheres in newtonian liquids. *Rheol. Acta*, 2:202, 1961.

[10] S. H. Maron. Rheological of synthetic latex. *J. Colloid Sci.*, 10:482, 1955.

[11] H. Eilers. The viscosity of emulsions of a highly viscous substance as a function of concentration. *Kolloid-Z*, 97:313, 1941.

[12] J.V. Robinson. The viscosity of dispersions of spheres. iii sediment volume as a determining parameter. *Trans. Soc. Rheology*, 1:15, 1957.

[13] A.P. Ting and R.M. Luebbers. Viscosity of suspensions of spherical and other isodimensional particles in liquids. *Amer. Inst. Chem. Eng. J.*, 3:111, 1957.

[14] K.H. Sweeney and R.D. Geckler. *J. Appl. Phys.*, 25:1135, 1954.

[15] F.L. Saunders. Rheological properties of monodisperse latex systems concentration dependence of relative viscosity. *J. Coll. Sci.*, 16:13, 1961.

[16] C.U. Thomas and M. Muthukumar. Three-body hydrodynamic effects on viscosity of suspensions of spheres. *J. Chem. Phys.*, 94:5180, 1991.

[17] C.W.J. Beenakker. The effective viscosity of a concentrated suspension of spheres (and its relation to diffusion). *Physica*, 128A:48, 1984.

[18] C.W. Macosko. *Rheology: principles, measurements, and applications (Foams, Emulsion and Blends*. Wiley-VCH, New York, 1994.

[19] J.M. Krieger and A. Dougherty. A mechanism for non-newtonian flow in suspensions of rigid spheres. *Tran. Soc. Rheol.*, 3:137, 1959.

[20] C.H. Hsueh and P.F. Becher. Effective viscosity of suspensions of spheres. *J. Am. Ceram. Soc.*, 88:1046, 2005.

[21] J. G. Oldroyd. The elastic and viscous properties of emulsions and suspensions. *Proc. R. Soc. London*, 218:122, 1953.

[22] S. J Choi and W. R Schowalter Rheological properties of non-dilute suspensions of deformable particles. *Physics of fluids*, 18:420, 1975.

[23] W.R. Hwang M.A. Hulsen and H.E.H. Meijer. Direct simulation of particle suspensions in sliding bi-periodic frames. *J. Comput. Phys.*, 194:742, 2003.

[24] W.R. Hwang and M.A. Hulsen. Toward the computation rheometry of filled polymeric fluids. *Korea-Australia Rheol.J.*, 18:171, 2006.

[25] G. DAvino, P.L. Maffettone M.A. Hulsen and G.W.M. Peters. A numerical method for simulating concentrated rigid particle suspensions in an elongational flow using a fixed grid.

[26] J.F. Brady. The einstein viscosity correction in n-dimensions. *Int. J. Multiphase Flow*, 10:113, 1984.

[27] G.J. Jarzebsky. On the effective viscosity of pseudoplastic suspensions. *Rheol. Acta*, 20:280, 1981.

[28] Donald L. Koch and G. Subramanian. The stress in a dilute suspension of spheres suspended in a second-order fluid subject to a linear velocity field. *J. Non-Newtonian Fluid Mech.*, 138:87, 2006.

[29] J.F.Palierne. Linear rheology of viscoelastic emulsions with interfacial tensions. *Rheol. Acta*, 29:204, 1990.

[30] R. Pal. Complex shear modulus of concentrated suspensions of solid spherical particles. *J. Colloid Sci*, 245:171, 2002.

[31] E. Guth. Theory of filler reinforcment. *J. Appl. Phy.*, 16:20, 1945.

[32] Y.P. Wu, Q.X. Jia D.S. Yu and L.Q. Zhang. Modeling young's modulus of rubber-clay nanocomposites using composite theories. *Polymer Testing*, 23:903, 2004.

[33] D. Graebling, R. Muller, and J.F. Palierne. Linear viscoelastic behaviour of some incompatible polymer blends in the melt. interpretation of data with a model of emulsion of viscoelastic liquids. *Macromolecules*, 26:320, 1993.

[34] S. E. Gleissle, W. Gleissle, G.H. Mckinley, and H. Buggish. The normal stress behaviour of suspensions with viscoelastic matrix fluids. *Rheol. Acta*, 41:61, 2002.

[35] J. Mewis and C.W. Macosko. *Suspension Rheology in: Rheology: Principles, measurements and applications*. C.W. Macosko ed., VCH Publishers, New York, 1994.

[36] N.Ohl and W.Gleissle. The characterization of the steady-state shear and normal stress functions of higly concentrated suspensions formulated with viscoelastic liquids. *J. Rheol*, 37:381, 1993.

[37] W.R. Hwang M.A. Hulsen and H.E.H. Meijer. Direct simulation of particle suspensions in a viscoelastic fluid in sliding bi-periodic frames. *J. Non-Newtonian Fluid Mech.*, 121:15, 2004.

[38] T. Kataoka, T. Kitano M. Sasahara and K. Nishijima. Viscosity of particle filled polymer melts. *Rheol. Acta*, 17:149, 1978.

[39] D.J. Highgate and R.W. Whorlow. Rheological properties of suspensions of spheres in non-newtonian media. *Rheol. Acta*, 9:569, 1970.

[40] D.L. Faulkner and L.R. Schimdt. Glass bead-filled polypropylene 1.rheological and mechanical properties. *Polym. Eng. Sci.*, 17:657, 1977.

[41] A.J. Poslinsky, M. E. Ryan R. K. Gupta S. G. Seshadri and F. J. Fechette. Rheological behaviour of filled polymeric systems. i. yeld stress and shear thinning effects. *J. Rheol.*, 32:657, 1988.

[42] H. See, P. Jang, and N. Phan-Thien. Concentration dependence of the linear viscoelastic properties of particle suspensions. *Rheol. Acta*, 39:131, 2000.

[43] B. K. Aral and D. M. Kalyon. Viscoelastic material function of noncolloidal suspensions with soherical particles. *J. Rheol.*, 41:599, 1997.

[44] J. A. Walberer and A. J. McHugh. The linear viscoelastic behavior of highly filled polydimethylsiloxane measured in shear and compression. *J. Rheol.*, 45:187, 2001.

[45] J. F. Le Meins, P. Moldenaers and J. Mewis. Suspensions in polymer melts. 1. effect of particle size on the shear flow behaviour. *Ind. Eng. Chem. Res.*, 41:6297, 2002.

[46] R.J. Manley S.G. Mason. The viscosity of suspensions of spheres:a note on the particle interaction coefficient. *Canadian Journal of Chemistry*, 32:763, 1954.

[47] D.D. Joseph. Flow induced microstructure in newtonian and viscoelastic fluids. *Proceedings of the 5th World Congress of Chemical Engineering, Particle Technology Track. American Institute of Chemical Engineers, San Diego Keynote presentation*, 6:3, 1996.

[48] F. Gadalamaria and A. Acrivos. Shear-induced structure in a concentrated suspensions of solid spheres. *J. Rheol*, 24:799, 1980.

[49] G. Segré and A. Silberberg . Radial particle displacements in poiseuille flow of suspensions. *Rheol. Acta*, 189:209, 1961.

[50] B.P. Ho and L.G. Leal. Inertial migration of rigid spheres in 2-dimensional unidirectional flows. *J. FLuid Mech.*, 65:365, 1974.

[51] E. Bartram, H.L. Goldsmith and S.G. Mason. Particle motions in non-newtonian media iii. further observations in elasticoviscous fluids. *Rheol. Acta*, 14:776, 1975.

[52] F. Gauthier, H.L. Goldsmith, S.G. Mason. Particle motions in non-newtonian media i. couette flow. *Rheol. Acta*, 10:344, 1971.

[53] F. Gauthier, H.L. Goldsmith, S.G. Mason. Particle motions in non-newtonian media ii. poiseuille flow. *Trans. Soc. Rheol.*, 15:297, 1971.

[54] M. Astruc, S. Vervoort, H.O. Nouatin, T. Coupez, Y. De Puydt, P. Navard, E. Peuvrel-Disdier. Experimental and numerical study of the rotation and the erosion of fillers suspended in viscoelaastic fluids under simple shear flow. *Rheol. Acta*, 42:421, 2003.

[55] F. Snijkers, G. D'Avino, P.L. Maffettone, F. Greco, M. Hulsen and J. Vermant. Rotation of a sphere in a viscoelastic liquid subjected to shear flow. part ii: Steady state experimental results. *submitted J. Rheol*, 2008.

[56] D.D. Joseph and J. Feng. A note on forces that move particles in a second order fluid. *J. Non-Newtonian Fluid Mech.*, 64:299, 1996.

[57] M.J. Riddle, C. Narvaez and R.B. Bird. Interactions between two spheres falling along their line of centers in viscoelastic fluid. *J. Non-Newtonian Fluid Mech.*, 2:23, 1977.

[58] G. Gheissary, B.H.A.A. van der Brule. Unexpected phenomena observed in particle settling in non-newtonian media. *J Non-Newtonian Fluid Mech.*, 67:1, 1996.

[59] J. Michele R. Patzold and R.Donis. Alignment and aggregation effects in suspensions of spheres in non-newtonian media. *Rheol. Acta*, 16:317, 1977.

[60] H. Giesekus. *Some new results in suspension rheology.* F. Wendt, 1981.

[61] H. Giesekus. Die bewegung von teilchen in stromungen nicht-newtonscher flussigkeiten. *ZAMM*, 58:T–26, 1978.

[62] L. Petit and B. Noetinger. Shear induced structures in macroscopic dispersions. *Rheol. Acta*, 27:437, 1988.

[63] M.K. Lyon, D.W. Mead R.E. Elliot and L.G. Leal. Structure formation in moderately concentrated viscoelastic suspensions in simple shear flow. *J. Rheol*, 45:881, 2001.

[64] R. Scirocco J. Vermant and J. Mewis. Effect of the viscoelasticity of the suspendind fluid on structure formation in suspensions. *J. Non-Newtonian Fluid Mech.*, 117:183, 2004.

[65] D. Won and C. Kim. Alignment and aggregation of spherical particles in viscoelastic fluid under shear flow. *J. Non-Newtonian Fluid Mech.*, 117:141, 2004.

[66] H.W. Jung D. Won and C. Kim. Hydrodynamic interaction between two cylinders in planar shear flow of viscoelastic fluid. *Korea-Australia Rheol. J.*, 14:203, 2002.

[67] P. Brunn. The behavior of a sphere in non-homogeneous flows of a viscoelastic fluid. *Rheol. Acta*, 15:589, 1976.

[68] B.P. Ho ann L.G. Leal. Migration of rigid spheres in a two-dimenisonal unidirectional shear flow of a second order fluid. *J. Fluid Mech.*, 76:783, 1976.

[69] J.F. Morris and J. Brady. Curvilinear flows of noncolloidal suspensions. the role of normal stresses. *J. Rheol.*, 43:1213, 1999.

[70] A. Karnis and S.G. Mason. Particle motions in sheared suspensions.xix. viscoelastic media. *Trans. Soc. Rheol.*, 10:571, 1966.

[71] D.J. Highgate. Particle migration in a cone plate viscometry of suspensions. *Nature*, 211:1390, 1966.

[72] H.J. Choi, D.C. Prieve, M. S. John. Anomalous lateral migration of a rigid sphere in torsional flow of a viscoelastic fluid - effect of plymer concentration and solvent viscosity. *J. Rheol.*, 31:317, 1987.

[73] T.E. Karis, D.C. Prieve and S.L. Rosen. Lateral migration of a rigid sphere in torsional flow of a viscoelastic fluid. *AIchE. J.*, 30:631, 1984.

[74] T.E. Karis, D.C. Prieve and S.L. Rosen. Anomalous lateral migration of a rigid sphere in torsional flow of a viscoelastic fluid. *J. Rheol.*, 28:381, 1984.

[75] D.C. Prieve, M.S. Jhon and T.L. Koenig. Anomalous lateral migration of a rigid sphere in torsional flow of a viscoelastic fluid. II. Effect of shear rate. *J. Rheol.*, 29:639, 1985.

[76] M.A. Jefri and A.H. Zahed. Elastic and viscous effects on particle migratrion in plane-poiseuille flow. *J. Rheol.*, 33:691, 1989.

[77] M.A. Tehrani. An experimental study of particle migration in pipe flow of viscoelastic fluids. *J. Rheol.*, 40:1057, 1996.

[78] D.D. Joseph and J. Feng. the motion of solid particles suspended in viscoelastic liquids under torsional shear. *J. Fluid Mech.*, 324:199, 1996.

[79] Kurata M. T. Kotaka and Tamura M. Normal stress effect in polymer solutions. *J. Appl. Phys.*, 30:1705, 1959.

[80] J. Meissner, R.W. Garbella and J. Hostettler. Measuring normal stress differences in polymer melt shear flow. *J. Appl. Phys.*, 33:843, 1989.

[81] T. Patrick Underhill, P.S. Doyle. Accuracy of bead-spring chains in strong flows. *J. Non-Newtonian Fluid Mech.* , 145:109, 2007.

[82] J.F. Brady. Computer simulation of viscous suspensions. *Chem. Eng. Sci.* , 56:2921, 2001.

[83] H. H. Hu. Direct simulation of flows of solidliquid mixtures. *Int. J. Multiphase Flow*, 22:335, 1996.

[84] H. H. Hu P. Y. Huang, J. Feng and D. D. Joseph. Direct simulation of the motion of solid particles in couette and poiseuille flows of viscoelastic fluids. *Int. J. Fluid Mech.*, 343:73, 1997.

[85] M. Belzons, M. blanc , R. Bouillot J.-L. Camoin. Viscosit d'une suspensions diluee et bidimensionnelle de spheres. *C.R. acad. Sc. Paris*, 292:939, 1981.

[86] R. Glowinski, T.W. Pan, T.I.Hesla and D.D. Joseph. A distributed lagrangian multiplier /fictitious domain method for particulate flows. *Intern. J. multiphase Flows*, 25:755, 1999.

[87] G. Batchelor. The stress system in a suspension of force-free particles. *J. Fluid Mech.*,41:545, 1970.

[88] A. Einstein. Eine neue bestimmung der molekuldimension. *Annalen der Physik Berlin*, 19:286, 1906.

[89] L. Raynaud. *Rheology of aqueous dispersions containing mixtures of particles*. Phd Thesis, Katholieke Universiteit Leuven, Belgium, 1997.

[90] Y. Almog, S. Reich and M. Levy. Monodisperse polymeric spheres in the micron size range by a single step process. *Brit. Polym. J.*, 14:131, 1982.

[91] R. Scirocco. *Rheology and rheo-optics of suspensions in viscoelastic media*. PhD thesis, Katholieke Universiteit Leuven, Belgium.

[92] T. Narayanan. *Synchrotron Small-Angle X-Ray Scattering*.

[93] H. Brumberger. *Modern aspects of small angle scattering*. Kluwer Academic, Dordrecht, 1995.

[94] S.M. Clarke, R.H. Ottewill and A.R. Rennie. Light scattering studies of dispersions under shear. *Coll. and Interf. Sci.*, 60:95, 1995.

[95] A. Cumming, P. Wiltzius, F.S. Bates and J.H. Rosedale. Light-scattering experiments on phase-separation dynamics in binary fluid mixtures. *Phys. Rev. Lett.*, 45:885, 1991.

[96] J.V. Degroot, C.W. Macosko, T. Kume and T. Hashimoto. Flow-induced anisotropic sals in silica-filled pdms liquids. *Coll. and Interf. Sci.*, 166:404, 1994.

[97] S.M. Clarke, J. Melrose, A.R. Rennie, D. Heyes, P.J. Mitchell, R.H. Ottewill, H.J.M. Stanley and G.C. Straty. The structure and rheology of hard sphere systems. *J. Phys. Condensed Matter*, 6:A333, 1994.

[98] L.M. Walker,W.A. Kernick III and N.J. Wagner. In situ analysis of the defect texture in liquid crystal polymer solutions under shear. *Macromolecules*, 30:508, 1997.

[99] Abramoff M.D., P.J. Magelhaes, S.J. Ram. Image processing with imageJ. *Biophotonics Int.*, 11:36, 2004.

[100] C. Kim. Migration in concentrated suspension of spherical particles disperded in polymer solution. *Korea-Australia Rheol. J.*, 13:19, 2001.

[101] A. Ponche, D. Dupuis. On instabilities and migration phenomena in cone and plate geometry. *J. Non-Newtonian Fluid Mech.*, 127:123, 2005.

[102] D. Gunes, R. Scirocco, J. Mewis and J. Vermant. Effects of aspect ratio and suspending medium rheology on flow-induced orientation of non-spherical particles. *J. Non-Newtonian Fluid Mech.*, 2007-submitted.

[103] R. Scirocco, J. Vermant, and J. Mewis. Effect of the viscoelasticity of the suspending fluid on structure formation in suspensions. *J. Non-Newtonian Fluid Mech.*, 117:183, 2004.

[104] E. Bartram, H.L. Goldsmith and S.G. Mason. Particle motions in non-newtonian media. III. Further observation in viscoelastic fluids. *Rheol. Acta*, 14:776, 1975.